NOTICE

The quality of this microform is heavily dependent upon the quality of the original thesis submitted for microfilming. Every effort has been made to ensure the highest quality of reproduction possible.

If pages are missing, contact the university which granted the degree.

Some pages may have indistinct print especially if the original pages were typed with a poor typewriter ribbon or if the university sent us an inferior photocopy.

AVIS

La qualité de cette microforme dépend grandement de la qualité de la thèse soumise au microfilmage. Nous avons tout fait pour assurer une qualité supérieure de reproduction.

S'il manque des pages, veuillez communiquer avec l'université qui a conféré le grade.

La qualité d'impression de certaines pages peut laisser à désirer, surtout si les pages originales ont été dactylographiées à l'aide d'un ruban usé ou si l'université nous a fait parvenir une photocopie de qualité inférieure.

"ELECTROCHEMISTRY OF LEAD AND LEAD ALLOY ANODES IN LEAD-ACID BATTERIES FOR PHOTOVOLTAIC ENERGY STORAGE."

by:

Abdulreza Tabe Mohammadi

A thesis submitted to the School of Graduate Studies and Research in partial fulfilment of the requirements for the degree of Master of Applied Science in the Department of Chemical Engineering University of Ottawa

ISBN 0-315-68005-9

UNIVERSITÉ D'OTTAWA
UNIVERSITY OF OTTAWA

TO MY WIFE PARASTOO

تقدیم به همسرم پرستو

ACKNOWLEDGMENTS

I wish to express my gratitude to my project supervisors Dr. Subrah Donepudi and Dr. William Adams as well as Dr. Magdi Girgis for their guidance and encouragements throughout this work.

I would also like to thank all ESTCO staff, especially Mr. Ray Dore, for help with the experimental work. Without them this work would not have been possible.

The acknowledgement is extended to Dr. Edward Ghali and Mr. Alain Adnot of Laval University, Quebec, for their kind and generous help in providing the possibility to use the surface analysis facilities in that university; and also to the University Research Incentive Fund (URIF) of the province of Ontario, Westinghouse Canada, and Integrated Power Corp., MD, USA, for their financial support of the project.

The supply of lead and lead alloys by Dr. E. Valeriote, Cominco Metals Ltd., Product Research Centre, Sheridan Park, Mississauga, Ontario, is gratefully acknowledged.

Special recognition is due to my friend Mr. Stephane Garneau for all his helps.

TABLE OF CONTENTS

LIST OF FIGURES:

LIST OF TABLES:

NOMENCLATURE

A	electrode surface area (cm^2).
a	anodic (as subscript).
C	concentration (mol cm^{-3}), with ∞ superscript: bulk concentration.
c	cathodic (as subscript).
D	diffusion coefficient (cm^2 s^{-1}).
E	potential (mV).
E^0	standard potential (mV).
E_e	potential at equilibrium (mV).
F	Faraday constant (96500 C).
h	height (cm).
i	current (mA).
J	molar flux (mol s^{-1} cm^{-2}).
K	rate constant (mol s^{-1} cm^{-3}).
M	molecular weight (g mol^{-1}).
N_0	total number of nuclei formed in unit surface area of electrode.
n	the number of electrons transferred in the electrochemical reaction.
O	the oxidant (in subscript form).
R	the reductant (in subscript form).
R	gas constant (J mol^{-1} $^oK^{-1}$).
r	radius (cm).
T	temperature (^oK).

t	time (s).
u	age of a nucleus (s).
V	volume (cm^3).
x	distance from the surface of the electrode.
α	transfer coefficient (constant between 0 and 1).
η	overpotential (mV).
λ	time at which the scan is reversed (s).
ν	scan rate ($mV\ s^{-1}$).
ρ	density ($g\ cm^{-3}$).

ABSTRACT

The performance of lead-acid batteries for energy storage in photovoltaic/diesel/battery hybrid systems strongly depends on several electrochemical and/or operational factors such as the alloying elements incorporated in the electrode plates, the addition of expander materials to the anode or to the electrolyte, temperature, and the charging regime of the battery.

In this study, the influences of the above mentioned factors on battery performance were investigated using cyclic voltammetry and potentiostatic transient techniques supplemented by surface analysis techniques including scanning electron microscopy (SEM) and x-ray photoelectron spectroscopy (XPS).

The behaviour of binary lead-calcium and lead-antimony, and ternary lead-calcium-tin and lead-antimony-selenium alloy anodes were compared to that of the pure lead anode. In addition, the effect of ammonium ligno-sulphonate (ALS), as an expander added to the electrolyte, on the anode behaviour, was studied at room (23°C) and cold (0°C) temperatures.

CHAPTER ONE: INTRODUCTION

1.1- PHOTOVOLTAIC HYBRID SYSTEMS

Photovoltaic (PV) systems convert solar energy directly into direct current electricity by means of photovoltaic cells.

Despite the fact that the electricity generated by these systems is more costly than that produced by conventional systems (e.g., nuclear power stations), they have found practical applications in remote areas where connection of the load to the general electric grid is not possible or economical.

The traditional methods of electrical energy production in remote areas is by diesel engine generators which have the disadvantage of high energy cost mainly due to the expenditures related to the transportation of fuel, spare parts, and maintenance. However, a hybrid system combining a PV array, diesel engine generator, and batteries is found to be cost effective in remote locations for applications such as general household electrical demands, water pumping, refrigeration, and radio and TV repeaters. Such a hybrid system has the advantage of reducing the capital costs related to the PV stand-alone system as well as the fuel costs for the diesel engine generator by reduction in fuel consumption and it also extends the time between maintenance visits.

Figure 1.1 shows schematically the components of a PV/diesel/

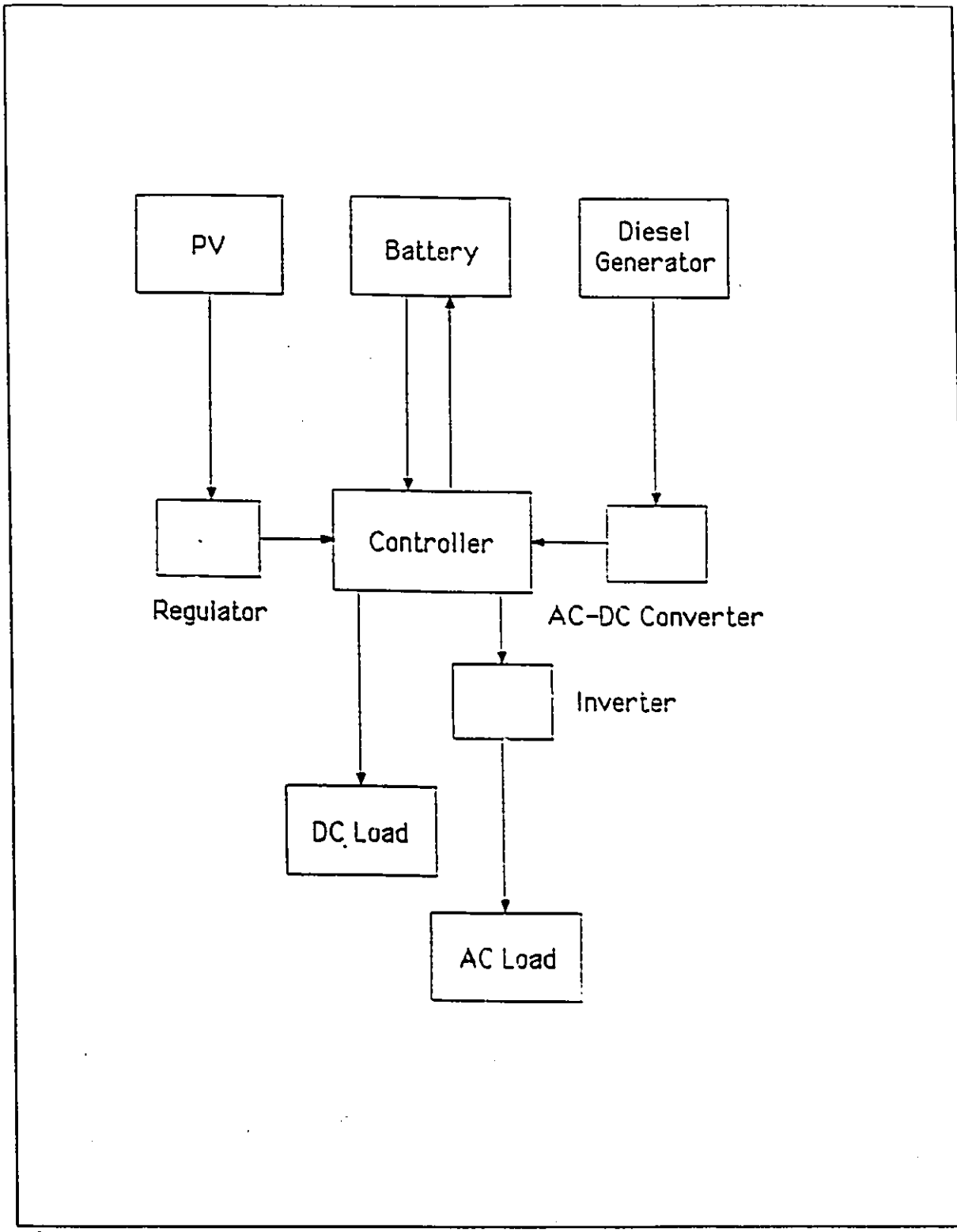

Figure 1.1: A typical PV/diesel/battery hybrid and its components.

battery hybrid. The system consists of the PV array, convertor, controller, battery subsystem, and diesel engine generator.

1.2- THE BATTERY SUBSYSTEM

The role of the battery subsystem in a hybrid PV system is to store the energy produced by the PV array and release it to the load during low light periods. This is illustrated in Figure 1.2a which shows a typical load profile for a hybrid system over 24 hours of operation. The battery subsystem also allows the diesel engine generator to operate at constant power which in turn increases both efficiency and life of the diesel generator and reduces fuel consumption and maintenance requirements.

In the early stages of the development of the PV technology, the price of the solar panels was as high as US$ 35.17 per peak-watt in the early 1970s [Sato, 1989], and the total PV system cost was controlled by this cost. Since then, however, due to technological innovations, the cost of solar panels has decreased, ($ 5.50/peak Watt in 1987 [Sol, 1989]), whilst that of the storage batteries, as a proportion of the total system cost, has increased. A typical break-down of the life cycle cost of the hybrid system shows [EMR, 1989; IPC, 1988] that the total cost is controlled, up to 24%, by the battery subsystem (see Figure 1.2b). Therefore, an accurate and predictable performance of the battery sub-system, with respect to operational and environmental conditions, is essential in order to minimize this cost by keeping the maintenance

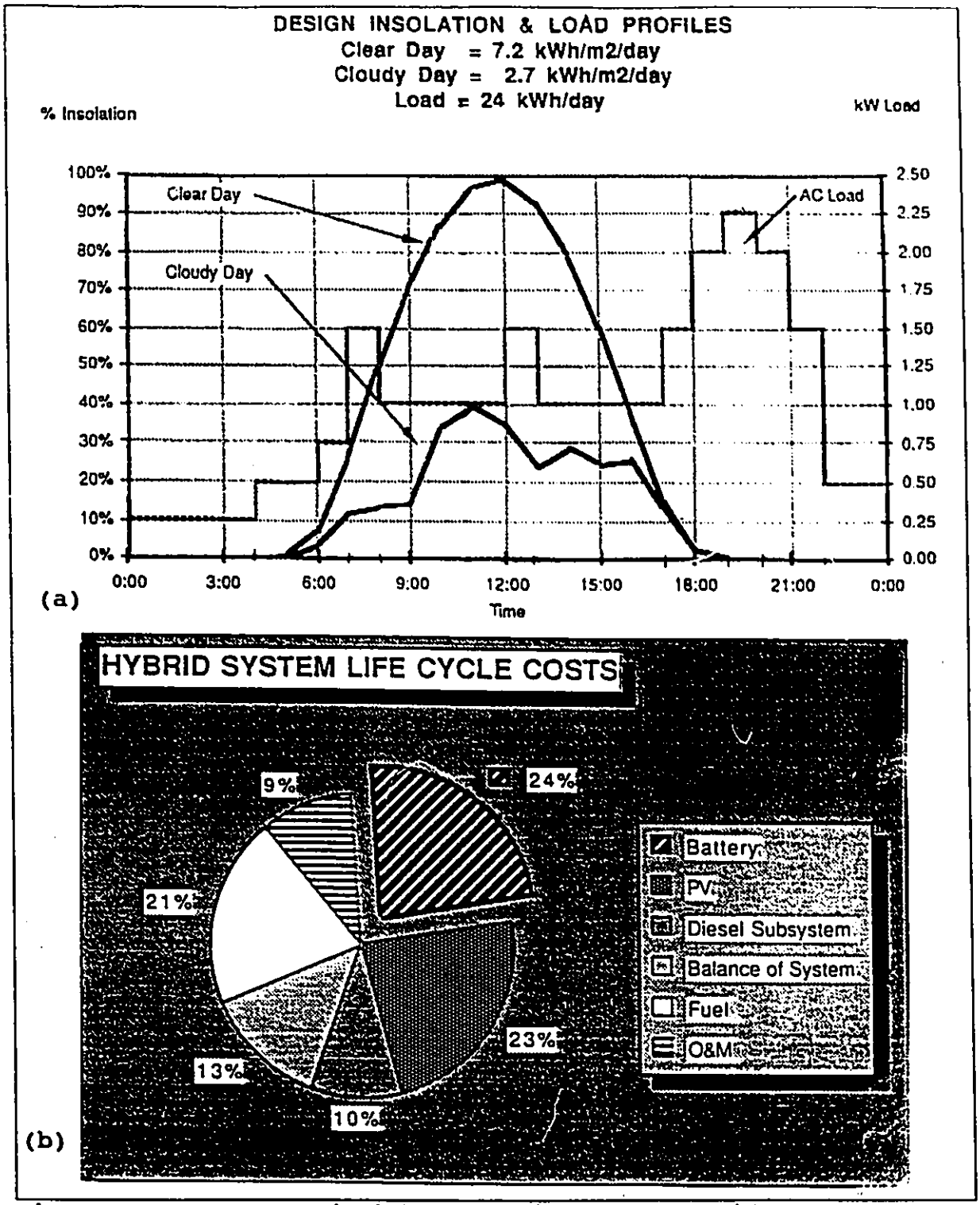

Figure 1.2: (a): A typical load profile for a hybrid system over 24 hours [EMR, 1989]. (b): Atypical breakdown of the total life cycle cost of a PV hybrid system [IPC, 1988].

as low as possible and extending the battery life to a maximum. To meet this goal, a good knowledge of battery operational parameters in PV systems is very important.

The most common types of storage (rechargeable) batteries which are in use in the PV/diesel/battery hybrid are of lead-acid sealed and flooded types, and nickel/cadmium flooded batteries.

In this study, the performance of materials used in lead-acid batteries was investigated.

1.3- THE KEY COMPONENTS OF THE LEAD-ACID BATTERY

In a lead-acid battery, the negative electrode is made of metallic lead or lead alloys, and the positive electrode is made of lead dioxide. Both these active materials are in contact with lead or alloyed lead grids which serve as the current collectors. A concentrated solution of sulphuric acid acts as electrolyte. A cutaway view of the inside of a battery case of a typical lead-acid battery built for SLI (starting/lighting/ignition) which is usually used in automobiles, is shown in Figure 1.3 [Linden, 1984]. This shows the electrode plates, separators, connectors, terminal post, and vents.

The discharge chemistry of this battery leading to the generation of electricity is as follows:

$Pb + HSO_4^- \longrightarrow PbSO_4 + H^+ + 2e^-$ (Anode)

$PbO_2 + HSO_4^- + 3H^+ + 2e^- \longrightarrow PbSO_4 + 2H_2O$ (Cathode)

$Pb + PbO_2 + 2H^+ + 2HSO_4^- \longrightarrow 2PbSO_4 + 2H_2O$ (Overall)

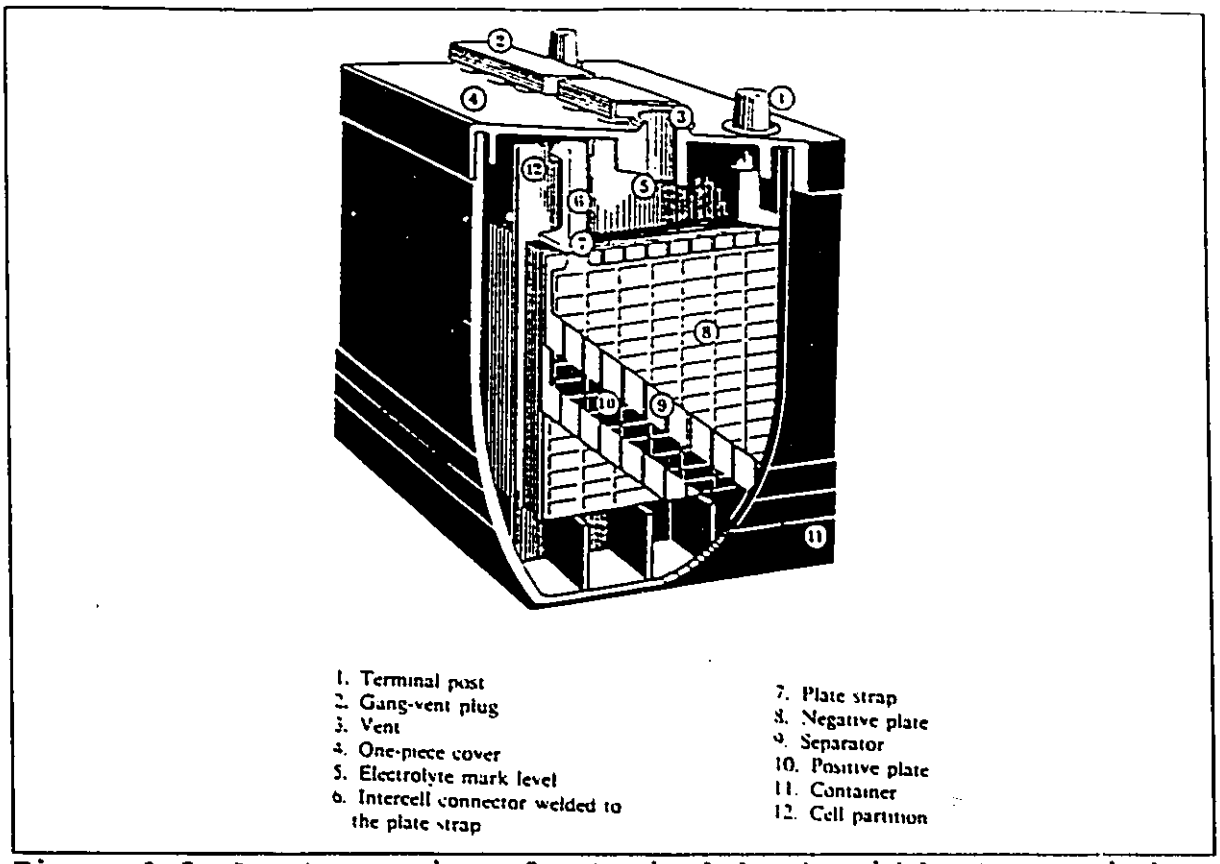

Figure 1.3: A cutaway view of a typical lead-acid battery [Linden, 1984].

These reactions are reversible and change direction during charging of the battery.

The high-rate and low-temperature performance of lead-acid batteries are two important factors to be considered in the design of the PV hybrid control system for northern Canadian applications. On the other hand, it is known [Mahato, 1977] that the high rate and low temperature performance of the battery are limited by its negative plate.

1.4- ELECTROCHEMISTRY OF LEAD-ACID BATTERIES.

1.4.1- GENERAL DESCRIPTION

The operation of lead-acid batteries can be explained on the basis of the double sulphate principle which was initially introduced by Gladstone and Tribe in 1882 [Bode, 1977]. According to this principle, the electrolyte in the solution, H_2SO_4, is not only an ion transport medium, but a reactant as well, and the discharge products of both the anode oxidation reaction and the cathode reduction reaction are lead sulphate.

The discharge curves for positive and negative electrodes are illustrated schematically in Figure 1.4 [Ruetschi, 1977]. The initial potential drop, A, after switching on the current, is due to the electrolyte resistance in the electrolyte-filled pores of the separators, the ohmic resistance in the grids, active material layers and solid-solid and solid-liquid interfaces. The sloping portion, B, arises from double layer capacity discharge, as coupled through the ohmic electrolyte resistance in the pores of the active mass. Supersaturation, nucleation and crystallization phenomena lead to the initial voltage drop, C, in the discharge curve of the positive electrode. This behaviour of the positive electrode may be related to the relatively poor charge acceptance of the positive electrode during recharge at low temperatures and high rates. Section D in Figure 1.4 represents the successive discharge of the active materials to lead sulphate. It is finally followed by rapid concentration polarization at E, due to acid depletion and pore

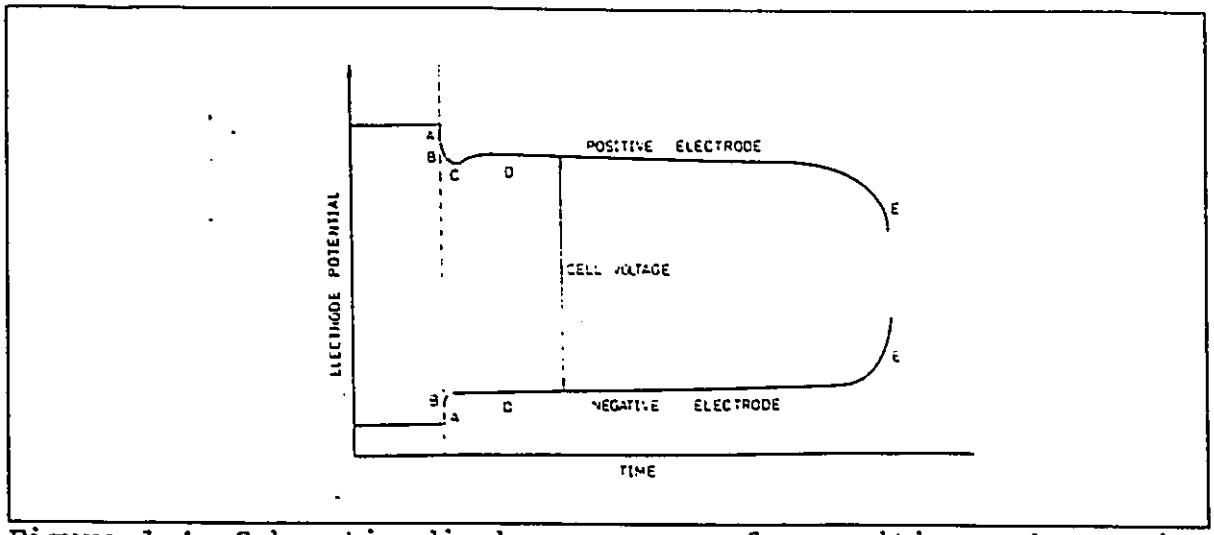

Figure 1.4: Schematic discharge curves for positive and negative plates [Ruetschi, 1977].

obstruction by lead sulphate crystals.

In particular, the discharge process of the lead negative electrode involves the dissolution of lead to form Pb^{2+} ions [Archdale, 1972a].

$Pb \longrightarrow Pb^{2+}$ (in solution) + $2e^-$

$Pb^{2+} + SO_4^{2-} \longrightarrow PbSO_4$ (crystal)

The rate is controlled by the gradual coverage of the electroactive surface by a resistive lead sulphate film leading to the eventual passivation of the electrode (see Figure 1.5).

The charging or the cathodic reduction of the lead electrode involves the electroreduction of the lead sulphate to metallic lead. The conventional reduction process occurs through chemical dissolution of $PbSO_4$ to Pb^{2+} ions followed by the electro-reduction of Pb^{2+} to metallic lead.

For the positive lead oxide electrode, the discharge reaction is believed to proceed via a dissolution-precipitation mechanism.

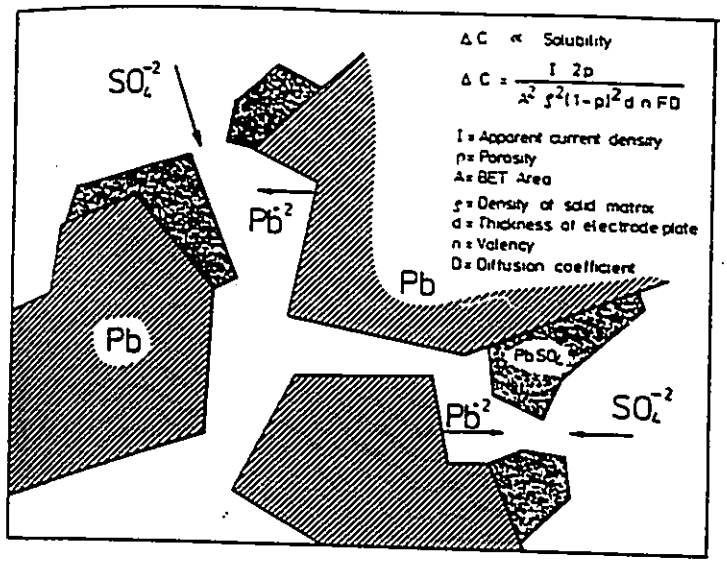

(a)

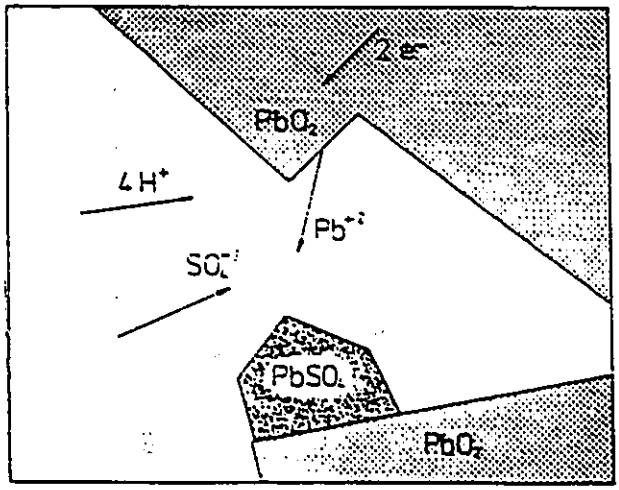

(b)

Figure 1.5: Schematic illustration of discharge process in the pores of (a): lead negative, and (b):lead oxide positive electrodes [Archdale, 1972a].

$2e^- + PbO_2 + 4H^+ \longrightarrow Pb^{2+} + H_2O$

$Pb^{2+} + SO_4^{2-} \longrightarrow PbSO_4$

Some more detailed discharge mechanisms involving further complex intermediates have been proposed by several authors [Laitinen, 1976; Hampson, 1968; Weininger, 1975]. Figure 1.5 simplifies the above discharge mechanism.

The free energy change of the system is:
ΔG^0 = -13.95 Kcal/mol (E_0 = 0.303 V vs. H_2/H^+, i.e., Normal Hydrogen Electrode, NHE) for the anodic reaction, and ΔG^0 = -74.99 Kcal/mol (E_0 = -1.627 V vs. H_2/H^+) for the cathodic reaction [Bode, 1977] giving ΔG^0 = -88.94 Kcal/mol (E_0 = 1.93 V vs. H_2/H^+), specific energy = 161 Wh/Kg, specific capacity = 83.5 Ah/Kg. However, in practice, the lead-acid battery exhibits significantly lower specific energy than theoretical.

1.4.2- PASSIVATION

While lead sulphate is the product of the electrochemical reaction leading to the electricity generation, it limits the rate and the extent of the reaction. Lead sulphate produces a dense, non-porous, and non-conducting layer on the electrode surface. Lead sulphate, which is a highly resistive material (approximately 10^8 ohm-cm) [Weissman, 1977], also occurs naturally as the mineral anglesite. It crystallizes in the orthorhombic system [Burbank, 1971a, b], and is present in a fine grain structure or as large crystals, constituting the so called "hard" sulphate [Chiku, 1971], which is not regenerable to the electrochemically active species of

lead and lead dioxide.

Chiku et al. [Chiku, 1971], identified morphological differences between the rechargeable and "hard" lead sulphate. Based on their study, the rechargeable lead sulphate was shown to nucleate preferentially in the early stages of the anodic oxidation of lead and grows dendritically afterwards. This was confirmed by the investigations of Archdale and Harrison [Archdale, 1972a, b, 1973a, b]. The latter authors showed that lead dissolves electrochemically in sulphuric acid solution to produce a soluble lead sulphate solution and a solid layer of lead sulphate. However, in a later work [Fleming, 1976], Fleming and Harrison suggest a precipitation mechanism prior to the formation of a $PbSO_4$ layer by a solid state reaction.

During discharge, the thickness of a freshly formed sulphate layer on the lead anode increases with the newly generated crystals. This layer is of the order of 0.1 to 10 μm in thickness [Weissman, 1977]. With time, and under deep-discharge conditions, significantly larger portions of the originally available lead becomes structurally encapsulated by the sulphate and unavailable for further discharges. The amount of active material utilized during the discharge depends on the thickness and porosity of the electrode plate. The electrode is performance-limited by its available reactive surface geometry and the degree of passivation of lead sulphate.

Electrode passivation is a result of the presence of a virtually insoluble and nonconducting lead sulphate film on the

electrode surface. The presence of intermediate compounds (i.e., basic lead sulphates and lead oxides) beneath the lead sulphate film have been confirmed [Ruetschi, 1964, 1973; Burbank, 1985; Ijomah, 1987]. Two theories , namely, "nucleation and growth (solid state reaction)" and " dissolution-precipitation" have both been used to explain electrode passivation [Ijomah, 1987]. In the solid state mechanism, $PbSO_4$ is believed to be deposited from the solution directly on the metal surface at a certain critical potential, followed by two or three dimensional growth until the surface is fully covered. However, in the dissolution-precipitation mechanism, nucleation of $PbSO_4$ was thought to occur in the solution, followed by its precipitation onto the metal surface (see Figure 1.5). Here, the growth is always three dimensional, and passivation is by physical blocking action. According to the passivation model proposed by Asai et al. [Asai, 1984], shown in Figure 1.6, for porous negative electrodes used in lower electrolyte concentrations, the plugging of pores by large sulphate crystals is responsible for passivation, whereas at higher electrolyte concentrations the predominant factor is coverage of the lead surface by the deposition of fine particles from solution. In other words, at the early stages of discharge, when the concentration of electrolyte is high, fine particles of lead sulphate form. As discharge proceeds, the concentration drops and larger crystals are produced and cover the fine ones. In porous positive electrodes, the plugging of pores is the main passivation mechanism.

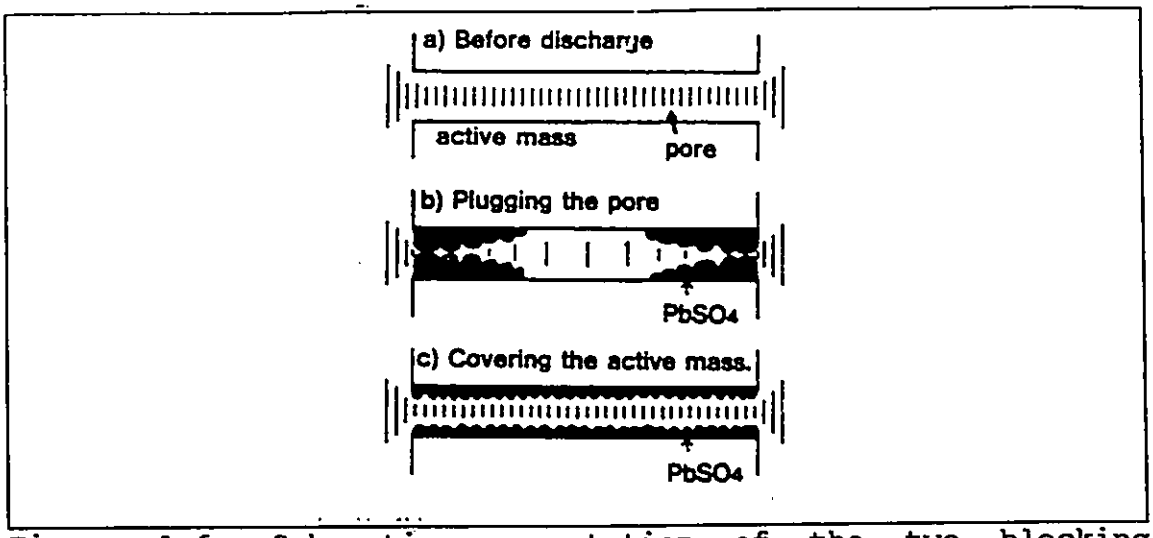

Figure 1.6: Schematicrepresentation of the two blocking mechanisms of lead sulphate crystals [Asai, 1984].

Pavlov and Popova [Pavlov, 1970] define two kinds of passivation: stable and unstable. The stable form is thought to be the result of a $PbSO_4$ layer in which distances between lead sulphate crystals are equivalent in magnitude to ionic diameters. This theory suggests that the anodic lead sulphate layer acts as a "permselective" membrane [Ruetschi, 1973] allowing free access of the H_3O^+, OH^-, and Pb^{2+} ions to the lead interface, but hindering the transport of SO_4^{2-} [Pavlov, 1970] and HSO_4^- [Weissman, 1977] ions when the lead sulphate film is at least 1 μm thick. Therefore, the rate controlling mechanism for anodic oxidation of lead is the diffusion of SO_4^{2-} and HSO_4^- ions [Carr, 1971]. Passivation then follows as a result of intercrystalline precipitation of lead monoxide and basic lead sulphates. Instability or self-depassivation, is the result of larger intercrystalline distances witnin the lead sulphate layer with passivation only possible during anodic polarization.

1.5- THE NEGATIVE ELECTRODE ALLOYS.

1.5.1- PURE LEAD

Metallic lead, in a highly reactive porous structure, is the base material used in lead-acid batteries as the negative electrode.

Pure lead has a density of 11.3 g/cm^3 at 20°C, melts at 327°C and possesses a resistivity of 2.1 X 10^{-5} ohm-cm at 18°C [ILZIC, 1977]. Lead is a very soft and ductile metal. It has low mechanical strength and poor creep resistance (plastic deformation under low stress at high temperatures). Therefore, alloying elements are added to improve the mechanical properties for fabrication processes and to optimize the performance of the electrode in the battery. However, small amounts of impurities will affect lead's electrochemical performance, e.g., hydrogen overvoltage, and mechanical characteristics, e.g., stress-strain relationship, appreciably [Mahato, 1983].

Pure lead, lead-antimony, and lead-calcium alloys are commonly used in lead-acid batteries with lead-antimony alloys presenting the known disadvantages of a higher tendency to self-discharge, and less life expectancy due to corrosion than lead and lead-calcium electrodes.

1.5.2- ANTIMONIAL ALLOYS

Pure lead is traditionally hardened by an addition of antimony. The amount of antimony has been varied between 5 to 12% by weight

with the maximum hardness at 12% [IBMA, 1973].

Some of the reasons for the wide acceptance and use of lead-antimony alloys in lead-acid batteries are improved strength, better corrosion resistance, and excellent castability. It has also been found that antimony addition to the positive grid extends the service life of the battery [Webster, 1988] as well as improving the adhesion of the active material to the grid [Burbank, 1971a, b].

The most well-known disadvantage of lead-antimony alloys is that it increases lead-acid battery gassing by reducing the lead electrode's hydrogen overpotential [Mahato, 1983, 1985]. This causes loss of water (and therefore the need for more frequent maintenance) and a higher rate of self-discharge as compared to pure lead (an average loss of 15% of the capacity per month, versus roughly 3% for the lead and lead-calcium systems [Linden, 1984]).

Toxic stibine gas (SbH_3) can also be evolved at the end of charging and during overcharge, causing a hazard when antimonial lead-acid batteries are used in an enclosed environment without an adequate charge control [Mahato, 1985]. The presence of antimony in the negative plate also reduces the charge efficiency.

One of the most important improvements in the last decade has been the reduction in the antimony level from 12% to less than 2% and ultimately the replacement of antimony with other alloying elements such as calcium and tin. Low antimony alloys (less than 3%) have been developed by overcoming the problems of a reduction in antimony content by the addition of other alloying elements such

as sulphur, copper, arsenic, and selenium. Selenium is the most efficient and most common addition, and only about 0.05% is required [Bagshaw, 1977; Prengaman, 1983]. However, low antimony alloys have a lower mechanical strength than the traditional alloys containing 6-12% antimony. Addition of tin to increase the fluidity of lead alloys during casting, and arsenic to reduce the age-hardening period (process of increasing the hardness of an alloy as a result of spontaneous structural changes which take place some time after casting [ILZIC, 1977]) is very common [Williams, 1966; Costa, 1970].

Although pure lead has been studied extensively, few investigations have been made to study the electrochemical properties of lead alloys. The morphological aspects of lead sulphate film formation on the surface of lead antimony alloys were investigated by Burbank [Burbank, 1971a, b, c]. She suggests a nucleation and growth mechanism which was confirmed by later transient experiments reported by Webster et al. [Webster, 1986]. The latter authors suggest a two-dimensional nucleation and growth of lead sulphate film followed by overlap of the crystals to cover the surface completely.

Ijomah [Ijomah, 1987], found a morphological dependency of the lead sulphate film on the nature and concentration of the alloying elements. He also detected a side reaction during the discharge of the negative electrode, namely oxidation of antimony, producing soluble tertiary antimony oxide. This, in turn, reduces the passivating nature of the lead sulphate layer by opening pores in

the layer [Ijomah, 1987; Webster, 1986].

Although low-antimony alloys are widely used in the battery industry, there still are some applications where even small amounts of antimony cause severe problems. Antimony poisoning of the negative plate (migration of antimony from positive grid to negative active material) and self-discharge of both plates will eventually occur even at low antimony contents. In the case of utilization of lead acid batteries in photovoltaic hybrid systems, it is absolutely essential to retain the high hydrogen overvoltage of lead in order to minimize the number of maintenance visits to the site for battery watering. Therefore, a substitute for antimony is required.

1.5.3- CALCIUM ALLOYS

Lead-calcium alloys were considered for use in batteries during the First World War and have been gaining increasing acceptance since the late 1950's [Jensen, 1957; Willingantz, 1959], and are now widely used for maintenance-free battery applications.

Calcium, is electronegative (anodic) relative to lead. It is usually present to the extent of 0.06 to 0.09 wt%. Although lead-calcium alloys have a poor creep resistance compared with lead-antimony-selenium alloys, their hydrogen overvoltage is similar to that of pure lead, hence there are lower rates of self-discharge and gassing in the battery which is therefore nearly maintenance-free.

The electrical conductivity characteristics of lead-calcium

alloys are quite favourable. A Pb/0.1 wt% Ca alloy exhibits a conductivity 20% higher than that of Pb/9 wt% Sb [Burbank, 1971c].

Bass [Bass, 1987] studied the effect of the calcium content on the exchange current density, and concluded that at calcium levels up to 0.07 wt% the more negative potentials involved with hydrogen evolution will give a super-saturated solution of Ca in Pb at the electrode surface which would, with time, form the stable intermetallic compound Pb_3Ca. This increases the apparent exchange current density, i_0, while the preferential adsorption of calcium ions at the electrode surface (preferred to protons) reduces the hydrogen evolution, hence an increase in exchange current density. At higher Ca concentrations the Ca rich sites, e.g., grain boundaries, will be covered by an insoluble, non-conducting layer of calcium sulphate, hence the observed electro- chemistry approaches that of pure lead.

To maintain the mechanical properties required for mass production, a ternary alloy containing Pb, Ca, and Sn with rigid control of Ca content between 0.07 and 0.1 wt% is now commonly employed [Bass, 1987]. The addition of tin increases the creep resistance of lead-calcium alloys, but it has little effect on the corrosion of these alloys [Bagshaw, 1977; Valeriote, 1981].

The significant advantage of lead-calcium-tin alloys is the lack of the poisoning of the negative plate, thus giving the possibility replacing lead-antimony alloys in the low or maintenance-free batteries. These alloys have presently found their applications in stationary batteries as well as automotive

starting, lighting, and ignition (SLI) batteries.

Although antimonial alloys possess higher mechanical strength characteristics immediately following the casting operation, aged lead-calcium-tin alloys yield stronger and more ductile grids in the long run [Caldwell, 1975].

1.6- EFFECT OF EXPANDERS

The high-rate, low-temperature performance of lead-acid batteries is improved by the addition of materials commonly known as expanders, which also increase the cycle life of the electrode [Simonsson, 1988]. The main purpose of the addition of expanders is to increase the active material utilization by changing the morphology of lead sulphate crystals and increasing the active material surface area.

The conventional expander is a mixture of a lignin derivative (ligno-sulphonate salts), barium sulphate, and carbon black [Bode, 1977; Mahato, 1980]. Out of these, ligno-sulphonate provides the most beneficial influence to the lead active mass. The barium sulphate and carbon black additives have very limited effects on the electrode characteristics [Simon, 1970, 1973, 1974]. Zachlin [Zachlin, 1951] studied the effect of adding an expander and $BaSO_4$ to a battery plate and concluded that $BaSO_4$ was only necessary for maintaining capacity during prolonged cycle life. It may also reduce passivation during discharge by providing alternative nucleation sites for $PbSO_4$ (as $BaSO_4$ is isomorphous to $PbSO_4$)

[Fleming, 1979].

Lignin is one of the three major components of wood and a by-product of pulp and paper mills. The basic structure of lignin is shown in Figure 1.7a. It is a polymer containing phenylpropane units with a poorly defined structure [Mahato, 1980, 1981; Szava, 1988]. The most accepted chemical formula is proposed by Freudenberg [Szava, 1988] shown in Figure 1.7b. Its molecular weight varies from a few hundreds to several thousands. It is non-ionic and has surfactant properties [Rosen, 1978] (i.e., it decreases the surface tension). It adsorbs on solids (lead and lead sulphate) [Sharpe, 1969] and has decreased solubility with increasing sulphuric acid concentration [Mahato, 1977]. Because lignin is not soluble in neutral and organic solvents [Szava, 1988], it is extracted from other compounds by sulphonation as shown in Figure 1.7c.

Many different salts of ligno-sulphonate have been identified and tested [Mahato, 1977] including sodium, ammonium, calcium and barium, which can be added either to the electrode or the electrolyte [Mahato, 1980]. Mahato [Mahato, 1977] examined these salts in cells and found very little differences in their performance based on the identity of the cation of the salts.

It is well established [Simonsson, 1988; Mahato, 1977, 1980, 1981; Szava, 1989; Ekdung, 1987, 1989; Hoffmann, 1984] that the expander is adsorbed on both lead and lead sulphate. During discharge, ligno-sulphonate forms an intermediate complex of "lead-lignin" [Mahato, 1981] which possibly alters the saturation

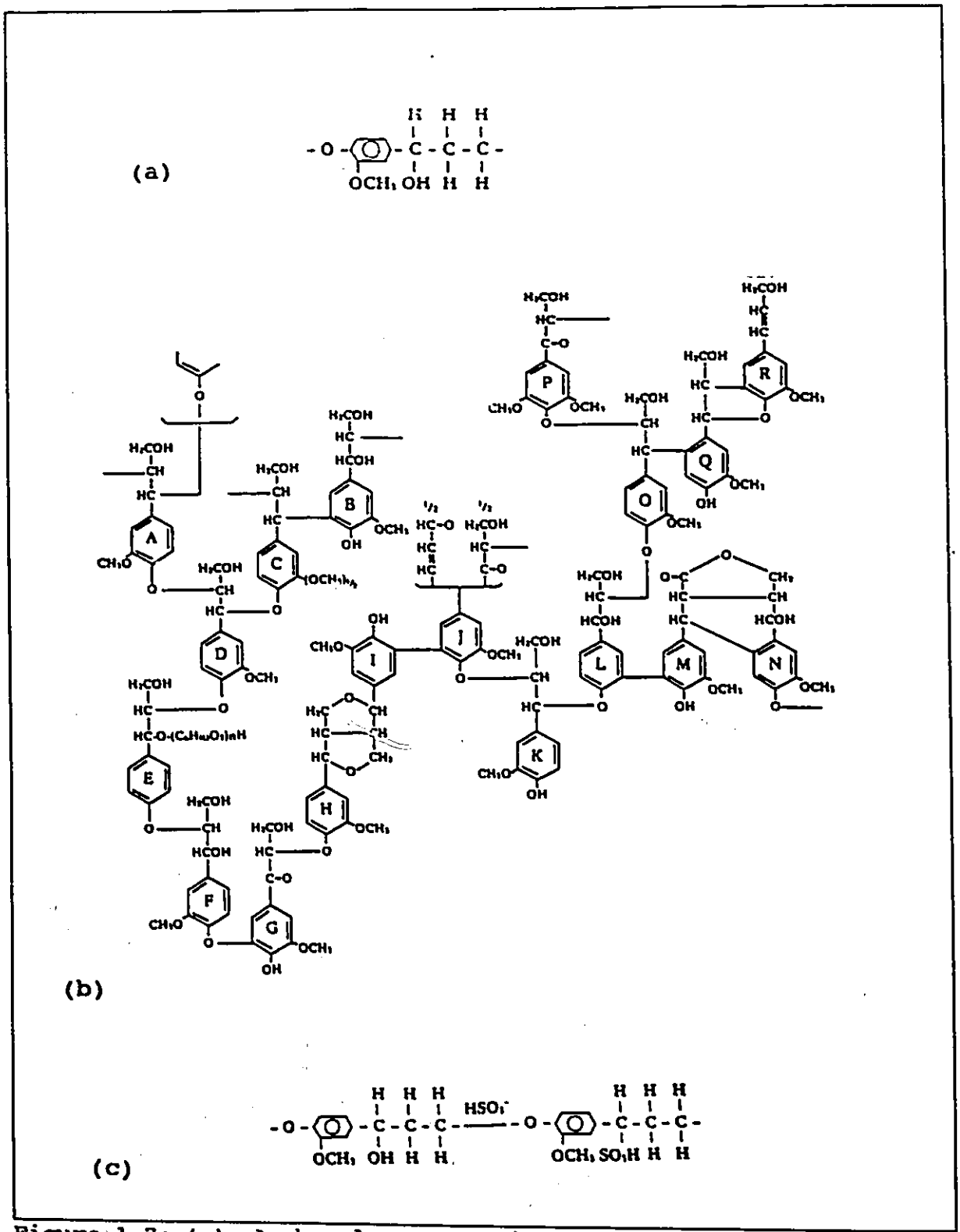

Figure 1.7: (a): A phenylpropane unit. (b): Freudenberg formula of lignin. (c): Sulphonation of lignin [Szava, 1988].

concentration of Pb^{2+} ion at the interface [Asai, 1984]. The adsorption of the expander on the growing faces of the lead sulphate crystals decreases the crystal growth rate, and affects the particle size and the ion permeability of the product layer. However, there is no general agreement on the effect of the expander on the particle size of the lead sulphate crystals [Ekdung, 1989]. Some authors [Simon, 1974; Pavlov, 1987; Iliev, 1985] believe that the lead sulphate crystals become smaller in size, while others reported the opposite effect [Ekdung, 1989; Asai, 1981] and still others have seen no substantial effect on the size of the lead sulphate crystals [Pavlov, 1984]. Also, the delayed passivation of the lead electrode in the presence of expander has been reported [Bode, 1977; Mahato, 1977, 1980; Simon, 1974; Brennan, 1973, 1974, 1976]. This delay was explained in terms of: the expander's contribution in decreasing the resistivity of the lead sulphate layer; altering the morphology of the lead sulphate; initiating the solid phase reaction between the Pb and SO_4^{2-} or HSO_4^- anions under the influence of anodic potential; and the formation of Pb^{2+} soluble intermediates.

The cation of ligno-sulphonate salt additives retards the hydrogen evolution potential as well as the solid phase reaction [Mahato, 1977]. It is also responsible for reducing the oxygen evolution reaction.

The high efficiency of electro-deposition of lead during charge, due to the high hydrogen overpotential on lead, causes the deposited lead particles to coalesce and form a low surface area

layer. Therefore, the conversion of lead sulphate particles to metallic lead would be incomplete and inefficient. The role of expander in this case is to adsorb on the lead sulphate particles as well as on lead deposited sites influencing the overall electroreduction kinetics [Hoffmann, 1984; Simon, 1974; Iliev, 1985]. The former mechanism controls the dissolution of $PbSO_4$, inhibits the complete sheathing of the lead sulphate particles by electrodeposited lead, and helps the overall electroconversion efficiency. The latter mechanism, by blocking coverage of the activation sites, prevents sintering of the freshly electrodeposited lead masses [Mahato, 1980; Pavlov, 1987] and helps to maintain or increase the surface area of the electrode after the charging operation [Mahato, 1980]. Mahato [Mahato, 1977] has also noted that the presence of expander in the pasted electrode increases the specific surface area from ca. 0.23 m^2/gr to 0.50 m^2/g which was confirmed by the BET measurements done by Ekdung et al. [Ekdung, 1987]. It was also found [Szava, 1989] that the presence of expander hinders the agglomeration of the active mass during pasting and cycling.

According to microscopy studies by Simon et al. [Pavlov, 1987], lignin suppresses the growth of dendritic lead and forms small lead crystals resulting in a larger active surface area and therefore increased capacity.

The effect of expander concentration has been investigated by some authors [Mahato, 1980, 1981; Szava, 1988; Hoffmann, 1984]. Based on these studies an optimum expander concentration of around

10 PPM [Mahato, 1980; Hoffmann, 1984] has been established at which the desired influences are maximized. At concentrations exceeding this optimum value, the effect of expander is reversed. This reverse effect at higher concentrations is explained by blockage of the active surface area and restriction of the dissolution rate of lead sulphate precipitate by the expander itself [Mahato, 1980; Hoffmann, 1984]. The research group in the Farrington Lockwood Co. Ltd. [FLCL, 1989] studied the correlation between the physical and chemical properties of various ligno-sulphonate salts and their functioning at lead electrolyte interface. Using UV absorption technique, they monitored the changes in the concentration of expanders in aqueous electrolyte with different pH's, as a function of their rate of precipitation. Among the favourable expander properties they suggest are: (i) low sugar contents in sodium salt expanders; (ii) high degree of precipitation in 1.28 s.g. H_2SO_4; and (iii) expanders which require small amount of lead nitrate for precipitation.

1.7- OBJECTIVES

The major requirement of lead-acid storage batteries used in remote photovoltaic hybrid systems is low maintenance. That is because visits must be kept to the minimum level possible.

This requires continuous and accurate control of both the battery's charge/discharge regime and state-of-charge, with respect to the temperature of the battery.

To achieve this goal, a detailed knowledge of the battery behaviour is required, including hydrogen evolution potential, and temperature dependency of battery performance which is especially important in northern Canadian applications.

Although lead-acid batteries are more than 150 years old and much research and development has been conducted to develop their science and technology, there still is a significant potential for improvement and numerous gaps to be filled in understanding their performance.

The effects of different alloys on mechanical and physical properties of the negative electrode plates have been investigated and reasonably well established. However, our knowledge of the influence of these alloys on the electrochemistry of the plates is not yet satisfactory. Some of the remaining questions are the number of electrons transferred in the electrochemical reaction, the ion transport mechanism, and the electrochemical behaviour when the battery undergoes overcharge.

In addition, information about the effect of expanders is limited to their effects on pure lead electrodes, while photovoltaic lead-acid battery anodes are mostly made with calcium or antimonial alloys, and there is little information concerning their behaviour in the presence of expanders. The majority of researchers dealing with the effect of expanders have concentrated their efforts on the normal operation of the battery excluding overcharge conditions.

The effect of temperature is another major factor to be

considered in battery design especially for applications in the cold arctic and subarctic conditions prevailing in Northern Canada.

Therefore the objectives of this research was to study the following subjects:

1- The influence of alloying elements, based on a pure lead standard, including binary alloys of lead-calcium and lead-antimony, and ternary alloys of lead-calcium-tin and lead-antimony-selenium, on anode parameters such as number of electrons transferred in the electrochemical reaction, ion transport mechanisms, and hydrogen overpotential.

2- The effect of ammonium ligno-sulphonate (ALS) as an expander on fresh and aged lead anodes (pure lead, lead-antimony, and lead-calcium). Study of changes in peak anodic potential, peak anodic current, and hydrogen overpotential under overcharge conditions.

3- The comparison of cold (0°C) and room (23°C) temperatures performance of the lead alloy anodes with respect to the differences in their peak anodic potential, peak anodic current, and hydrogen evolution potential. Investigation of the desired and/or non-desired influences of ALS in cold temperatures.

4- To study the mechanism of lead sulphate film growth on the lead and lead alloys, the size and the shape of crystals, and the effects of alloying materials and expanders.

The first three objectives were studied using the cyclic voltammetry technique while the last one took advantage of the potentiostatic transient technique and was confirmed by scanning

electron microscopy and X-ray diffraction.

The results from this research were presented at three conferences [Tabe Mohammadi, 1990a, b, c]. For the abstracts of these presentations see Appendix II.

CHAPTER TWO: THEORY

An electrochemical reaction can be simplified as:

$$O+ne^- \leftrightarrows R \qquad (2.1)$$

where O and R represent the oxidant and the reductant respectively. Five separate steps can be considered in the conversion of O to R:

(1)- Transport of O from the bulk solution to the interface.

(2)- Adsorption of O onto the surface.

(3)- Charge transfer at the electrode to form R.

(4)- Desorption of R from the surface.

(5)- Transport of R from the surface to the bulk solution.

The rate of the reaction and the resulting current, is determined by the rate of the overall sequence, and is dependent on the slowest step. Thus, to understand the characteristics of such an electrode reaction, both mass transport and the electron transfer process must be known. If it is assumed that mass transport into and out of the interface occurs only by diffusion, then the rates of steps 1 and 5 depend upon the concentration gradient at the interface in accordance with Fick's law.

$$\frac{-i}{nFA}=J_O=-D_O\left(\frac{\partial C_O}{\partial x}\right)_{x=0} \qquad (2.2)$$

$$\frac{i}{nFA} = J_R = -D_R\left(\frac{\partial C_R}{\partial x}\right)_{x=0} \qquad (2.3)$$

where J is flux (mol sec^{-1} m^{-2}) normal to the surface, A is the area of the surface (m^2), and D the diffusion coefficient (m^2 sec^{-1}). The mathematical solution of the above equations lead to the exact form of the i-t transient, i.e.:

$$i = -\frac{nFD^{1/2}C_o^{\infty}}{\pi^{1/2}t^{1/2}} \qquad (2.4)$$

The graphical representation of the above equations are shown in Figure 2.1 [Southampton group, 1985]. With reference to equations 2.2 to 2.4 and Figure 2.1, it is clear that the rates of steps 1 and 5, and hence the total current, decrease with time.

The objective of the transient techniques in electrochemistry is to develop theoretical expressions relating rate (current) to time in order that the effect of diffusion can be removed by extrapolation. These expressions may involve some time dependent parameters such as potential scan rate in cyclic voltammetry techniques (Section 2.1), or time directly as in the potentiostatic transient techniques (Section 2.2). The perturbations and the responses in these two techniques are illustrated in Table 2.1 [Mcdonald, 1977].

2.1- CYCLIC VOLTAMMETRY TECHNIQUES

The variation of current with potential is a useful tool to

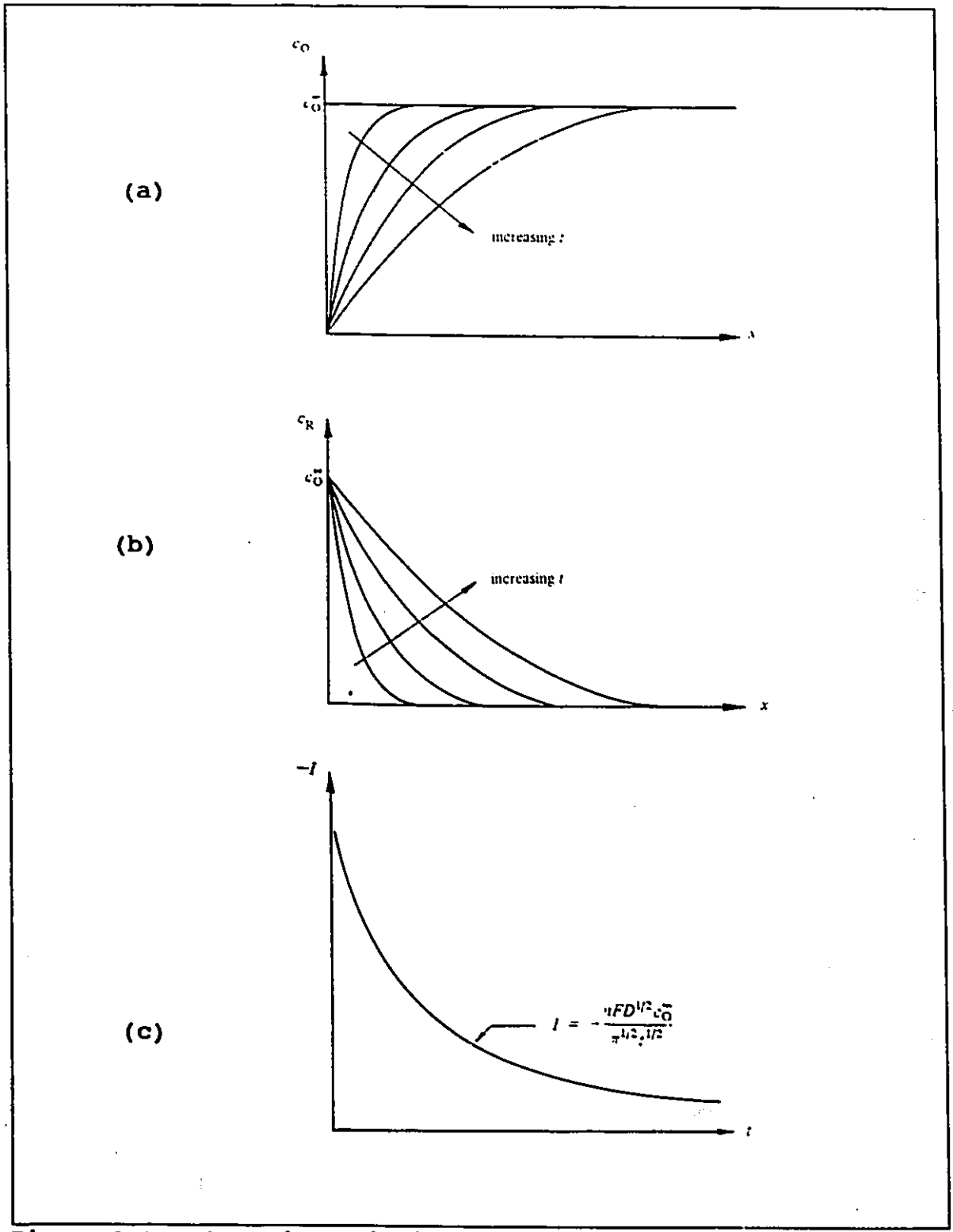

Figure 2.1: Schematic variation of the oxidant concentration (a), reductant concentration (b), and the total current (c), with time under potentiostatic control [Southampton group, 1985].

TABLE 2.1

Two potential perturbation techniques commonly used in electrochemistry: potential step (potentiostatic transient method), and cyclic voltammetry.

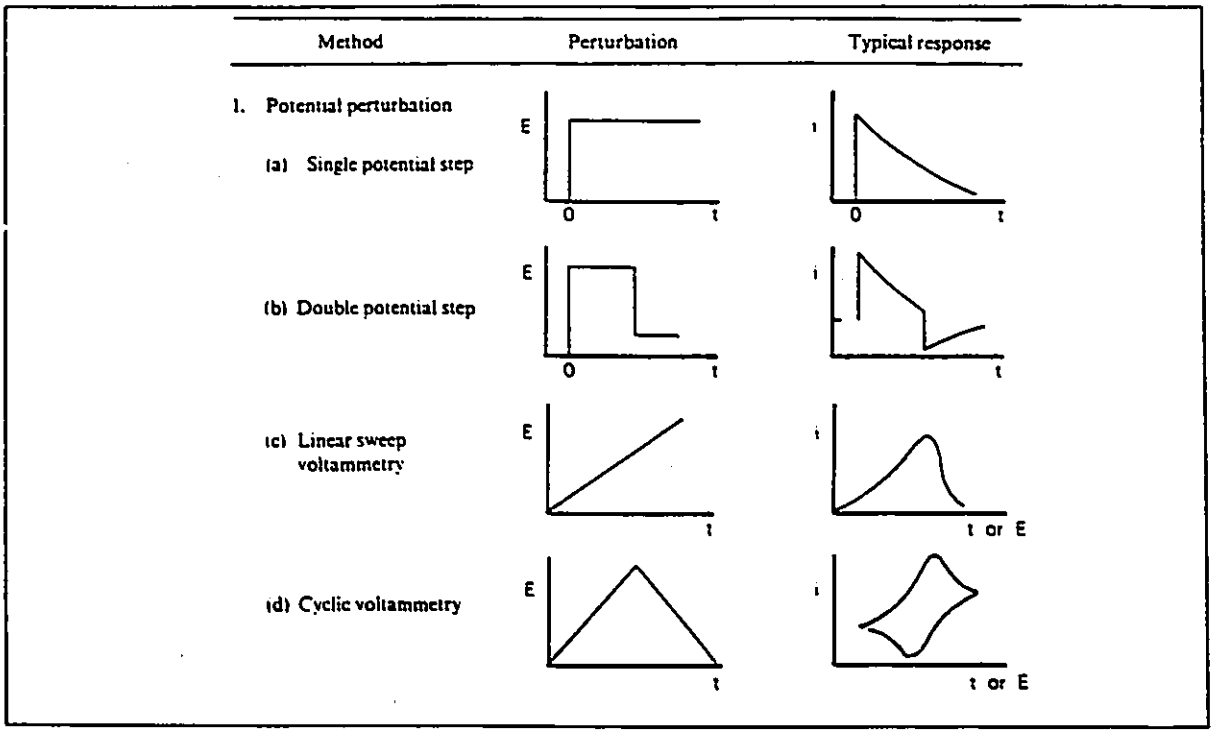

understand the electrochemistry of a particular reaction. These variations can be monitored using "potential sweep techniques", among them the most commonly used is the "cyclic voltammetry technique". In this technique, the electrode potential is scanned between limits E_1 and E_2 at a known scan rate, v. The current is recorded (using an X-Y recorder or a microcomputer) as a function of potential. At a certain potential where the electrochemical reaction occurs, the current rises. After the potential reaches E_2 value, the scan is reversed to reach the initial potential E_1. Figure 2.2 illustrates a typical i-E curve for anodic oxidation reaction of a lead electrode. In this figure, the anodic current is

taken to be positive. The peak indicates the occurrence of the electrochemical reaction. The product of the oxidation reaction is lead sulphate which covers the surface as the reaction proceeds and slows down and eventually stops the reaction. Therefore, current passes through a maximum and approaches zero when the whole surface is covered by lead sulphate. In the reverse scan (cathodic direction), the lead sulphate particles are reduced causing a cathodic current. The process of the cyclic voltammetry simulates an overall charge/discharge cycle in a battery.

The maximum anodic current is called the peak anodic current (PAC) and is shown by i_p. The corresponding potential is called the peak anodic potential (PAP) and is shown by E_p. Similar current and potential at the cathodic side are called peak cathodic current (PCC), and peak cathodic potential (PCP). In a voltammogram, the PAP (and PCP) represents the potential at which an electrochemical reaction occurs, and PAC (or PCC) represents the rate (kinetics) of the reaction.

2.1.1- TRANSPORT MECHANISM

The cyclic voltammetry techniques can be used to understand the transport mechanism in the vicinity of the electrode.

The mathematical form of the cyclic voltammogram can be obtained starting from Fick's 2nd Law of diffusion for O and R:

$$\frac{\partial c_o}{\partial t} = D_o \frac{\partial^2 c_o}{\partial x^2} \qquad (2.5)$$

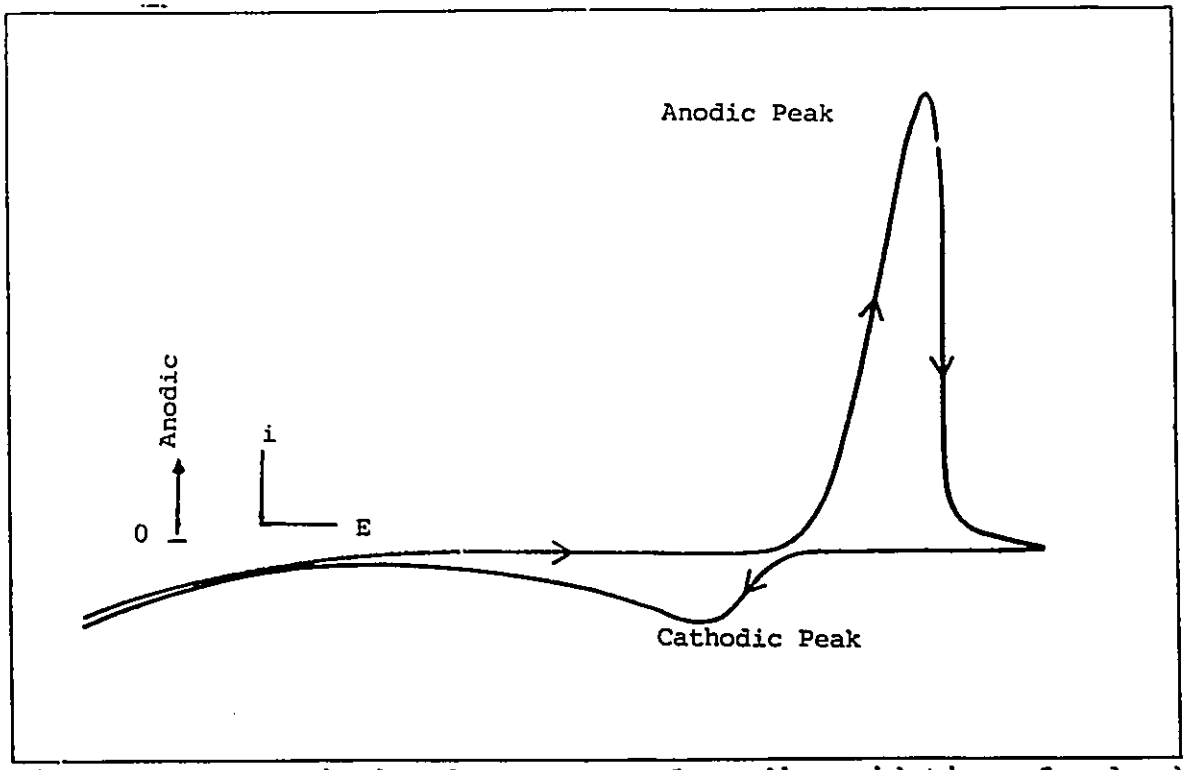

Figure 2.2: A typical voltammogram of anodic oxidation of a lead electrode.

$$\frac{\partial c_R}{\partial t} = D_R \frac{\partial^2 c_R}{\partial x^2} \qquad (2.6)$$

Under diffusion control, with only O initially present in solution and assuming $D_O = D_R = D$ under the equilibrium conditions, the initial and the boundary conditions are:

$t = 0,\ x>0,\ c_O = c_O^*$ and $c_R = 0$

$$t>0,\ x=0,\ D\left(\frac{\partial c_O}{\partial x}\right) + D\left(\frac{\partial c_R}{\partial x}\right) = 0$$

$$\left(\frac{c_O}{c_R}\right)_{x=0} = \exp\left[\frac{nF}{RT}(E - E_e^0)\right]$$

$$-i = nFD\left(\frac{\partial c_o}{\partial x}\right)_{x=0}$$

Where E^0 is the standard potential, and c_0^* is the bulk concentration in mol/cm^3. For a scan rate of ν

$0 < t < \lambda \qquad E = E_1 - \nu t$

$t > \lambda \qquad E = E_1 - 2\lambda\nu + \nu t$

where E_1 is the initial potential and λ the time at which the sweep is reversed. The solution for planar diffusic. (with F=96500 C, R=8.31 J/mol °C, and T=298 °K) is [Southampton Group, 1985]:

$$i_p = -0.4463nF\left(\frac{nF}{RT}\right)^{1/2} c_o^* D^{1/2}\nu^{1/2} \qquad (2.7)$$

This equation is called the Randles-Sevčic equation, and can be applied to reversible, irreversible, and quasi-reversible reactions. At room temperature the equation reduces to the form:

$$i_p = -(2.69\times10^5)\, n^{3/2} c_o^* D^{1/2}\nu^{1/2} \qquad (2.8)$$

In this equation, all variables except ν are independent of the time. Therefore, the equation can be written as:

$$\log(i) = (const.) + \frac{1}{2}\log(\nu) \qquad (2.9)$$

Therefore, based on the assumption of a diffusion controlled mass transport, the slope of log (i) vs. log (scan rate) is 0.5. This is a diagnosis for determining whether or not a reaction is diffusion controlled.

2.1.2- NUMBER OF ELECTRONS TRANSFERRED

One of the marked features of a reversible electrochemical reaction is that the peak anodic and cathodic potentials are independent of the scan rate [Southampton Group, 1985]. In the irreversible and quasi-reversible reactions, however, this is not the case. In the quasi-reversible reactions (e.g., anodic oxidation of lead), the peak potentials vary with the scan rate according to the following equation:

$$E_p = K - \frac{2.3RT}{2\alpha nF}\log v \qquad (2.10)$$

where

$$K = E_\theta^0 - \frac{RT}{\alpha nF}\left(0.78 - \frac{2.3}{2}\log\left(\frac{\alpha nFD}{k^{0^2}RT}\right)\right)$$

where α is constant (between 0 and 1 and generally approximately 0.5) known as the transfer coefficient. Subscript $_a$ and $_c$ indicate anodic and cathodic reactions respectively. The symbol n indicates the number of electrons transferred up to, and including, the rate determining step in the electrochemical reaction. For definition of other variables look at the Nomenclature.

Substituting the values for R (8.31 J/mol °K), T (298 °K, room temperature), α (0.5) and F (96,500 C), and with E_p measured in mV (instead of V), Equation 2.8 can be approximated and simplified to:

$$E_p = (const) - \frac{59}{n}\log(v) \qquad (2.11)$$

where v is the scan rate. In other words, a plot of peak anodic potential (PAP) vs. logv has a slope equal to {59/(number of

electrons)}, or:

$$n=\frac{59}{slope} \quad \text{(for PAP vs. log } \nu\text{)} \qquad (2.12)$$

The slope of the plot of PAP vs. log ν is known as the Tafel slope. The Tafel slope and the number of electrons can also be calculated in other way independent of the scan rate. The analysis as follows [Linden, 1985]:

Equations 2.2 and 2.3 can be written as:

$$i_o=nFAk_oC_o \qquad (2.13)$$

$$i_R=nFAk_RC_R \qquad (2.14)$$

where k with subscript of O and R are the rate constants for the oxidation and reduction reactions (unit cm/s) and A is the area of the electrode (cm^2). These potential dependent rate constants are mathematically expressed as:

$$k_o=k_o^0\exp\left(\frac{-\alpha nFE}{RT}\right) \qquad (2.15)$$

$$k_R=k_R^0\exp\left(\frac{(1-\alpha)nFE}{RT}\right) \qquad (2.16)$$

Under equilibrium condition, no net current flows and

$$i_o=i_R=i_0 \qquad (2.14)$$

Therefore,

$$C_ok_o^0\exp\left(\frac{-\alpha nFE}{RT}\right)=C_Rk_R^0\exp\left(\frac{(1-\alpha)nFE}{RT}\right) \qquad (2.18)$$

or rearranging,

$$E=\frac{RT}{nF}\ln\frac{k_R^0}{k_O^0}+\frac{RT}{nF}\ln\frac{C_O}{C_R} \qquad (2.19)$$

The first term of Equation 2.19 is defined as the standard potential, E_e^0, which is taken as the reference point of the potential scale. This helps to define the standard rate constant k:

$$k_O^0=k_R^0=k \qquad (2.20)$$

Equation 2.19, then, can be written as:

$$E=E^0+\frac{RT}{nF}\ln\frac{C_O}{C_R} \qquad (2.21)$$

which is consistent with the Nernst equation.

Combining Equations 2.13, 2.15, 2.19, and 2.20, the exchange current density is calculated:

$$i_0=nFAkC_O^{(1-\alpha)}C_R^{\alpha} \qquad (2.22)$$

Calculating C_R from Equation 2.21 and substituting in 2.22 yields:

$$i=nFAkC_O\exp\left(\frac{-\alpha nF\eta}{RT}\right) \qquad (2.23)$$

where η is called overpotential and is the potential with reference to the standard potential $(E - E^0)$. Now when $\eta = 0$, $i = i_0$, then

$$i=i_0\exp\left(\frac{-\alpha nF\eta}{RT}\right) \qquad (2.24)$$

and

$$\eta = \frac{RT}{\alpha nF} \ln i_0 - \frac{RT}{\alpha nF} \ln i \qquad (2.25)$$

This is called the Tafel equation. Substituting values for R (8.31 J/mol °K), T (298 °K, room temperature), α (0.5), and F (96,500 C), and converting (ln) to (log), the number of electrons transferred in each reaction (oxidation or reduction) can be calculated. With the potential measured in mV, Equation 2.25 is simplified as:

$$\eta = (const.) - \left(\frac{59}{n}\right) \log i \qquad (2.26)$$

Therefore, if the over potential, η, is plotted against log (i), the slope, (Tafel slope), leads to the calculation of the number of electrons transferred in the electrochemical reaction:

$$n = \frac{59}{slope} \qquad (2.27)$$

2.2- POTENTIOSTATIC TRANSIENT (CHRONOAMPEROMETRY)

In this technique, the electrode undergoes a sudden change in the potential. Two kinds of responses are frequently monitored: (a) the current as a function of time (chronoamperometry), and (b) the charge as a function of time (chronocoulometry). The two methods yield essentially the same information. If the chronoamperometry response of a system to a potential perturbation is i(t), then the chronocoulometry response is:

$$Q(t) = \int_0^t i(t)\,dt \qquad (2.28)$$

An application of this technique, which is of importance to this study, is to investigate the electrode surface processes, including electrocrystallization. The theoretical analysis of surface processes under potentiostatic transient is greatly simplified by the fact that the electrochemical rate "constants" are in fact constant for t>0. Therefore, the only time-dependent quantities in the differential equations that will be constructed to describe the relaxation processes are surface coverage by intermediates, film thicknesses, diameters of nuclei, and related parameters.

2.2.1- FILM GROWTH MODELS

For the simplest case, it is assumed that after the potential step is imposed, nuclei form at discrete centres and grow across the surface. It is also assumed that the rate of growth (current) is proportional to the area (A) onto which the deposition occurs, and that the growth area may be modified by overlap with the adjacent nuclei. Figure 2.3 [Southampton Group, 1985] simplifies the formation and overlap of crystals on the electrode surface. Then, the current can be written as:

$$i = nFKA \qquad (2.29)$$

where K is the rate constant (mol sec^{-1} m^{-2}). The current is also equal to the rate of change of accumulated charge with time on the surface. Therefore, application of Faraday's law yields [MacDonald,

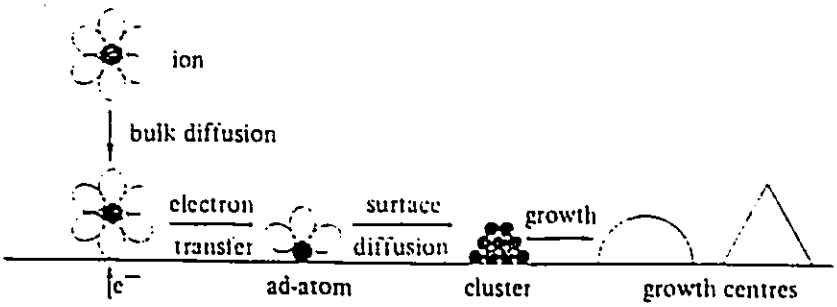

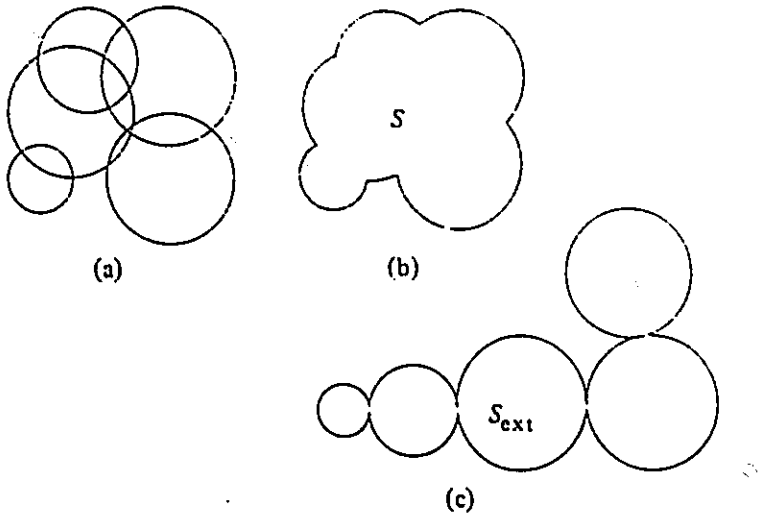

Figure 2.3: Some of the steps involved in the electrocrystallization of a metal (top), and the overlap problem (bottom). S_{ext}: extended area. The figure illustrates how the overlap of growth centres shown in (a) gives rise to the real area corresponding to (b) and the extended area shown in (c) [Southamton group, 1985].

1977]:

$$i=nF\rho\left(\frac{dV}{dt}\right)/M \tag{2.30}$$

where ρ and V are density and volume, respectively, of the deposited phase of molecular weight M. The derivative (dV/dt) may be expanded with respect to the radius r. Equating 2.29 and 2.30 then yields:

$$\left(\frac{dr}{dt}\right)=\frac{MKA}{\rho}\left(\frac{dV}{dr}\right) \tag{3.31}$$

Assuming a disk shape for the nucleus (see Figure 2.4), the corresponding area and volume are:

$$A=2\pi rh \tag{2.32}$$

$$V=\pi r^2h \tag{2.33}$$

gives

$$\frac{dr}{dt}=\frac{MK}{\rho} \tag{2.34}$$

Equation 2.34 is then integrated with respect to time to yield the time dependence of the radius of a single nucleus, i.e.,

$$r=\frac{MKt}{\rho} \tag{2.35}$$

Substitution for r in equation 2.32 followed by the insertion of A into equation 2.29 gives the current for the growth of a single centre as a function of time:

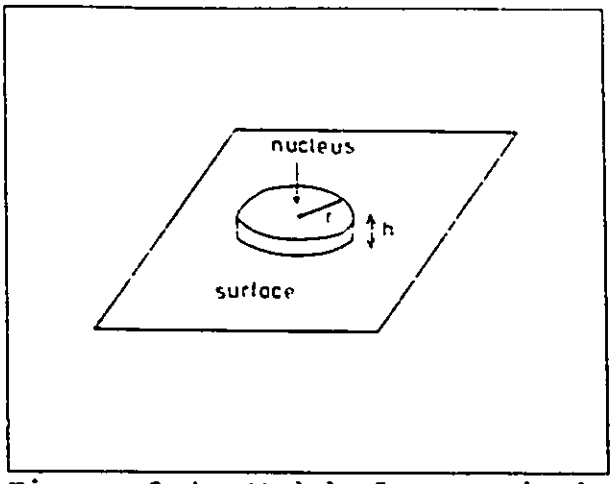

Figure 2.4: Model for a single two-dimensional disk nucleus.

$$i = \frac{2\pi n F K^2 h M t}{\rho} \qquad (2.36)$$

The latter equation considers the growth of only one nucleus. It is necessary to introduce into the model the time dependence of the nuclei population. In the simplest case (instantaneous nucleation), it is assumed that for t>0 there exists a total of N_0 nuclei, and that no new growth centres are established after perturbation is imposed. The total current is then:

$$i = \frac{2\pi n N_0 F K^2 h M t}{\rho} \qquad \text{(instantaneous nucleation)} \quad (2.37)$$

One might also suppose that nucleation and growth occur simultaneously (progressive nucleation), i.e., the population of the nuclei is time dependent. Thirsk and Harrison [Thirsk, 1972] argue that the number of the new growth centres should increase exponentially with time in a manner given by:

$$N=N_0(1-e^{-Zt}) \tag{2.38}$$

where Z is a constant. The rate of change of N is obtained by differentiation of the latter equation. If the analysis is restricted to short times such that $N<<N_0$, then the differential dN/dt is given by:

$$dN/dt=N_0Z \tag{2.39}$$

Since the nucleation and growth occur simultaneously, then the total current at time t after the start of the deposition can be written as:

$$i=\int_0^t i(u)\,(dn/dt)_{t-u}du \tag{2.40}$$

where u is the age of a nucleus for which the local current is i(u). Substitution of equations 2.36 and 2.39 into equation 2.40 yields the total current due to simultaneous nucleation and growth:

$$i=\frac{n\pi FK^2hMN_0Zt^2}{\rho} \qquad \text{(progressive nucleation)} \tag{2.41}$$

To take into account the effect of overlapping, Macdonald [Macdonald, 1977] introduces exponential terms to equations 2.38 and 2.41:

$$i=\left(\frac{2nF\pi MN_0K^2ht}{\rho}\right)\exp(-\pi M^2N_0k^2t^2/\rho^2) \qquad \text{(instantaneous)} \tag{2.42}$$

$$i=\left(\frac{nF\pi MN_0ZK^2ht^2}{\rho}\right)\exp(-\pi M^2N_0Zk^2t^3/3\rho^2) \qquad \text{(progressive)} \tag{2.43}$$

The analysis given above for instantaneous and progressive

nucleation and growth of the two-dimensional phases is easily extended to other geometries for the growth centres by the use of the appropriate expressions for area and volume. For instance, for the hemispherical growth centres area and volume are:

$$A=2\pi r^2 \tag{2.44}$$

$$V=2\pi r^3/3 \tag{2.45}$$

Substitution of these equations into equation 2.31 and following the same procedure, as before results in the following two equations:

$$i=\frac{2\pi nFK^3N_0M^2t^2}{\rho^2} \qquad \textbf{(instantaneous)} \tag{2.46}$$

$$i=\frac{2\pi nFK^3ZN_0M^2t^3}{\rho^2} \qquad \textbf{(progressive)} \tag{2.47}$$

The effect of overlap on transients for three-dimensional growth (right circular cone) has been considered by Armstrong et al. [Armstrong, 1966]. The following expression as a function of time was obtained:

$$i=nFk_2\left[1-\exp\left(\frac{-\pi M^2k_1^2N_0Zt^3}{3}\rho^2\right)\right] \tag{2.48}$$

where k_1 and k_2 are the rate constants for growth parallel and perpendicular to the plane, respectively. This expression predicts a transient of the form shown in Figure 2.5. Note that at long times the current becomes constant rather than approaching zero as

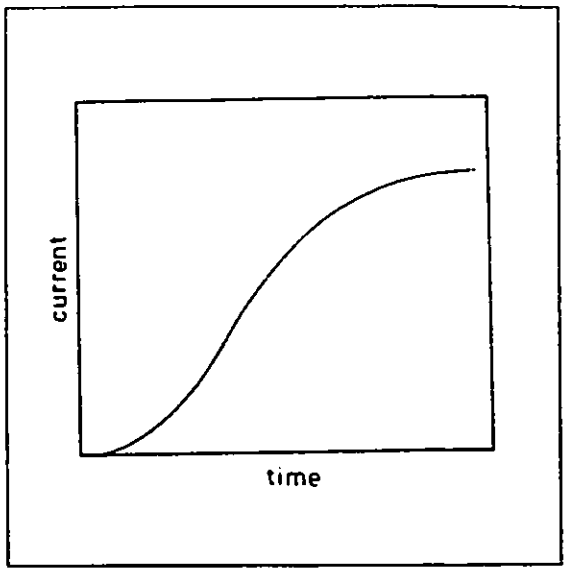

Figure 2.5: Potentiostatic transient for 3-D nucleation and growth including the effect of overlap.

predicted for the two-dimensional case.

In equations 2.37, 2.41, 2.42, 2.43, 2.46, 2.47, and 2.48, all parameters are constant with respect to time. Therefore, the experimental summary shown in Table 2.2 can help to predict the growth mechanism on the electrode surface.

TABLE 2.2

Summary of approaches for interpretation of experimental data from potentiostatic transient experiments.

TYPE OF CURVE	REQUIREMENTS	INTERPRETATION
i vs. t	approaching zero	2-Dimensional grow
	approach. non-zero constant	3-Dimensional grow
log(i) vs. log (t)	slope = 1	2D inst. disk
	slope = 2	2D prog. disk
		2D inst. hemisphere
	slope = 3	2D prog. hemisphere
ln (i/t) vs. t^2	linear	2D inst. overlap
ln (i/t^2) vs. t^3	linear	2D prog. overlap

CHAPTER THREE: EXPERIMENTAL

3.1- LIST OF EXPERIMENTS

In order to meet the objectives of this study, the following experiments were performed on the anode:

1- The effect of alloying materials.

2- a) The effect of aging (cycling).

   b) Comparison of the anode operational parameters in fresh and aged (cycled) electrodes.

3- The expander's concentration effect (ammonium ligno-sulphonate (ALS) in electrolyte).

4- Potentiostatic transient experiments in presence and absence of ALS.

5- Effect of ALS on the anode operational parameters (room temp.).

6- Effect of ALS on the anode operational parameters (at 0°C).

7- a) Scanning Electron Microscopy (SEM), and

   b) X-ray Photoelectron Spectroscopy (XPS), on fresh and aged (cycled) electrodes.

The experiments 1 to 3, 5 and 6 were performed using cyclic voltammetry techniques. The variables recorded were the peak anodic potential (PAP), the peak anodic current (PAC), and the hydrogen evolution potential (HEP). The potentiostatic transient technique was employed in experiment 4. The theoretical treatments of both these techniques are provided in Chapter two.

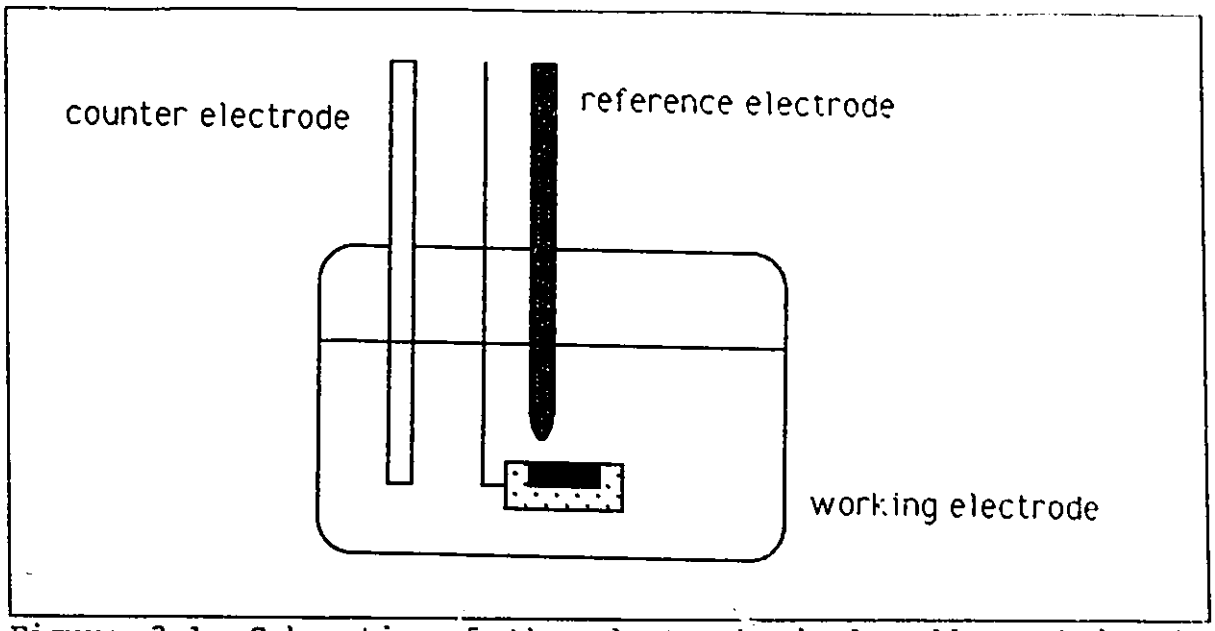

Figure 3.1: Schematic of the electrochemical cell used in the experiments.

3.2-APPARATUS

The electrochemical cell consisted of a working electrode (the electrode under study, i.e., lead and lead alloys), a counter electrode made of pure lead, and a reference electrode (Calomel Saturated Electrode) to measure the potential of the working electrode independent of the counter electrode. A 30% (by volume) solution of sulphuric acid (98% pure) in distilled water was used as electrolyte (see figure 3.1).

The electrochemical cell was connected to an EG&G potentiostat model 273 through an interface and a Keithley voltmeter model 175. This set-up was used for cyclic voltammetry and transient experiments. The cyclic voltammograms were plotted using a Honey-Well XY-recorder. The apparatus set-up for cyclic voltammetry and

transient experiments is schematically illustrated in Figure 3.2.

3.3- MATERIALS AND METHODS

The list of lead alloys that were used in these studies and their nominal compositions are shown in table 3.1.

TABLE 3.1

Lead alloy anodes used in the experiments and their compositions.

Group A: lead and binary alloys
1- Lead (99.99% Pb)
2- Lead/1.66% Antimony
3- Lead/0.09% Calcium
Group B: Ternary Calcium Alloys
4- Lead/0.09% Calcium/0.3% Tin
5- Lead/0.06% Calcium/0.3% Tin
6- Lead/0.06% Calcium/0.8% Tin
Group C: Ternary Antimonial Alloys
7- Lead/0.85% Antimony/0.03% Selenium
8- Lead/0.68% Antimony/0.015% Selenium

All the alloys in groups A, B, and C were used to study the alloying effects, whereas only those listed under group "A" were used for studying the other variables, i.e., scan rate, ALS, and temperature effects.

The cast alloys used in the present studies were provided by Cominco Metals, Mississauga, Ontario, Canada, who also provided the compositions. The electrodes having the area of 64mm^2 were cut from

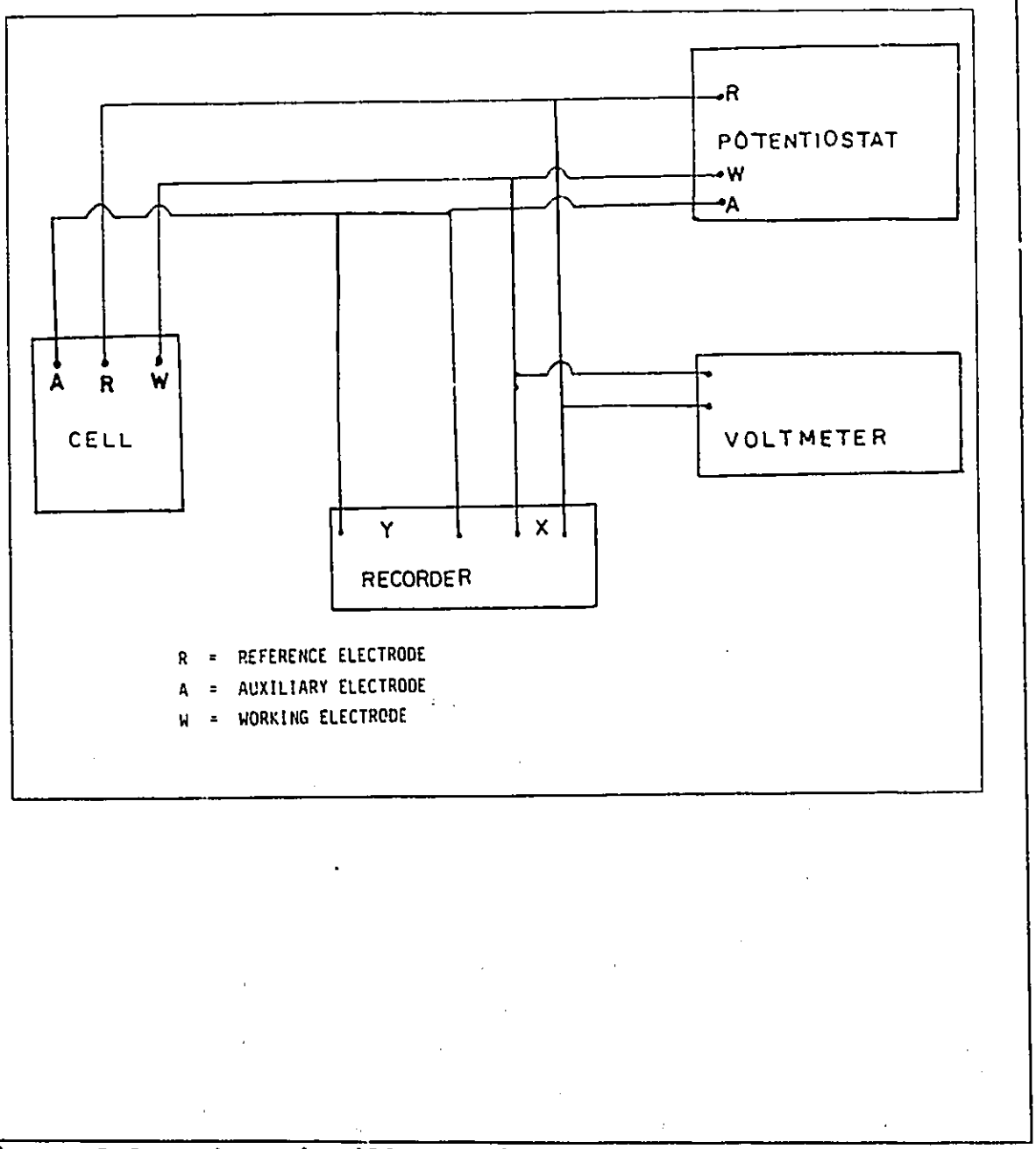

Figure 3.2: Schematic illustration of the apparatus set-up for cyclic voltammetry and transient measurements.

strips of approximately 1.5mm thickness. The electrodes #1, and 3-6 are considered the same as the most widely used non-antimonial commercial materials. The electrodes #2, 7, and 8 are experimental strip samples which could be used commercially if the production process is improved.

The electrodes were soldered to a copper wire rod, and set in hard plastic, such that only the electrodes were exposed to the electrolyte.

A powdered ammonium ligno-sulphonate (ALS) produced by Lignosol Chemicals, Quebec, Quebec, Canada, was used as the expander material. The effect of the concentration of ALS on the behaviour of the negative electrode was studied at concentrations of 0, 10, 30, and 50 PPM of ALS in the electrolyte. For the rest of experiments with ALS, a concentration of 10 PPM was used.

All the experiments were performed at room temperature (23-24°C) some low temperature experiments were also conducted at 0°C.

Cyclic voltammograms were obtained in the potential range of -1300 mV to -350 mV (vs. the Calomel electrode), with sweep rates of 10, 30, 50, 70, 100, 150, and 200 mV/s.

For the transient experiments, the electrodes were kept at a potential of -1300 mV for 15 seconds in order to attain pseudo-steady-state conditions. The potential was then jumped to the peak anodic potential for each electrode. Data were recorded every 0.5 - 1 ms by a computer.

Surface analyses were performed using Scanning Electron Microscopic and X-ray Photoelectron Spectroscopic techniques. Fresh

and aged electrodes, after 5 and 1000 cycles respectively, without and with ALS were chosen for these studies.

3.4- PRETREATMENT

The pretreatment of the electrodes had three stages. First, the electrodes were polished using hard, medium, and soft polishing papers (120, 240, and 400 grit respectively), and washed with distilled water. The electrodes were then etched in diluted nitric acid (50% by volume) for 1-2 seconds in order to remove oxide film and relive polishing cold work, and washed again with distilled water. Finally they were conditioned under hydrogen evolution potential (-1300 mV) for 30 to reduce air formed oxide films.

For surface analyses, the electrodes were washed with distilled water and acetone after electrochemical conditioning, dried, and kept in a vacuum desiccator before undergoing the experiments.

CHAPTER FOUR: RESULTS AND DISCUSSION

In previous chapters, the needs for investigating near and long term electrochemical behaviour of lead alloy anodes used in photovoltaic lead-acid batteries were established (Chapter one), the theory underlying the use of some important electrochemical techniques such as cyclic voltammetry and potentiostatic transient were highlighted, (Chapter two), and a selection of a series of experiments together with the experimental procedures were described, (Chapter three). In this chapter, a description of the experimental results together with a discussion of the observed trends, will be presented. In the sections described below, the following aspects will be dealt with:

4.1- Description of cyclic voltammogram for a lead alloy anode.

4.2- Effect of alloying.

4.3- Effect of aging.

4.4- Effect of expander, i.e., ammonium ligno-sulphonate, ALS.

4.5- Effect of temperature.

4.6- Transient electrochemistry.

4.7- Surface analyses.

4.1- DESCRIPTION OF CYCLIC VOLTAMMOGRAM FOR A LEAD ALLOY ANODE.

A typical cyclic voltammogram (CV) for a polished, nitric acid etched lead anode immersed in an un-stirred 30% sulphuric acid

solution at room temperature, (23°C ± 1), is shown in Figure 4.1. This electrode was cycled between -1300 and -350mV (vs. a saturated calomel reference electrode, SCE, and referred to the same scale hereafter) at a scan rate of 50 mV/s. In this cyclic voltammogram, the anodic component (top half of the CV) signifies the anodic dissolution during a battery discharge process. On the other hand, the cathodic component (bottom of the CV), signifies the charging process, i.e., the reduction of the anodic products, and hydrogen evolution. In the anodic part, it can be seen that a peak occurs around -450 mV corresponding to the maximum anodic dissolution rate as evidenced by a sharp rise in current, subsequently followed by a sharp decline in the current, signifying a passivation process. The peak anodic potential is designated as the PAP, and the corresponding current density as the PAC. In the cathodic branch, the peak cathodic potential for product reduction is designated as the PCP, and the corresponding current density as the PCC. In the cathodic peak, the reduction rate is a maximum. Following this, there is an inflection in the cathodic current curve. The inflection point corresponds to an onset of the hydrogen evolution process. The potential corresponding to the point of inflection is designated as the HEP.

Qualitatively, it can be seen from the areas under the PAP and PCP of this CV, that the ratio of the anodic to the cathodic charge, a symptom of reversibility, is less than 1.

In the subsequent sections, the changes in i) peak anodic potential and current and ii) hydrogen evolution potential

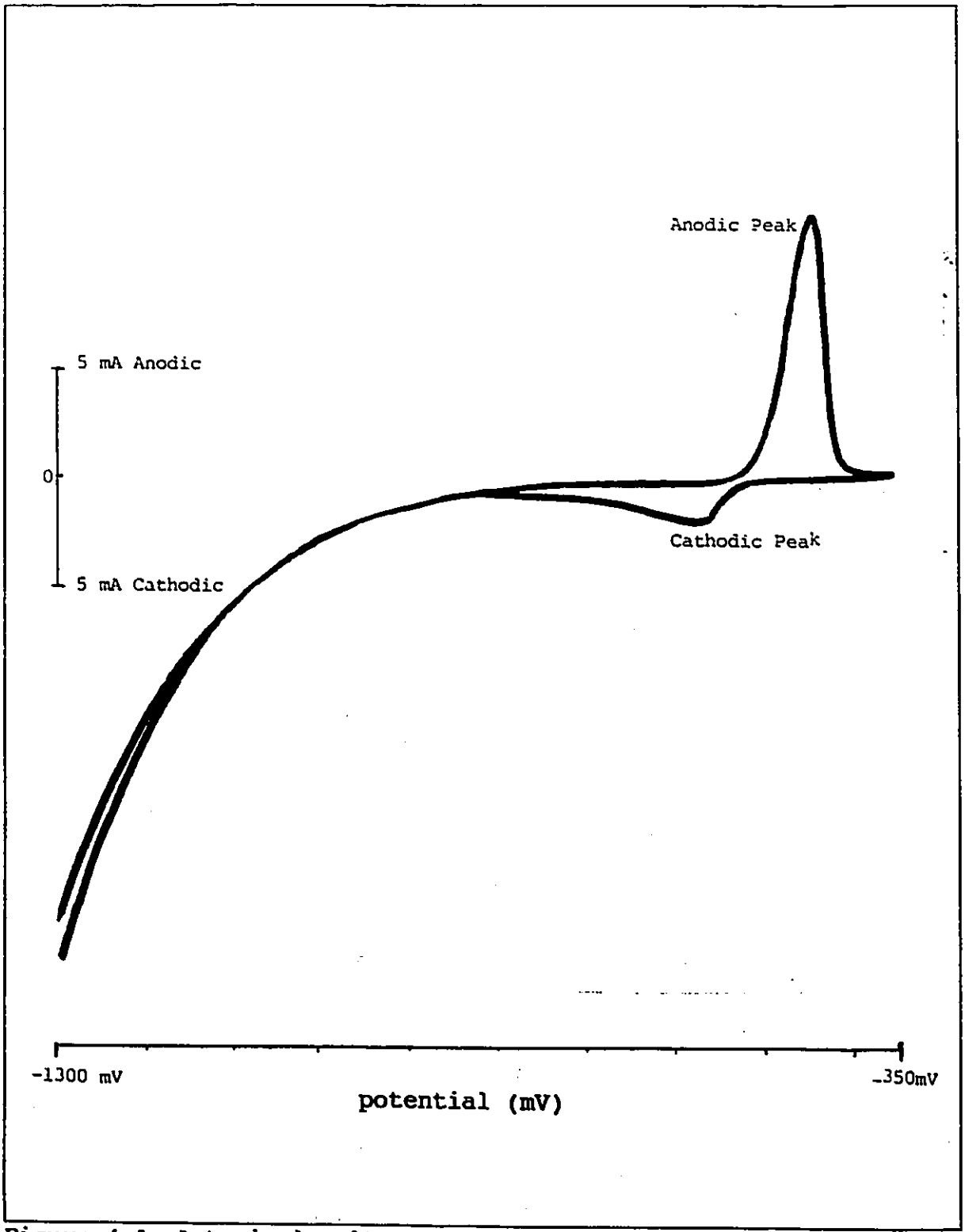

Figure 4.1: A typical voltammogram for a lead anode immersed in an un-stirred 30% sulphuric acid solution at room temperature (23°C ± 1).

hereafter referred to as PAP, PAC, and HEP were followed as a function of: i) alloying elements; ii) scan rate at 10, 30, 50, 70, 100, and 200 mV/s; iii) aging as simulated by continuous cycling; iv) expander, i.e., battery electrode or electrolyte additive; and v) temperature, i.e., 23 ± 1 °C and 0 ± 0.2 °C.

4.2- EFFECT OF ALLOYING ELEMENTS

4.2.1- GENERAL REMARKS

Conventionally, lead-antimony or its ternary alloys containing selenium for example, are used in flooded type lead-acid batteries. Lead-calcium, or its ternary alloys containing tin and strontium are used in maintenance-free lead-acid batteries. Some sealed (maintenance-free) and flooded lead-acid battery characterization work has been performed in a related part of the PV/diesel/ battery hybrid program at ESTCO [Song, 1990], in addition to the fundamental electrochemical studies on the anode behaviour presented in this work [Tabe Mohammadi, 1990a, b, c]. Therefore, CVs were obtained for the lead-calcium and lead-antimony alloys as per the list that has already been shown in Table 3.1.

The PAP, the Tafel slope, the intercept, and the number of electrons transferred are shown in Table 4.1. Table 4.2 shows the PAC, and the slope of the curve of log current vs. log scan rate for lead and lead alloys. The regression coefficients of the plots, designated as R^2, which are measure of the linearity of the plots,

TABLE 4.1

(a) Peak anodic potential (PAP), (mV), variation with scan rate in the potential range of -1300 to -350 mV for lead and lead alloys in stagnant 30% sulphuric acid at room temperature. (Precision: ±1%). Composition of the alloys are in weight% in all tables.

Scan mV/s	Pb	Pb/ .09Ca	Pb/ 1.66 Sb	Pb/ .85Sb .03Se	Pb/ .69Sb .01Se	Pb/ .06Ca .8Sn	Pb/ .06Ca .3Sn	Pb/ .09Ca .3Sn
10	-502	-535	-530	-509	-526	-529	-526	-530
30	-490	-522	-512	-492	-524	-510	-508	-511
50	-483	-515	-505	-490	-514	-500	-499	-514
70	-480	-510	-500	-488	-502	-496	-494	-503
100	-474	-510	-493	-484	-492	-490	-487	-491
200	-465	-495	-480	-457	-472	-479	-476	-485

(b) The calculated data from table (a). Slope: the Tafel slope (the slope of PAP vs. log scan rate) (unit mV); Int'pt: the intercept of the same curve; R^2: the regression factor; No. e^-: the number of electrons transferred in the electrochemical reaction.

Slope	29	29	36	47	45	36	36	36
Intpt	-533	-563	-568	-575	-581	-567	-565	-568
R^2	98.3%	99.1%	98.0%	97.9%	98.2%	98.7%	98.5%	98.1%
No.e-	2.0	2.0	1.6	1.3	1.3	1.6	1.6	1.6

are also shown in these Tables.

4.2.2- PEAK ANODIC POTENTIAL (PAP)

The plots of PAP vs. log scan rate for pure lead, lead-calcium, and lead-antimony alloys are shown in figure 4.2.

The relationships between potential, E_a, and log scan rate, v (in mV/s), are linear and are as follows:

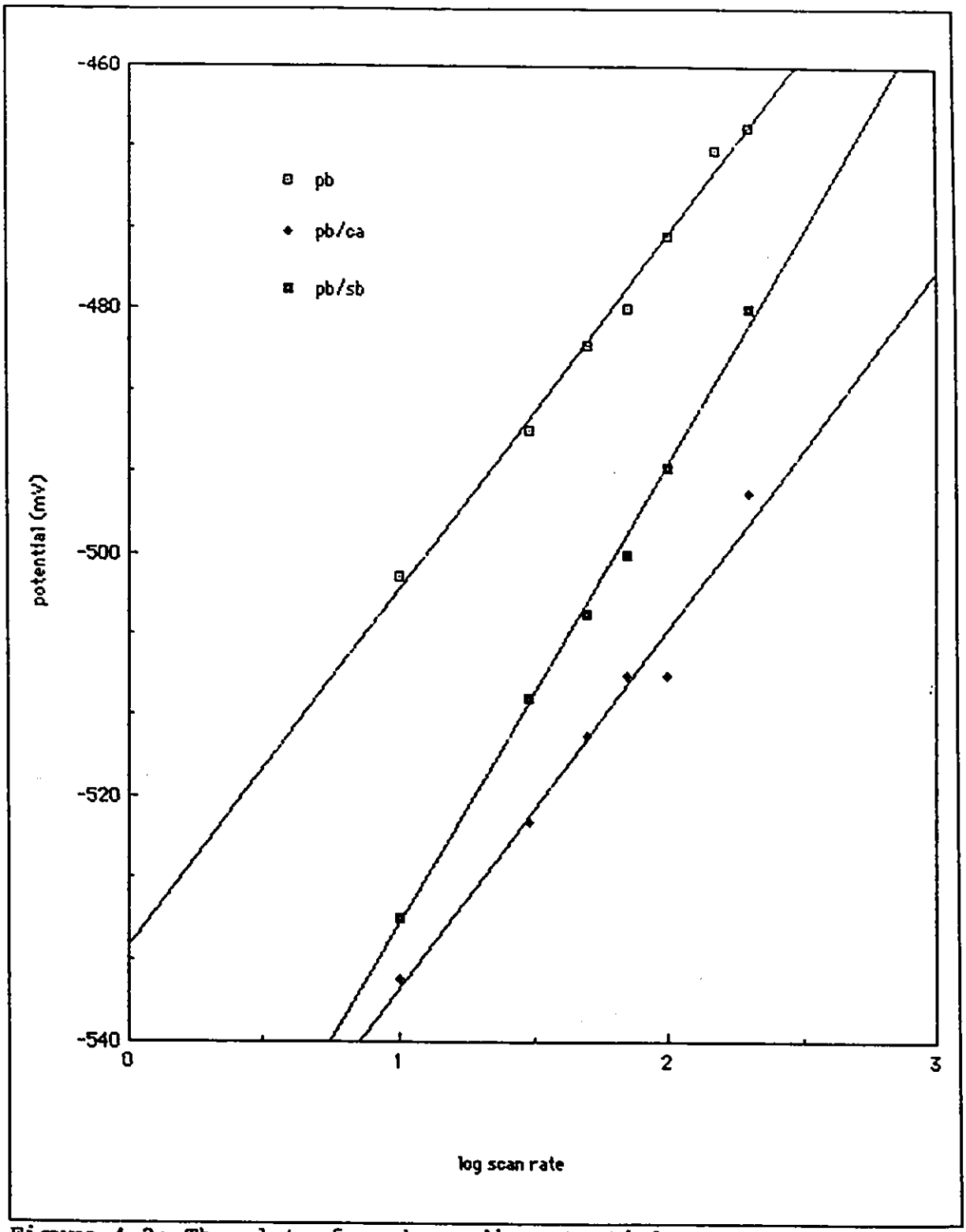

Figure 4.2: The plot of peak anodic potential (PAP) vs. log (scan rate) for lead, lead-0.09% calcium, and lead-1.66% antimony alloy anodes in stagnant 30% sulphuric acid at room temperature.

Pb: $E_a = -533 + 29 \log v$

Pb/Ca: $E_a = -563 + 29 \log v$

Pb/Sb: $E_a = -568 + 36 \log v$

Figure 4.2 and the above relationships illustrate that both alloying materials depolarize the anodic reaction but at lower peak currents than pure lead. The significance of this phenomenon will be discussed later. The slope of the curve does not change with the addition of calcium (29 mV for both lead and lead-calcium), consequently the number of electrons transferred is not influenced by the presence of calcium (2.0 for both lead and lead-calcium alloys). Antimony increases the slope from 29 to 36 mV and therefore reduces the number of electrons to 1.6.

Similar treatments were applied to ternary calcium and antimony alloys. The results for all anode alloys are shown in Table 4.1b. Addition of selenium increases the slope from 36 to 46 mV, and consequently reduces the number of electrons from 1.6 to 1.3. The same effect is observed when tin is added to lead-calcium alloy. The slope increases from 29 to 36 mV when tin is added, the resulting decrease in the number of electrons is from 2.0 to 1.6.

The slope of both the binary lead-antimony and the ternary lead-calcium-tin alloys is equal to 36 mV. The intercepts of these two curves are also slightly decreased such that the curves approach that of lead-antimony. These observations suggest that tin and calcium together provide the same electrochemical effects as does antimony alone.

TABLE 4.2

(a) Peak anodic current (PAC) density, (mA/cm^2), variation with scan rate for lead and lead alloys in stagnant 30% sulphuric acid at room temperature. (Precision: ±4%)

Scan mV/s	Pb	Pb/ .09Ca	Pb/ 1.66 Sb	Pb/ .85Sb .03Se	Pb/ .69Sb .01Se	Pb/ .06Ca .8Sn	Pb/ .06Ca .3Sn	Pb/ .09Ca .3Sn
10	4.4	3.4	3.4	4.9	5.0	4.1	6.1	3.8
30	8.7	4.7	6.1	10.4	9.2	8.3	12.0	8.0
50	11.5	8.1	7.6	12.2	11.2	10.2	12.7	10.2
70	15.0	9.6	11.0	14.4	12.5	13.4	12.5	12.4
100	16.5	10.9	11.5	19.5	15.6	13.3	15.8	17.0
200	29.4	18.2	22.5	28.4	24.5	21.6	24.0	25.6

(b) The calculated data from table (a). Slope: the slope of log PAC vs. log scan rate. R^2: regression coefficient of the plots.

Slope	0.63	0.58	0.61	0.56	0.49	0.42	0.53	0.63
R^2	97.0%	96.9%	96.4%	96.8%	96.1%	97.5%	96.3%	96.9%

4.2.3- PEAK ANODIC CURRENT (PAC)

Table 4.2a shows the current densities for lead and lead alloys. The addition of calcium or antimony reduces the anodic current density, this can be seen in Figure 4.3.

Figures 4.4a and b illustrate the effect of the addition of the third alloying element on the PAC. The current density is significantly improved and approaches that of pure lead with the introduction of the third alloying element. Increase in current density was found to be proportional to the amount of tin and selenium in lead-calcium and lead-antimony alloys respectively.

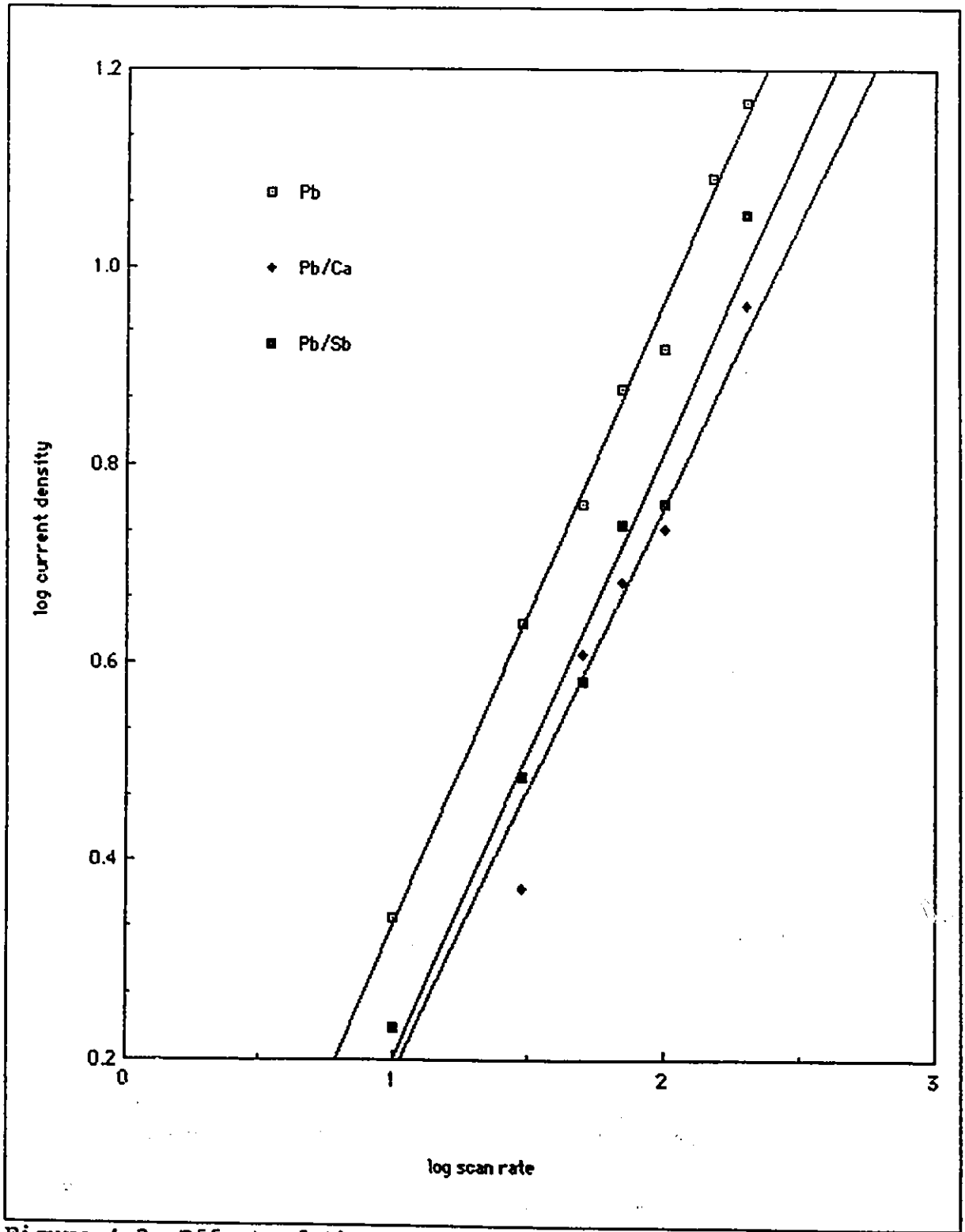

Figure 4.3: Effect of the presence of calcium and antimony in the binary lead alloys on the reduction of anodic current in stagnant 30% sulphuric acid solution at room temperature.

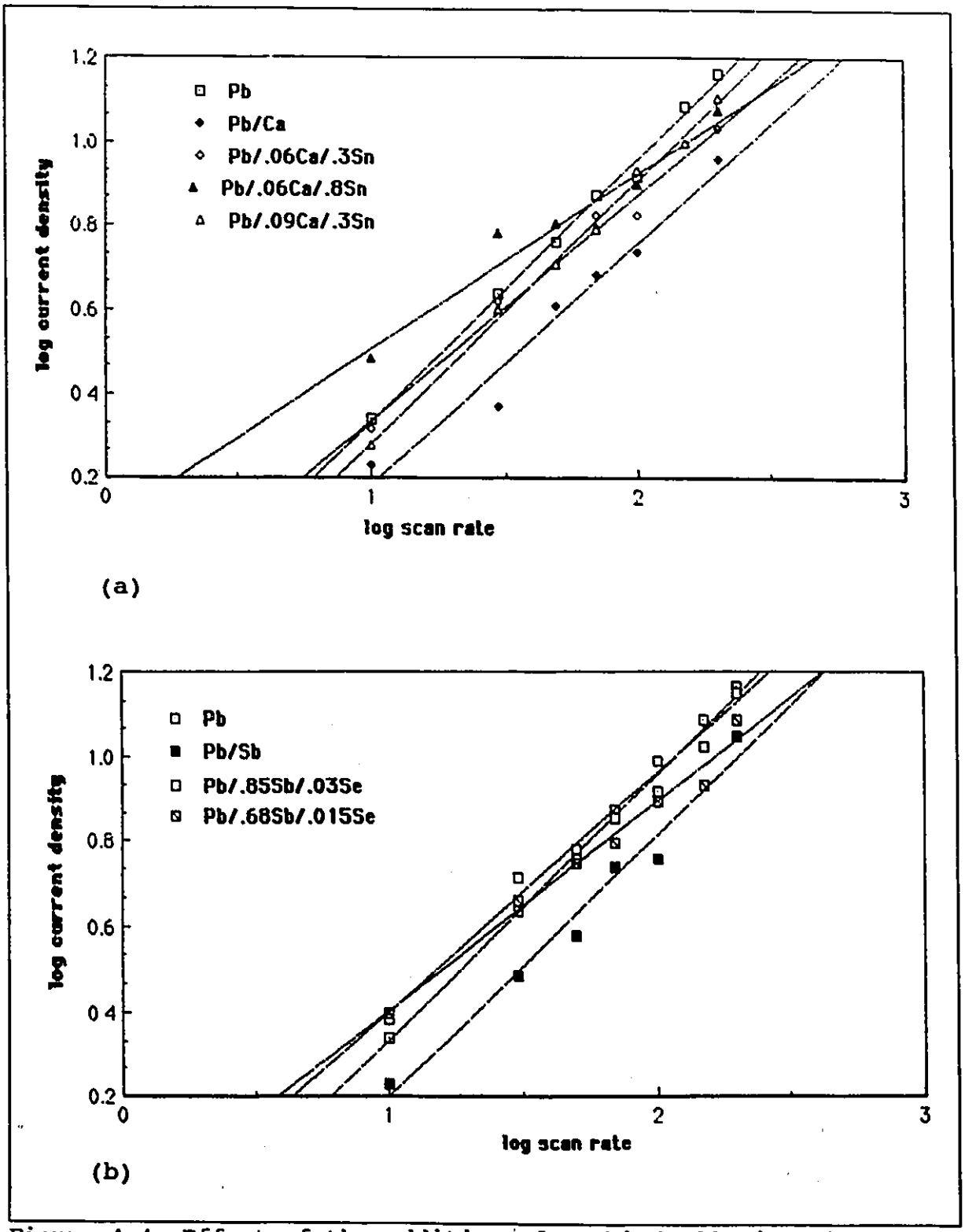

Figure 4.4: Effect of the addition of a third alloying element on the magnitude of peak anodic current. (a) Calcium alloys, (b) antimony alloys, in stagnant 30% sulphuric acid at room temp.

From the plots of log (current) vs. log (scan rate) shown in Figures 4.3 and 4.4, the slopes can be calculated. The values are shown in Table 4.2b. These slopes are all nearly equal or close to 0.5 which suggest a diffusion controlled transport mechanism.

It is important to note that the number of electrons transferred as a function of alloying composition is estimated from the Tafel slope data, i.e., PAP vs. log (scan rate) plots (refer to Figure 4.2 and Table 4.1). The changes in number of electrons transferred as influenced by alloying composition need not necessarily be attributed to additional reaction steps, either electrochemical or non-electrochemical. This behaviour can be interpreted as being due to effects of: i) diffusion control that might exist in un-stirred electrolytes and, ii) the CVs not being compensated for "iR" drops existing at the electrode-electrolyte interface.

In summary, the addition of antimony or calcium alone to form binary alloys of lead appear not to produce favourable effects in terms of depolarizing the anodic reaction, or, enhancing the current output. On the other hand, the addition of tin to lead-calcium and selenium to lead-antimony alloys seems to exert a favourable influence by shifting the anodic peak potentials in the noble direction and enhancing the current output under those conditions.

4.3- AGING EFFECTS

The behaviour of active materials in lead-acid batteries varies with time. Major processes that limit the battery cycle life are: i) the passivation of the anode, ii) loss of cathode activity, iii) electrolyte degradation, and iv) separator failures. Understanding the electrochemistry of processes leading to the passivation of the battery can help in extending the cycle life of the battery. Therefore, the variation of anode parameters were studied in the two following areas: i) time (number of cycles) dependency of PAP, and PAC; and ii) the scan rate dependency of these parameters in the fresh and aged electrodes. For the first part, lead, lead-calcium, and lead-antimony anodes were subjected to prolonged cycling up to 1700 cycles at a constant scan rate of 50 mV/s. The peak anodic potential (PAP), and the peak anodic current (PAC) were recorded at different time periods and compared. The data were plotted against the number of cycles. In the second part of the procedure, the scan was interrupted after 5 and 1200 cycles. The scan rate was then changed to 10, 30, 50, 70, 100, 150, and 200 mV/S. The PAP, PAC, and HEP (hydrogen evolution potential) were recorded. The number of electrons and transport mechanisms were compared in the fresh and aged electrodes.

A white powder precipitate was observed at the bottom of the cell after a few hundred cycles.

4.3.1- CYCLING EFFECTS

The changes in the PAP of lead, lead-calcium, and lead-antimony

as a function of cycle number, are shown in Figure 4.5. All three curves pass through a maximum. The maximum occurs at around 300 cycles for lead-calcium and lead-antimony, and around 500 cycles for pure lead. The maximum value represents the shift of peak anodic potential towards more positive values, postponing the onset of anode passivation. The curves then stabilize at around 700 cycles. The general trend is similar for all the three alloys.

Figure 4.6 illustrates the changes in the PAC of the three anodes. These curves complement the current-time curve obtained at a constant potential thus reflecting the diminished or enhanced anodic activity of an aged electrode. The initial current densities of all three anodes are reasonably close, stable, and around 11 mA/cm^2, but the presence of antimony and calcium reduces the current density after a few cycles. The curves pass through a maximum, which occurs earlier for lead alloys (after 300 cycles), and later for pure lead (around 500 cycles). The final current stabilizes at around 700 cycles. The final current density is very close for Pb/Ca and Pb/Sb (around 20 mA/cm^2), and less than that of pure lead (around 25 mA/cm^2).

4.3.2- ELECTROCHEMISTRY OF FRESH AND AGED ELECTRODE

The Tafel plots, and the plots of log (current) vs. log (scan rate) for lead, lead-calcium, and lead-antimony alloys are shown in Figures 4.7 to 4.9. The results calculated for the data are shown in Table 4.3.

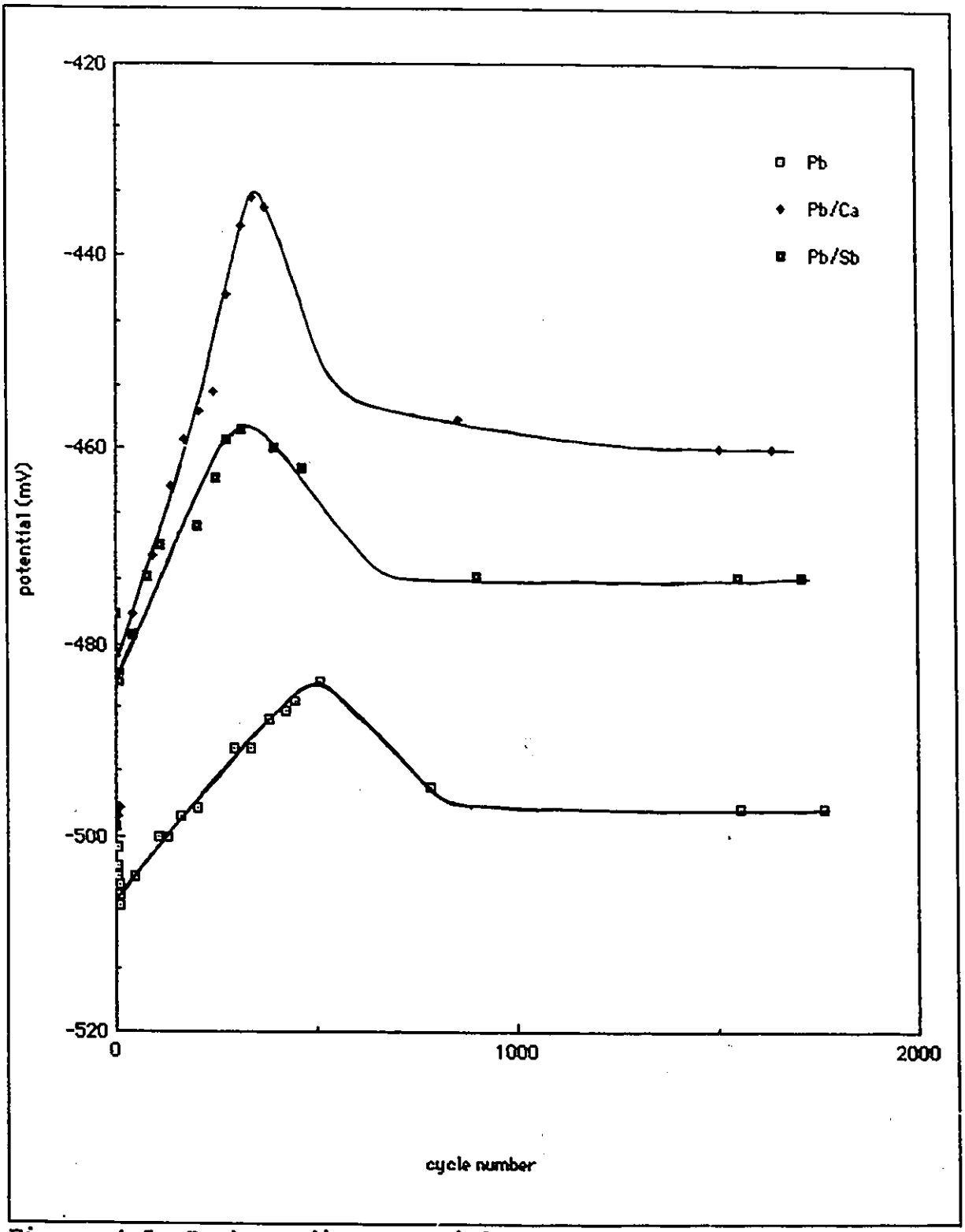

Figure 4.5: Peak anodic potential vs. number of cycles plots for lead, lead-calcium, and lead-antimony in stagnant 30% sulphuric acid at room temperature. Scan rate: 50 mV/s.

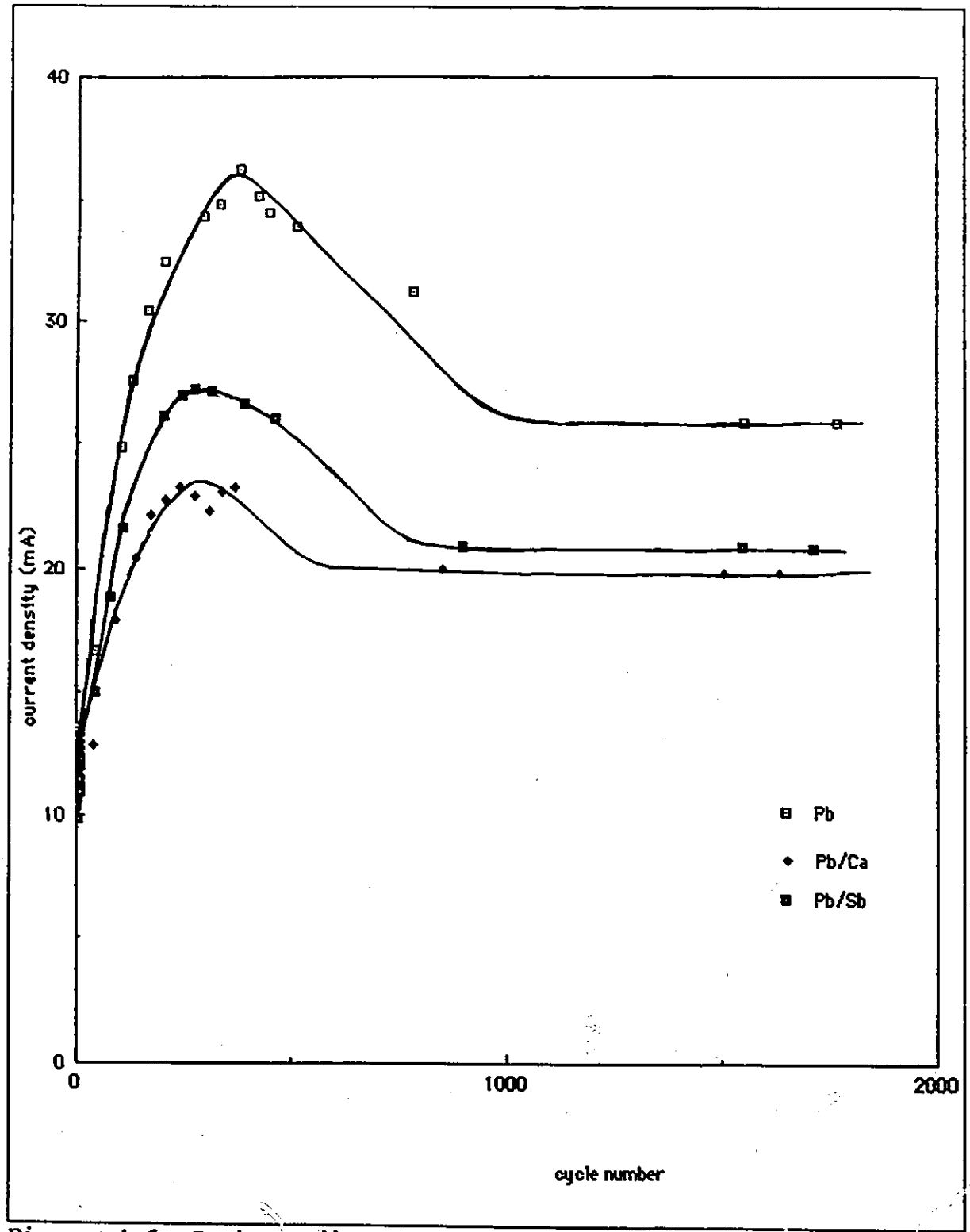

Figure 4.6: Peak anodic current vs. number of cycles plots for lead, lead-calcium, and lead-antimony in stagnant 30% sulphuric acid at room temperature.

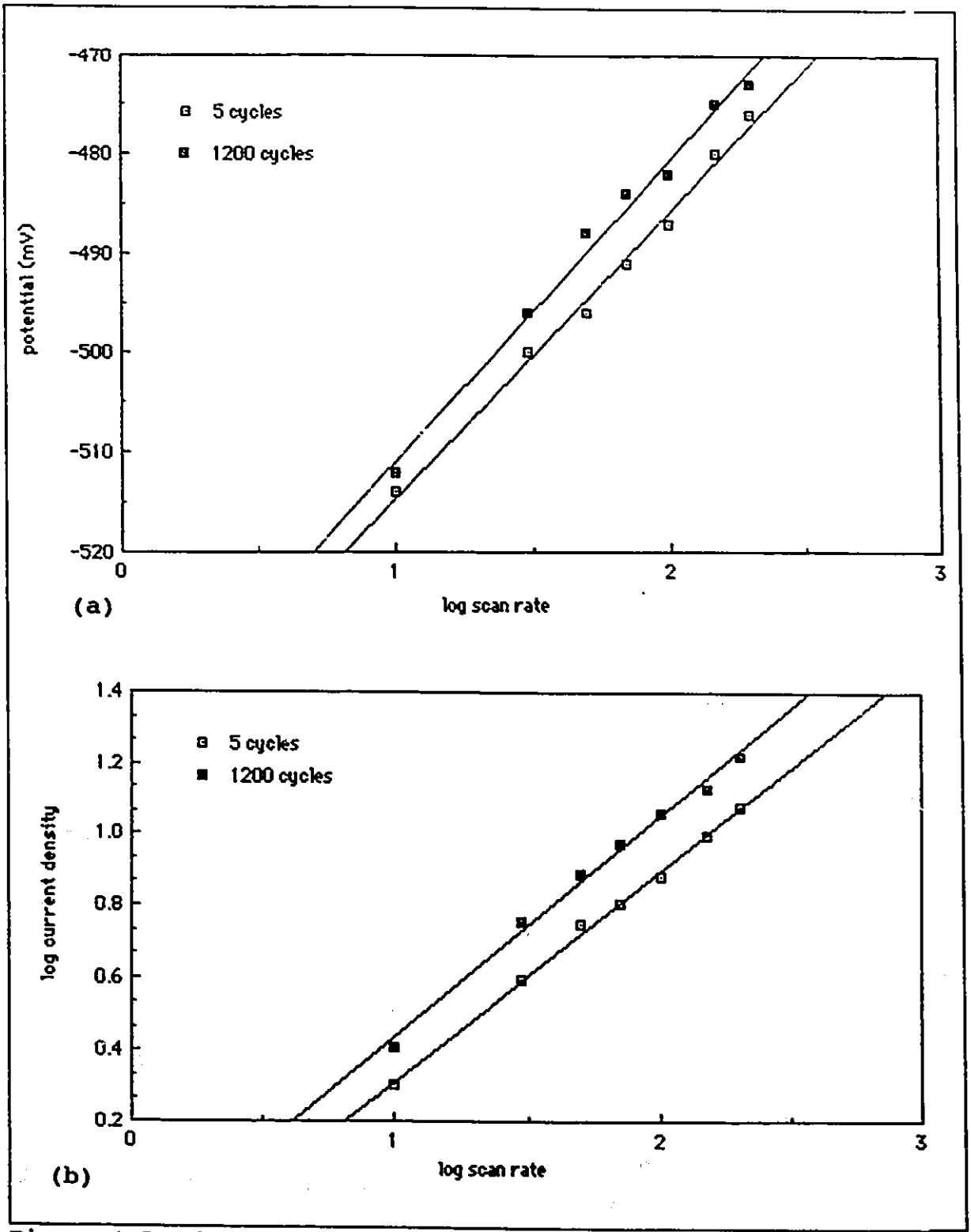

Figure 4.7: The plots of (a): PAP vs. log (scan rate), and (b): log (current) vs. log (scan rate) for lead anode in stagnant 30% sulphuric acid at room temperature.

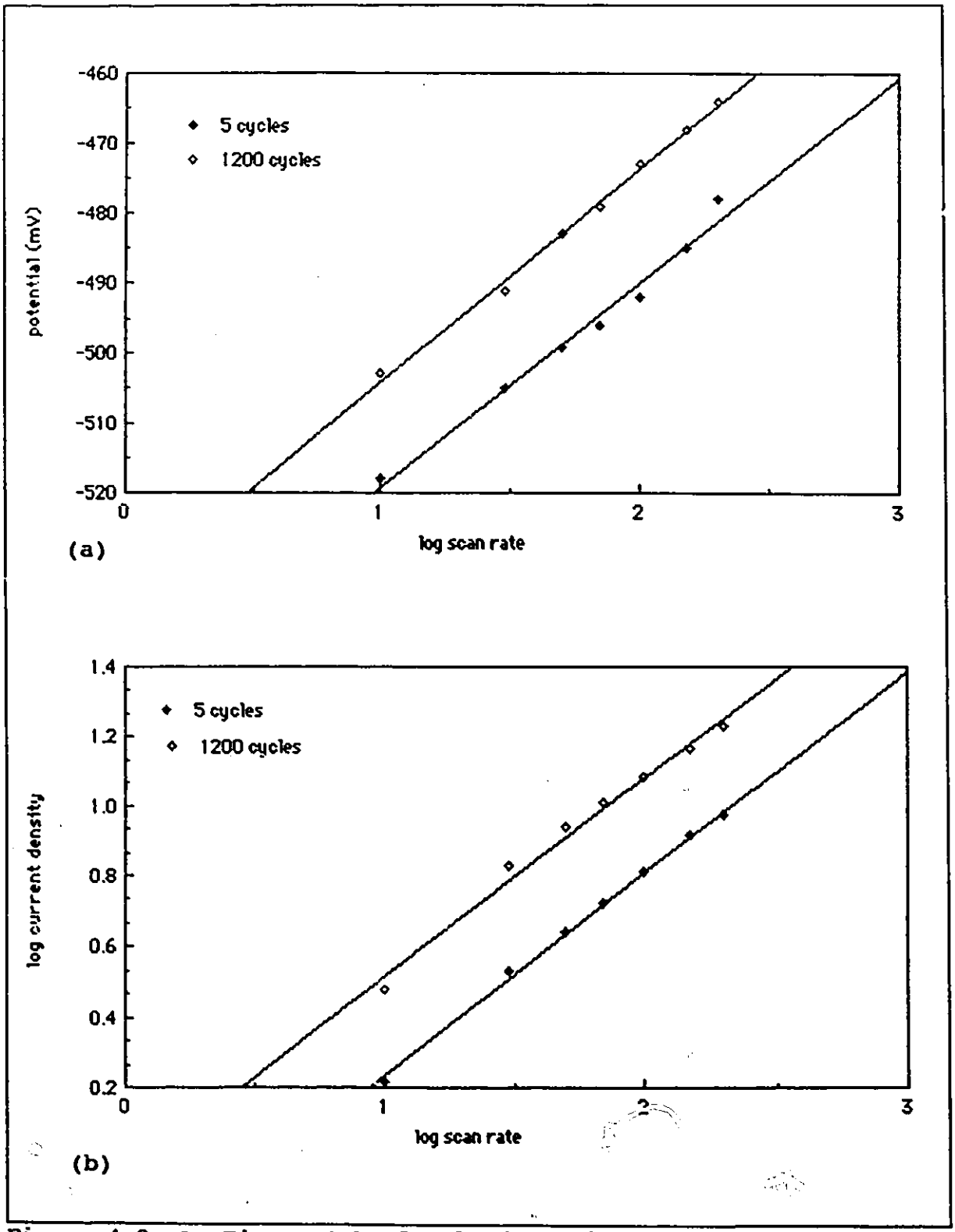

Figure 4.8: As Figure 4.7, for lead-calcium alloy.

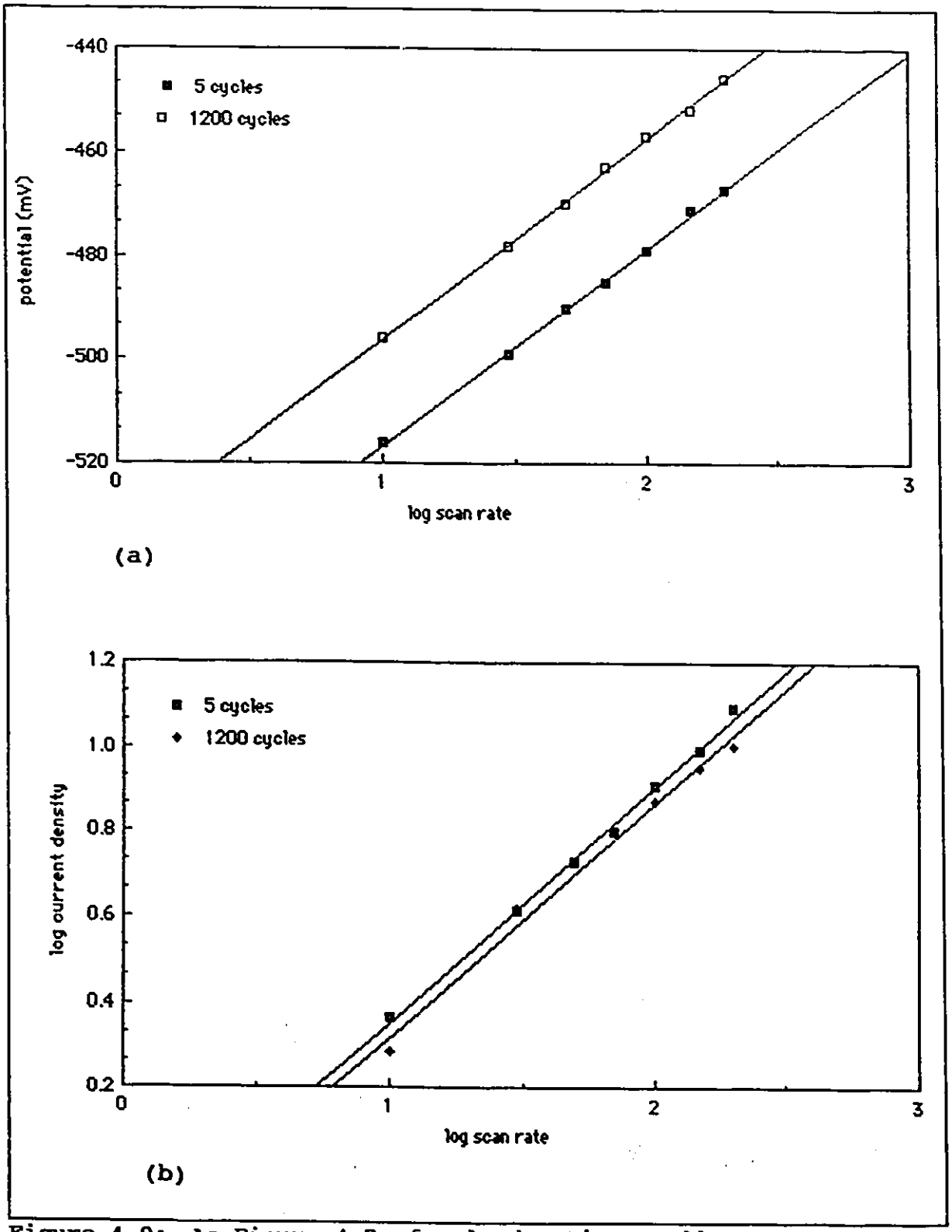

Figure 4.9: As Figure 4.7, for lead-antimony alloy.

Table 4.3

Comparison of the properties of electrodes after 5 and 1200 cycles in stagnant 30% sulphuric acid solutions at room temperature.

ANODES	Pb		Pb/Ca		Pb/Sb	
CYCLE NO.	5	1200	5	1200	5	1200
PAP slope	29	30	29	30	38	38
R^2 factor	99.0%	98.9%	98.8%	99.4%	99.9%	100%
No of e-	2.0	2.0	2.0	2.0	1.6	1.6
PAC slope	0.59	0.61	0.58	0.57	0.55	0.55
R^2 factor	99.5%	99.4%	99.8%	99.4%	98.5%	99.1%
H_2 potential	-1045	-1050	-1045	-970	-990	-925

Looking at the PAP vs log (scan rate) plots, it can be seen that as a result of aging, the PAPs are depolarized in all three alloys (Figures 4.7 to 4.9). The shift is negligible for pure lead with only 3 mV difference. The differences between the PAP of fresh and aged lead-calcium and lead-antimony anodes are 17 and 22 mV respectively. However, the changes in the Tafel slope estimated from the PAP vs. log (scan rate) plots, are not significant, and consequently, the number of electrons transferred in the electrochemical reaction remained the same for both the fresh and aged electrodes (Table 4.3).

The slope of the curves of log (current) vs. log (scan rate) remained reasonably similar, and close to 0.5, from which it can be concluded that the diffusion controlled transport mechanism is independent of the electrode aging. The Tafel slope and the slope of log (current) vs. log (scan rate) plots can also be compared to the corresponding data in Table 4.1.b and 4.2.b which represents

the first cycle results. This comparison confirms the independence of these two slopes from the age of the electrode.

The hydrogen evolution potential (HEP) was also found to be independent of scan rate in both fresh and aged electrodes, see Table 4.3. The HEP is retarded in pure lead but accelerated in lead-calcium and lead-antimony as a result of aging.

4.4- EFFECTS OF EXPANDER, AMMONIUM LIGNO-SULPHONATE, (ALS)

4.4.1- CONCENTRATION EFFECTS

As was mentioned earlier, the problem of loss in battery performance due to compact lead sulphate film formation on the surface of the electrode is usually treated by the addition of chemical compounds known as expanders, either to the electrode structures or to the electrolyte. The favourable influences of these substances have been discussed in detail in Chapter one. In these experiments, ammonium ligno-sulphonate (ALS) was added to the electrolyte in concentrations of: 10, 30, and 50 PPM, and the results were compared with those when there was no expander present in the electrolyte.

First, the rest potentials, i.e., open circuit potentials, of the electrodes were measured as a function of ALS concentration, and then cyclic voltammetry experiments in the potential range of -1300 to -350 mV were performed at a scan rate of 50 mV/s. The peak anodic potential (PAP), peak anodic current (PAC), and hydrogen

evolution potential (HEP) were estimated from the cyclic voltammograms that were obtained after five cycles. The dependency of these parameters on the concentration of ALS are illustrated in Figures 4.10 to 4.14.

Figure 4.10 shows the effect of concentration of ALS on the rest potential of the electrodes. Addition of ALS shifts the rest potential towards less negative values up to 10 PPM, shifting back to no-expander case at higher concentrations.

The dependence of PAP on the concentration of ALS is shown in Figure 4.11. The PAPs shifted in anodic direction up to a concentration of 10 PPM. Beyond this point, the PAP shifted back to the non-expander case. The trend that is noted in this figure complements that in Figure 4.10.

The shift of the PAP is accompanied by a decrease in the PAC which is shown in Figure 4.12. The current densities are minimum at a concentration of 10 PPM and do not change significantly with the additional concentrations of ALS. The decrease is highest for the lead-calcium alloy and lowest for lead-antimony.

The effect of ALS concentration on HEP is shown in Figure 4.13. The addition of ALS retards the hydrogen evolution potential (HEP), which is a favourable effect in actual battery operation. The evolution of hydrogen is postponed with any amount of ALS addition. The concentration of 10 PPM is the most effective in this respect.

The results obtained in these experiments are in contradiction with the results reported in the literature [Mahato, 1977, 1980, 1981, 1983, 1985; Pavlov, 1970; Bode, 1977; Simon, 1974; Brennan,

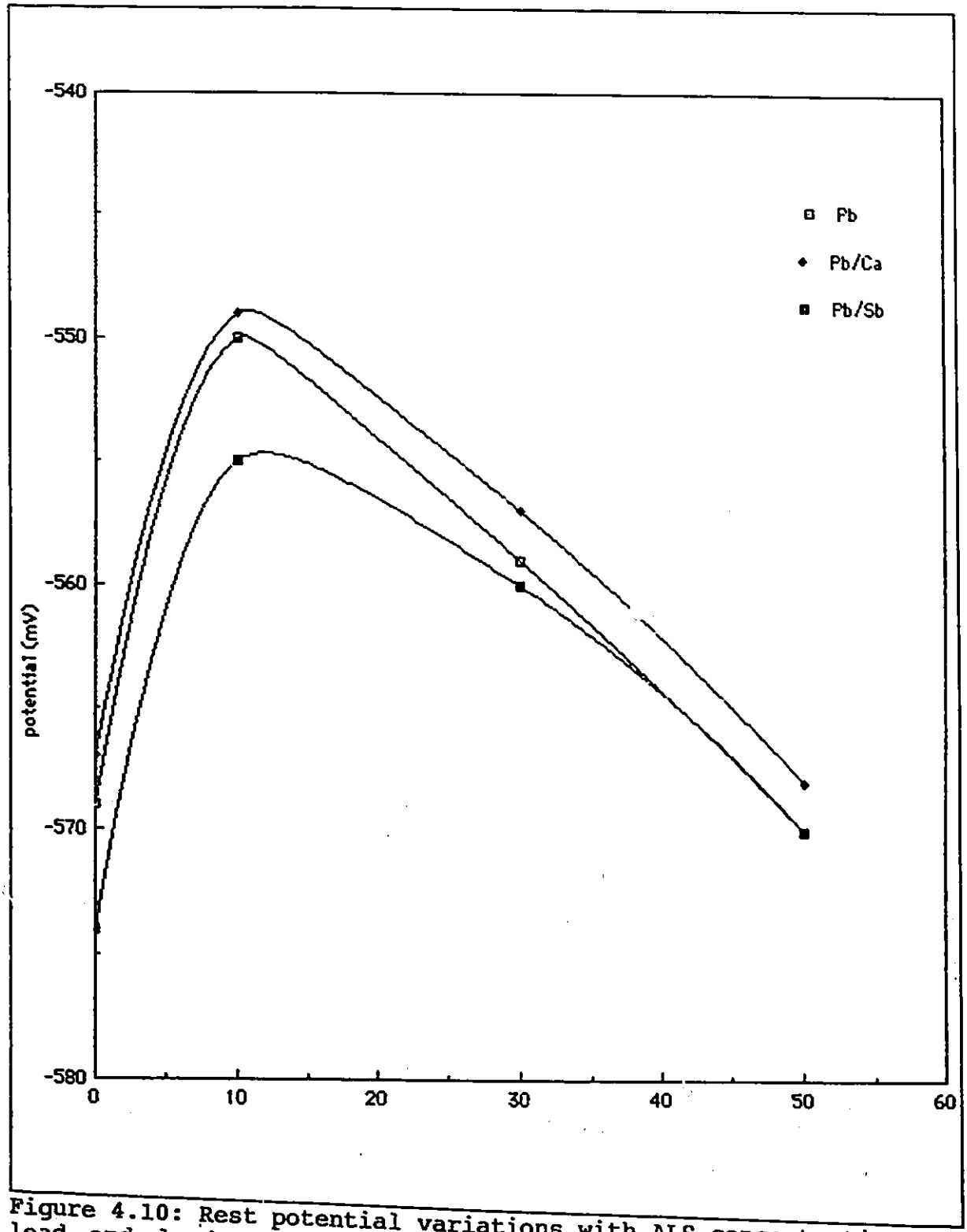

Figure 4.10: Rest potential variations with ALS concentration for lead and lead alloys in stagnant 30% sulphuric acid at room temperature.

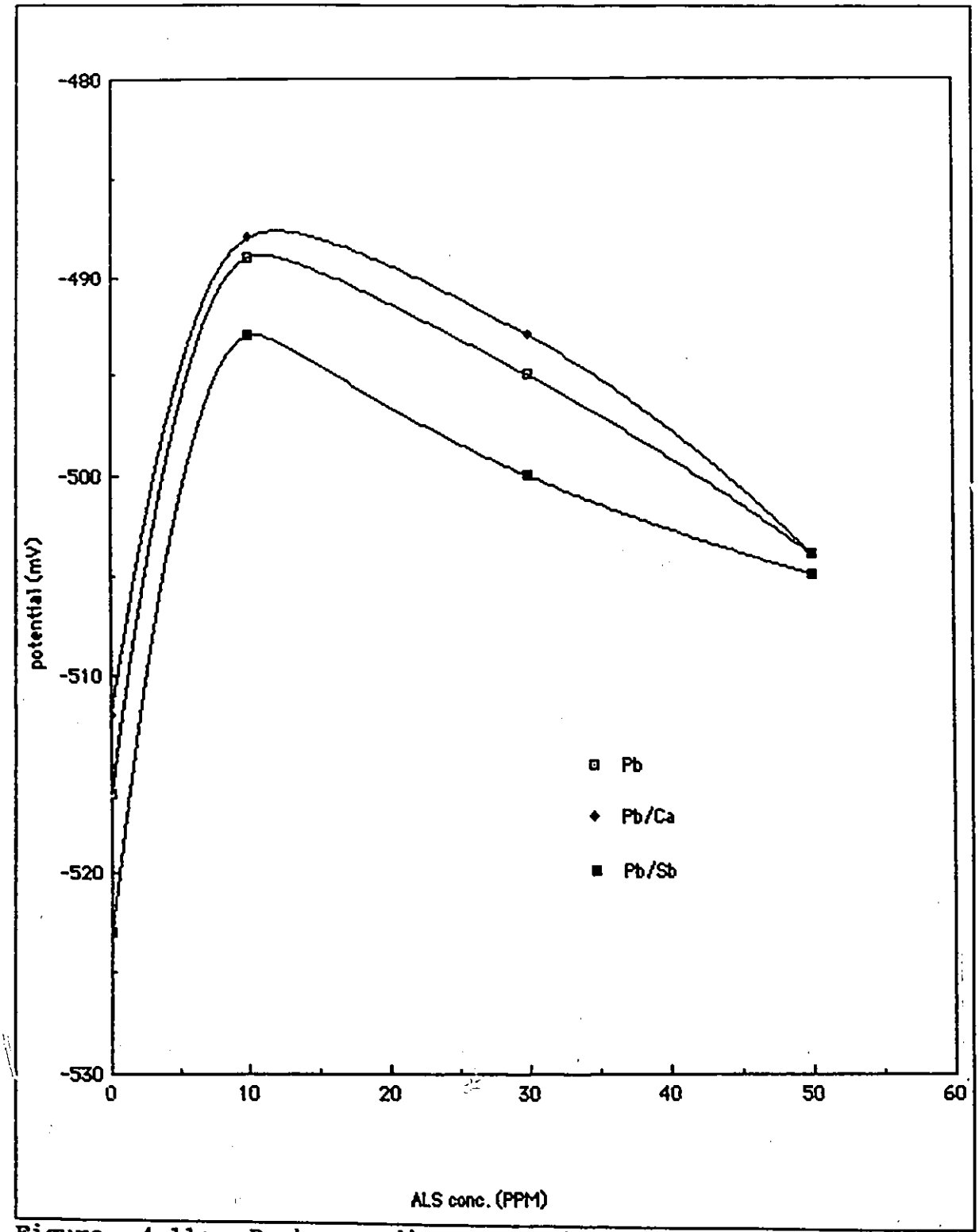

Figure 4.11: Peak anodic potential variations with ALS concentration for lead, lead-calcium, and lead-antimony alloys in stagnant 30% sulphuric acid at room temperature.

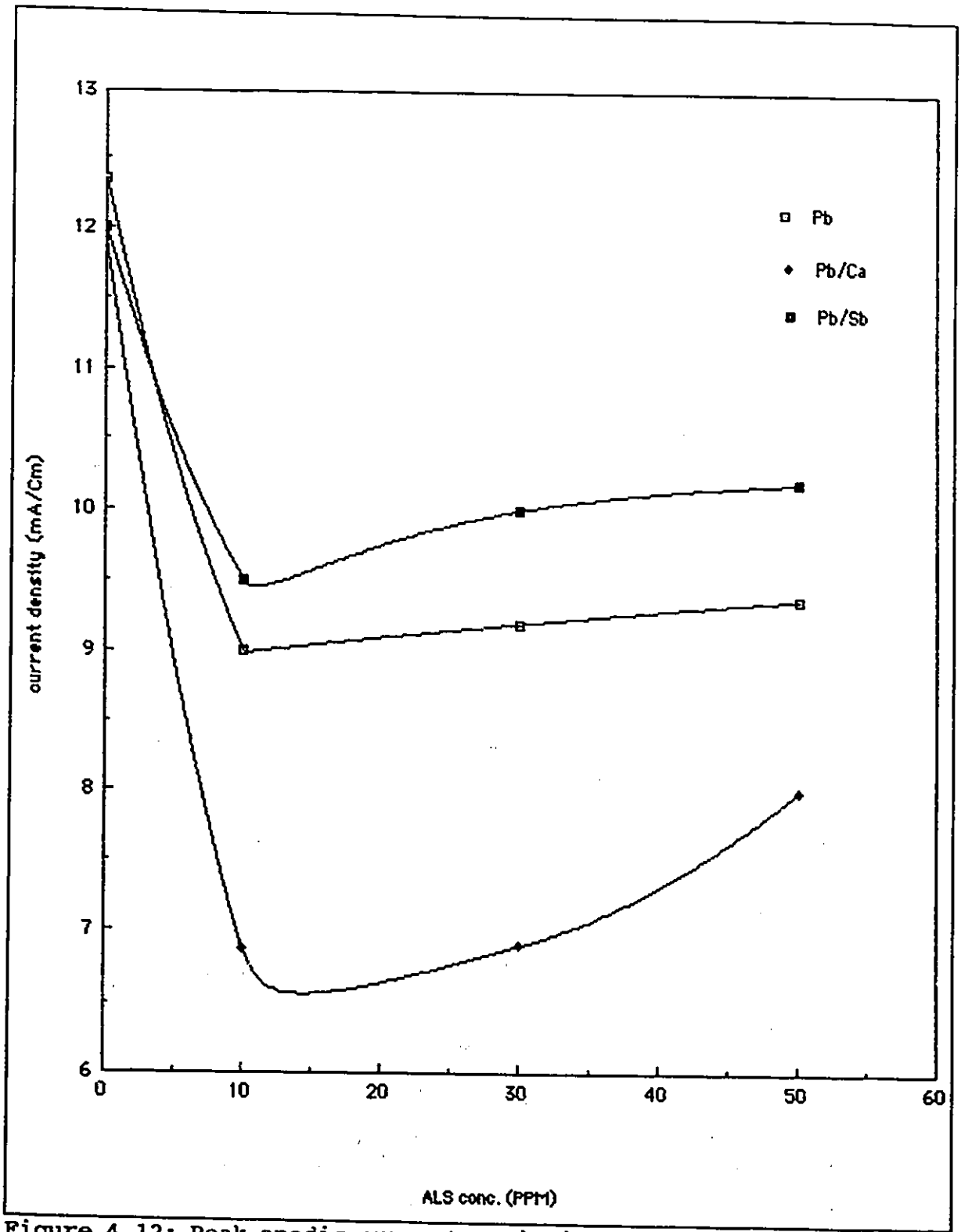

Figure 4.12: Peak anodic current variations with ALS concentration for lead, lead-calcium, and lead-antimony alloys in stagnant 30% sulphuric acid solution at room temperature.

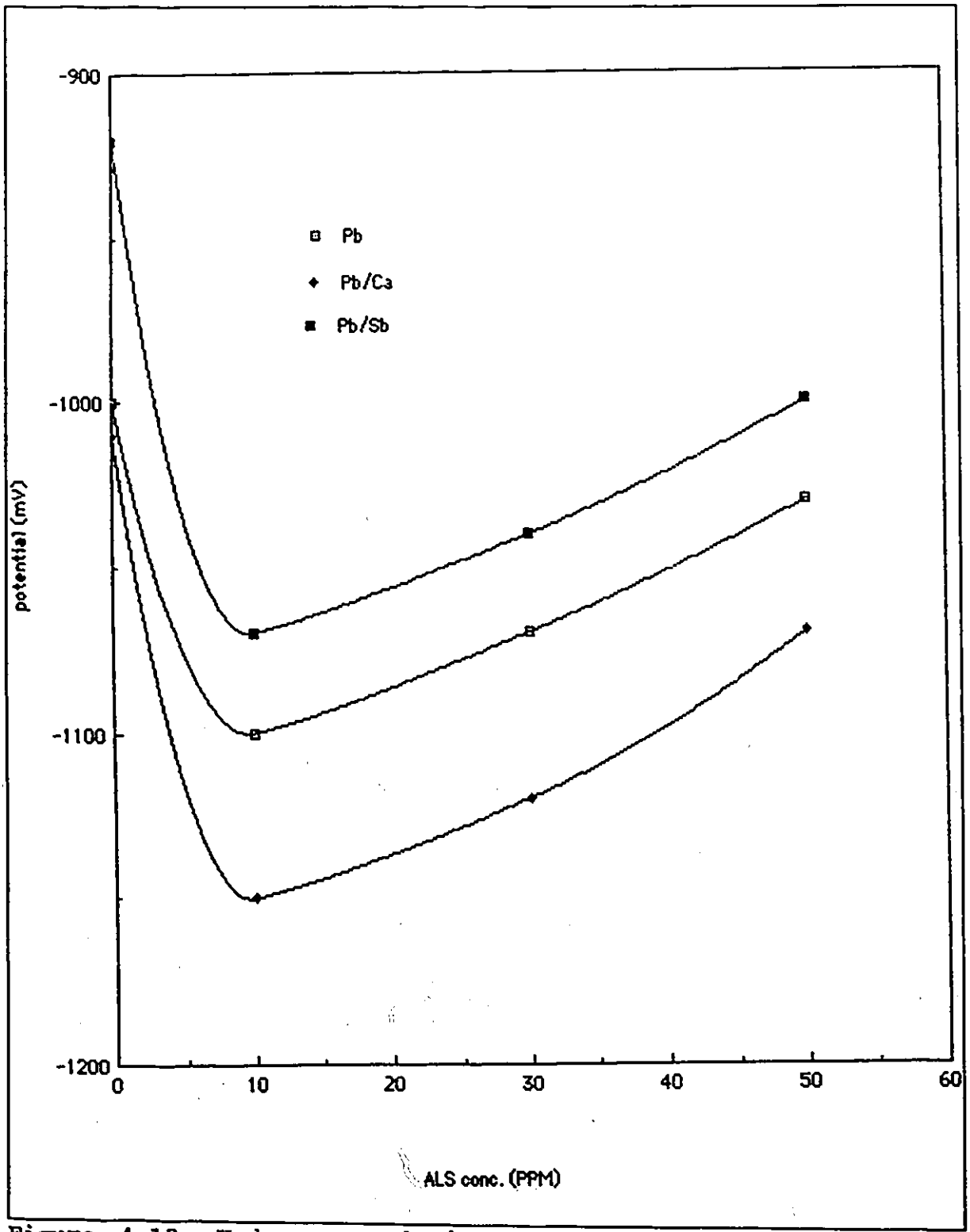

Figure 4.13: Hydrogen evolution potential variations with ALS concentration for lead, lead-calcium, and lead-antimony alloys in stagnant 30% sulphuric acid at room temperature.

1973, 1974, 1976]. The favourable ALS effects such as enhancement of the current density which have been reported by many authors [Mahato, 1980, 1981], were not observed in this set of experiments.

The reason for observing the opposite behaviour of ALS to that observed in other studies is the difference in potential range within which these experiments were performed, namely the range covering the hydrogen evolution potential (overcharge potential). All previous studies were performed in a potential range which only simulates the normal operation of the battery, excluding the gassing potential (e.g., -800 to -350 mV instead of -1300 to -350 mV vs. calomel reference electrode). The experiments performed by Mahato [Mahato 1980, 1981] are shown in Figure 4.14 which shows an enhancement effect of lignosulphonate salts on the current density. Mahato's experiments were repeated and the enhancement effect of ALS on the current density was confirmed. However, the potential range was extended to cover HEP which led to the opposite results being obtained in the current investigation.

The following interpretation is offered to explain these opposing observations: first, hydrogen evolution during the charge of the battery desorbs ALS from the lead sulphate particles, and allows for a coverage of the active surface area by larger lead sulphate crystals, hence, reducing the current density and postponing the PAP; second, ALS itself may degrade at the HEP producing complexes containing lead ions with the same properties as lead sulphate, thus enhancing the blocking effect of lead sulphate.

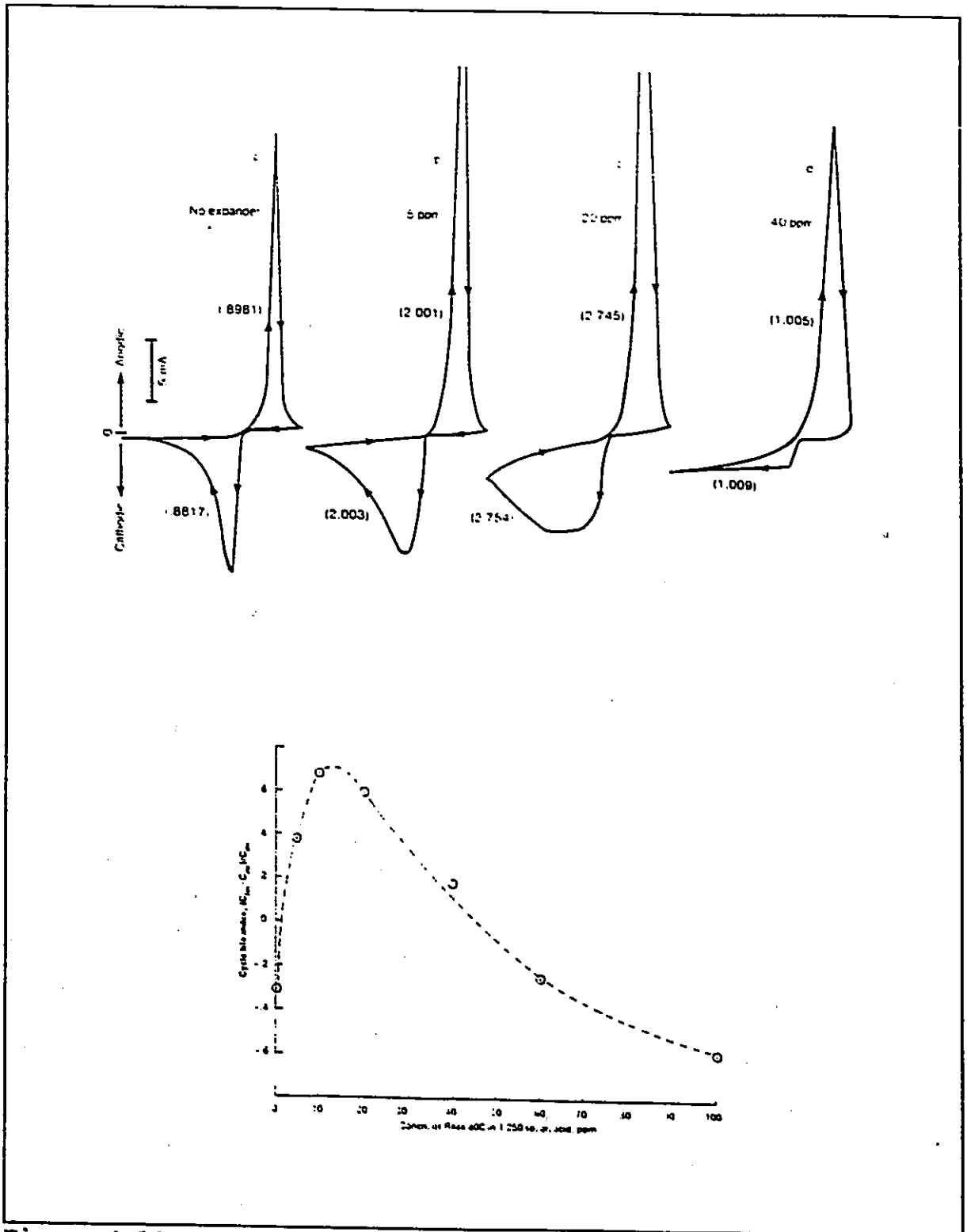

Figure 4.14: Results from the experiments made by Mahato [Mahato, 1980, 1981] on the effect of expanders on the enhancement of the current density.

This observation is of great importance to the battery industry. In actual battery operations, the gassing phenomenon occurs when the lead-acid battery undergoes overcharge. Therefore, the remote operation of sealed lead-acid batteries (e.g., photovoltaic applications) requires an accurate charge control that can prevent the battery from overcharging. Otherwise, the addition of ALS is of no benefit to the performance of the battery.

The interpretation above is supported by the SEM micrographs which show the crystal shape and size differences on the surface of electrodes scanned in solution with and without ALS. In the presence of ALS, the lead sulphate crystals are finer and cover the surface of the electrode more uniformly (see Section 4.7).

In summary, although ALS is known to be a beneficial additive with favourable effects on the performance of the battery, it is not beneficial when the battery is overcharged. Mahato [Mahato, 1980, 1981] has found ALS performs best when added at the concentration of 10 PPM. In this experiment, the same concentration was found to be a critical value at which both the desired and undesired effects of ALS are maximum. The desired effect of ALS for this condition is to postpone the evolution of hydrogen, and the undesired effects are reducing the current density and retarding the peak anodic potential.

4.4.2- EFFECTS OF ALS ON THE ELECTROCHEMISTRY OF ELECTRODES

The variations of the electrochemical properties of lead alloy

anodes in the presence of a 10 PPM concentration of ammonium lignosulphonate (ALS) solution were investigated in these experiments. At room temperature, the cyclic voltammograms were obtained between -1300 and -350 mV as a function of scan rate. The electrodes were scanned for 5 cycles at a scan rate of 50 mV/s until the pseudo-steady-state was reached. The scan rate was then changed to 10, 30, 50, 70, 100, 150, and 200 mV/s.

Figures 4.15 to 4.17 compare the PAP and PAC of lead, lead-calcium, and lead-antimony anodes in the presence and the absence of ALS. The PAP of all three anodes decreased (depolarized) when ALS was added to the electrolyte. This means the expander modifies the electrochemical reaction. The effect is more significant in the case of lead-antimony alloy. The slopes of the curves are lower in presence of ALS, see Table 4.4. These lower slopes represent greater numbers of electrons transferred (greater than 2) which is not physically realistic. This misleading observation can be explained in two ways: either a competitive side reaction occurs in addition to the principal one when the expander ions are presented, or at the experimental conditions, i.e., overcharging, hydrogen evolution and probably degradation of ALS, the curves do not follow the rules explained in Section 2.1. The Tafel slopes were recalculated individually from the plots of overpotential vs. log (current) (discussed in Section 2.1.2) for each scan rate. This time the values were in the neighbourhood of 30 mV (see Table 4.4), representing a 2-electron mechanism. The latter calculations support the second explanation above, namely, the PAP vs. log (scan

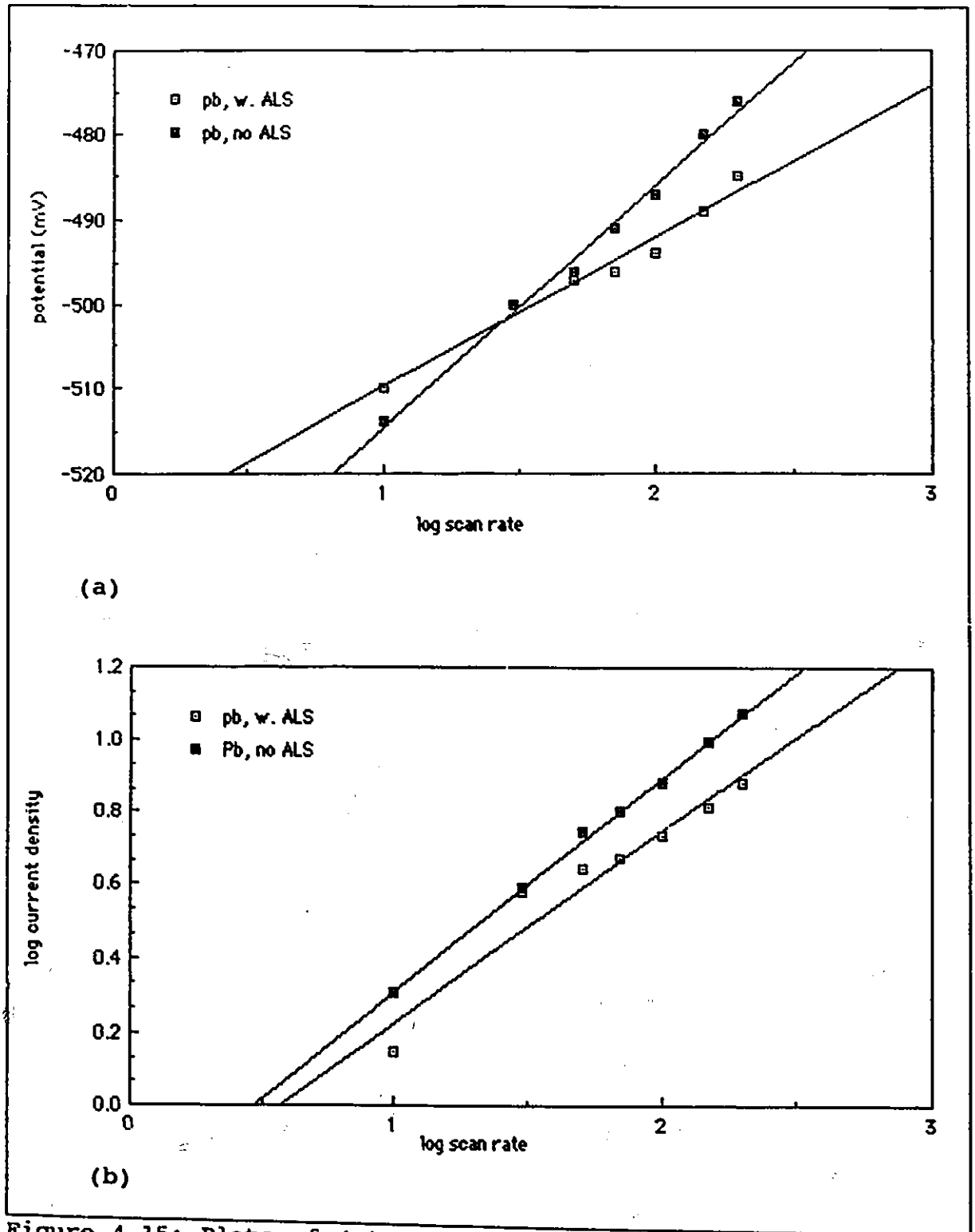

Figure 4.15: Plots of (a): PAP vs log (scan rate), and (b): log (current) vs. log (scan rate) for pure lead in the presence and absence of ALS (conc. 10 PPM), in stagnant 30% sulphuric acid at room temperature.

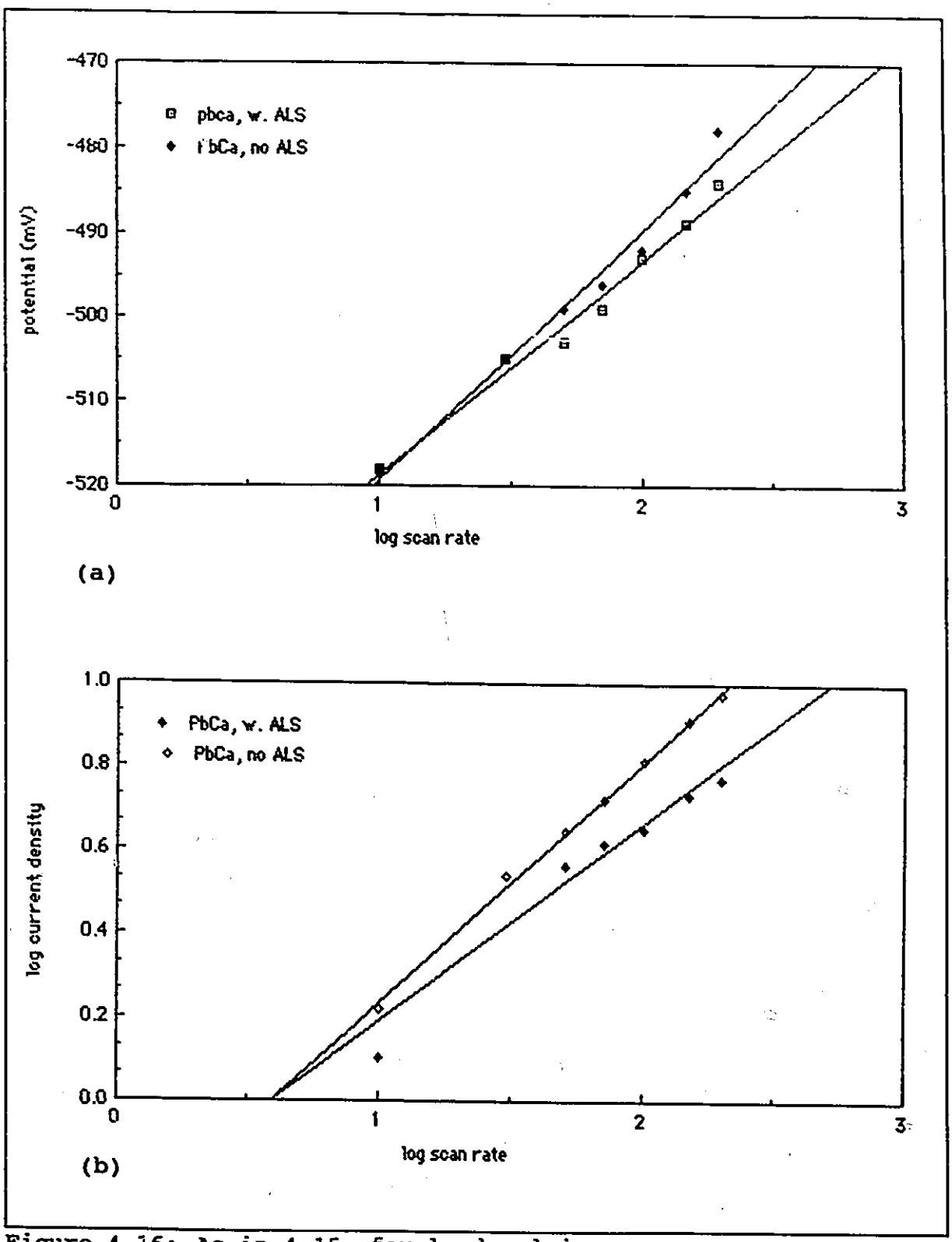

Figure 4.16: As in 4.15, for lead-calcium.

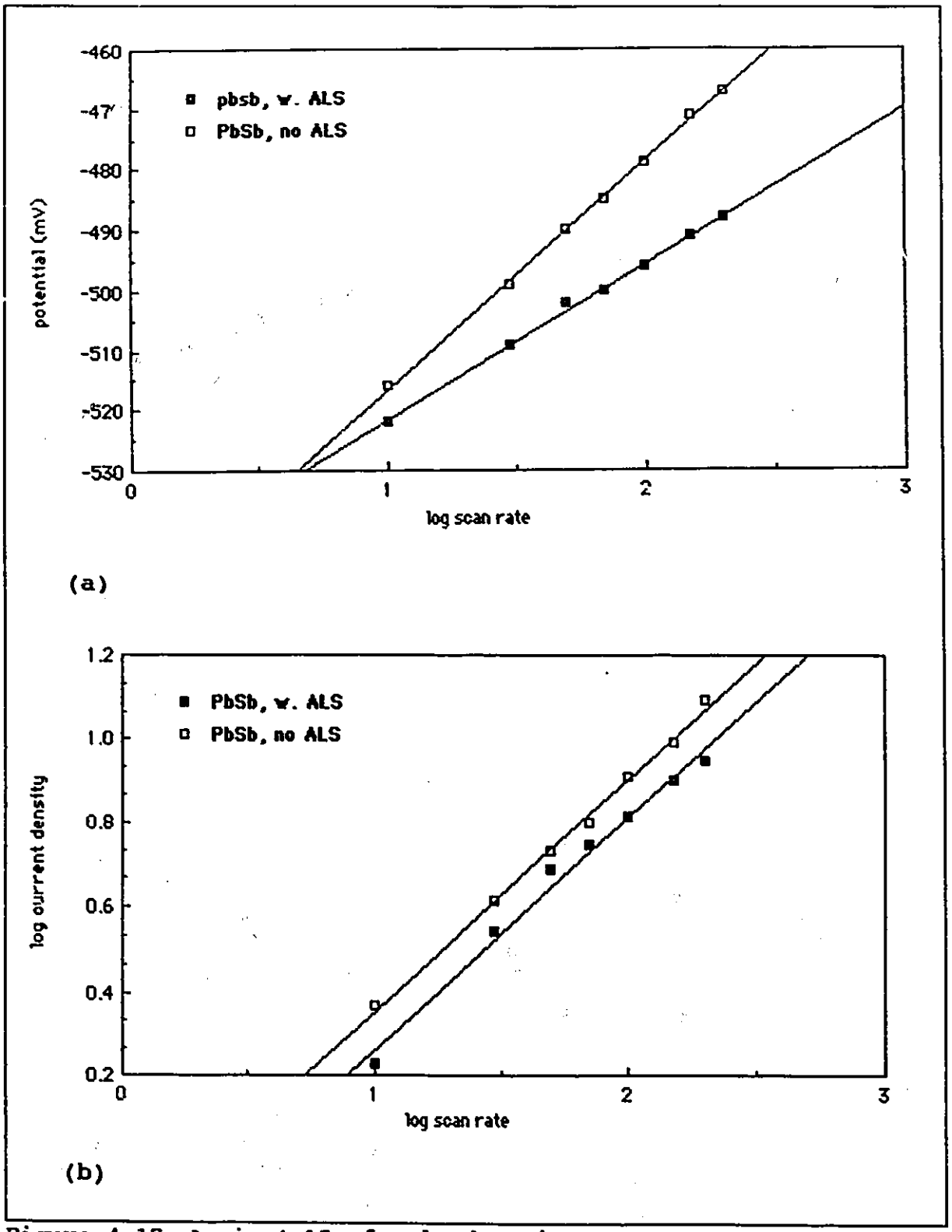

Figure 4.17: As in 4.15, for lead-antimony.

TABLE 4.4

The electrochemical properties of lead, lead-calcium, and lead-antimony alloys in the presence of ammonium ligno-sulphonate. Electrolyte: 30% sulphuric acid solution with 10 PPM concentration of ALS, at room temperature. [Description of variables: PAP slope: the slope of PAP vs. log (scan rate), (unit mV). Tafel: the Tafel slope calculated from the plot of potential vs. log (current). No. of e^-: the number of electrons transferred. PAC slope: the slope of log (current density) vs. log (scan rate). R^2 factor: the regression coefficient for the latter plot.]

Anodes	Pb		Pb/Ca		Pb/Sb	
Paramet.	no ALS	w. ALS	no ALS	w. ALS	no ALS	w. ALS
PAP slope	29	18	29	25	36	26
Tafel	30	30	30	31	35	36
No. of e^-	2.0	2.0	2.0	2.0	1.6	1.6
PAC slope	0.59	0.52	0.58	0.48	0.55	0.55
R^2 factor	99.8%	93.7%	99.8%	90.9%	99.7%	98.7%

rate) plots do not follow the Tafel rules under the above mentioned experimental conditions.

The current densities of all three anodes decreased in the presence of ALS. The log (current) vs. log (scan rate) plots of lead and lead-calcium are linear only in the scan rate range of 30 to 200 mV/s. These curves deviate slightly from linearity when the range is extended to scan rate of 10 mV/s with the regression coefficients of 93.7% and 90.9% for lead and lead-calcium respectively, see Table 4.4. The slopes are very close to 0.5.

The performance of the expander is the best with lead-antimony alloy showing a maximum of acceleration of the electrochemical reaction and an insignificant reduction in the current density.

4.5- TEMPERATURE EFFECT

One of the major factors affecting battery performance is the operational temperature. The capacity and the cycle life of the battery decrease significantly in cold weather and, addition of certain expanders are anticipated to affect the battery performance in cold climates differently than in moderate or hot climates. In order to verify this hypothesis, the influence of ALS at low temperature, i.e., 0°C, was studied by performing cyclic voltammetry experiments on lead, lead-calcium, and lead-antimony alloys exposed to sulphuric acid (30%) with and without ALS.

The peak anodic potential (PAP), and the peak anodic current (PAC) were recorded at scan rates of 10, 30, 50, 70, 100, 150, and 200 mV/s after the anodes were cycled 5 times at a scan rate of 50 mV/s in the potential range of -1300 to -350 mV to reach the pseudo-steady-state.

The results are shown in Figures 4.18 to 4. 20, and Table 4.5. At low temperature, the current density decreases significantly. The addition of ALS was expected to improve the current density at low temperatures. However, under the overcharge conditions, the ALS addition not only did not increase the current density, but caused a further decrease (the same effect of ALS as observed at room temperature).

The PAC curves are linear only in the scan rate range of 30 to 200 mV/s, with the regression coefficients of 97.8, 97.3, and 96.0 for lead, lead-calcium, and lead-antimony anodes respectively. The slopes are around 0.3 in the scan range of 30 to 200 mV/s (current

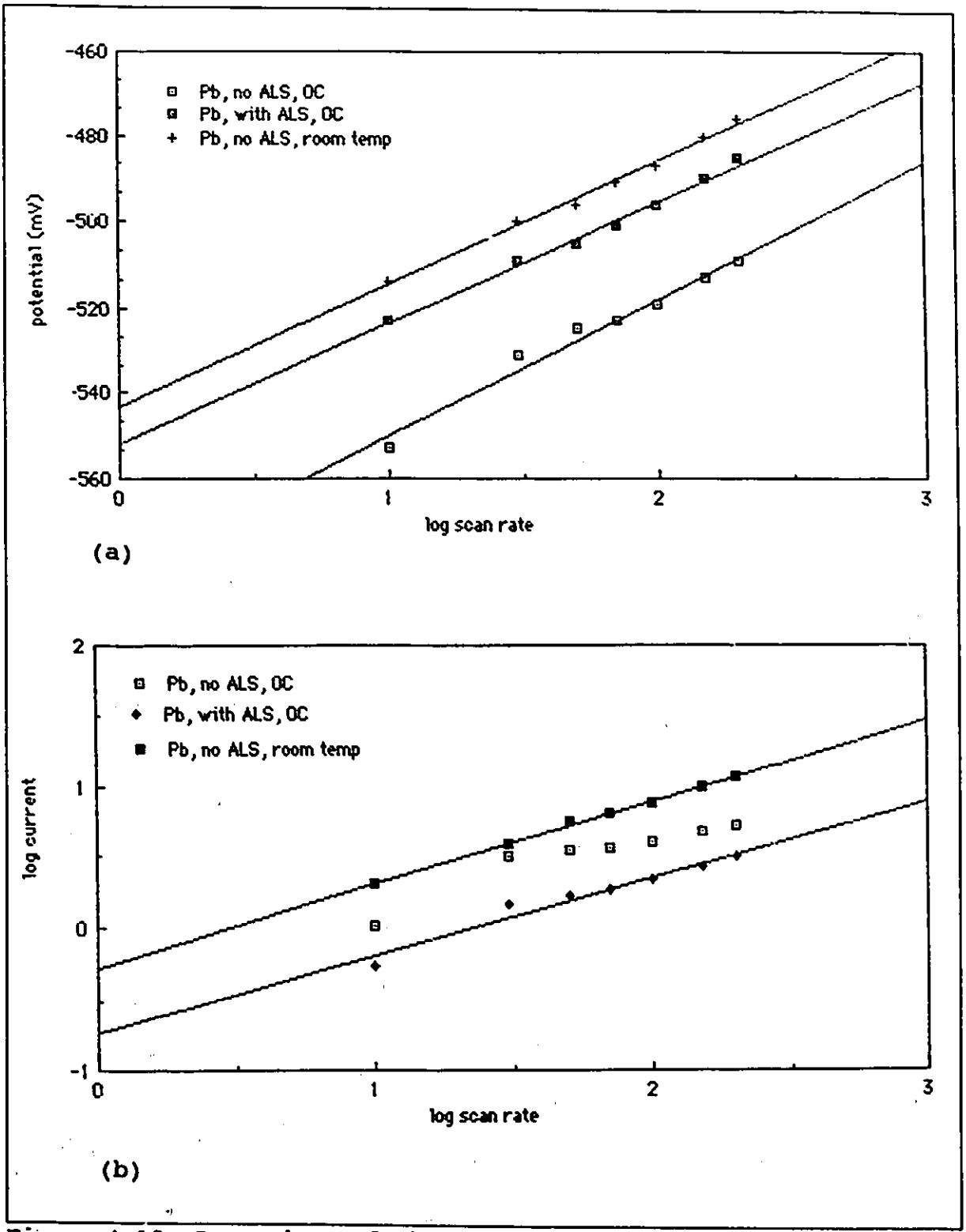

Figure 4.18: Comparison of plots of PAP vs log (scan rate) (a), and log (current) (bottom), vs. log (scan rate) (b), for lead anode at room temperature and 0°C with and without ALS.

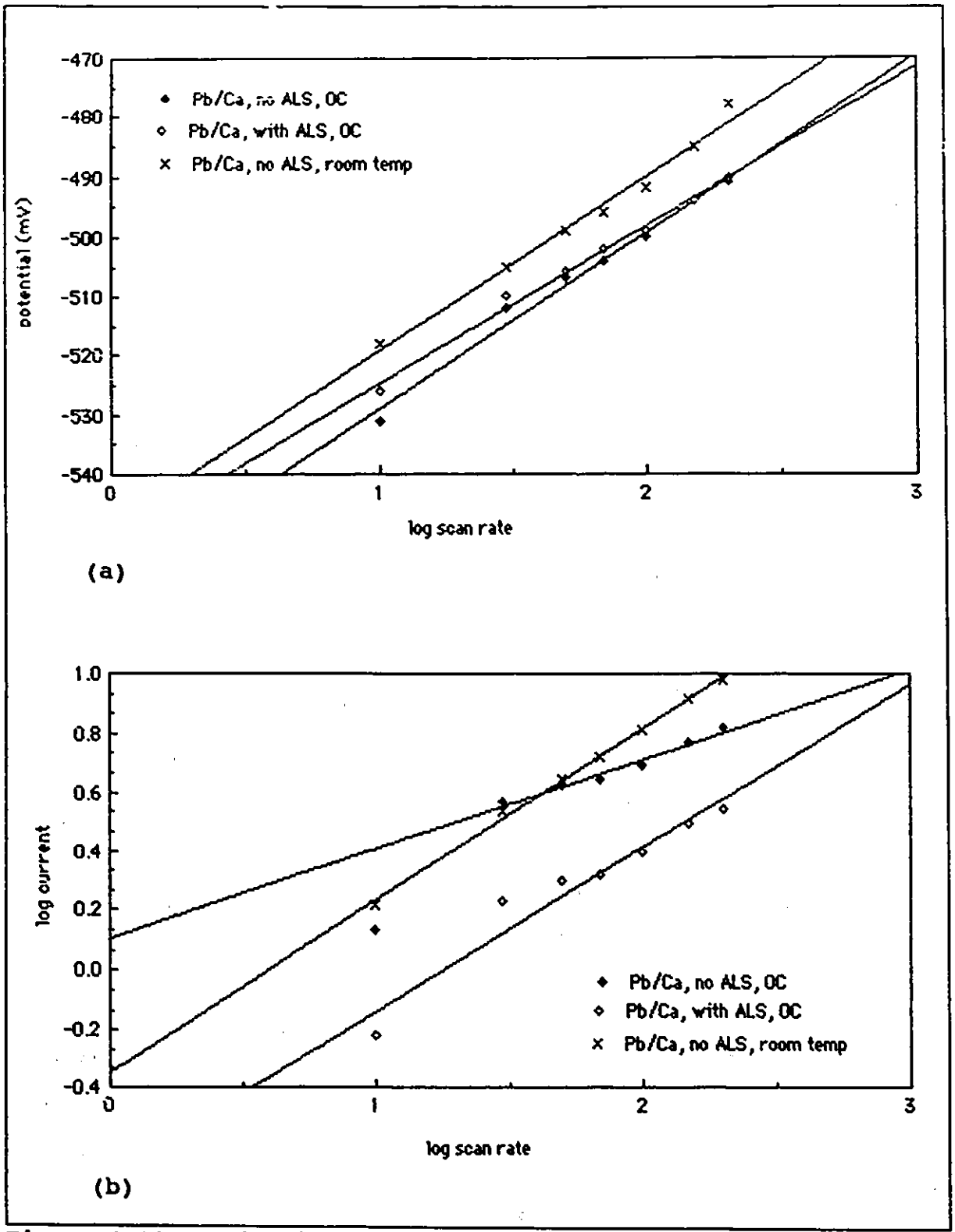

Figure 4.19: As in Figure 4.18, for lead-calcium.

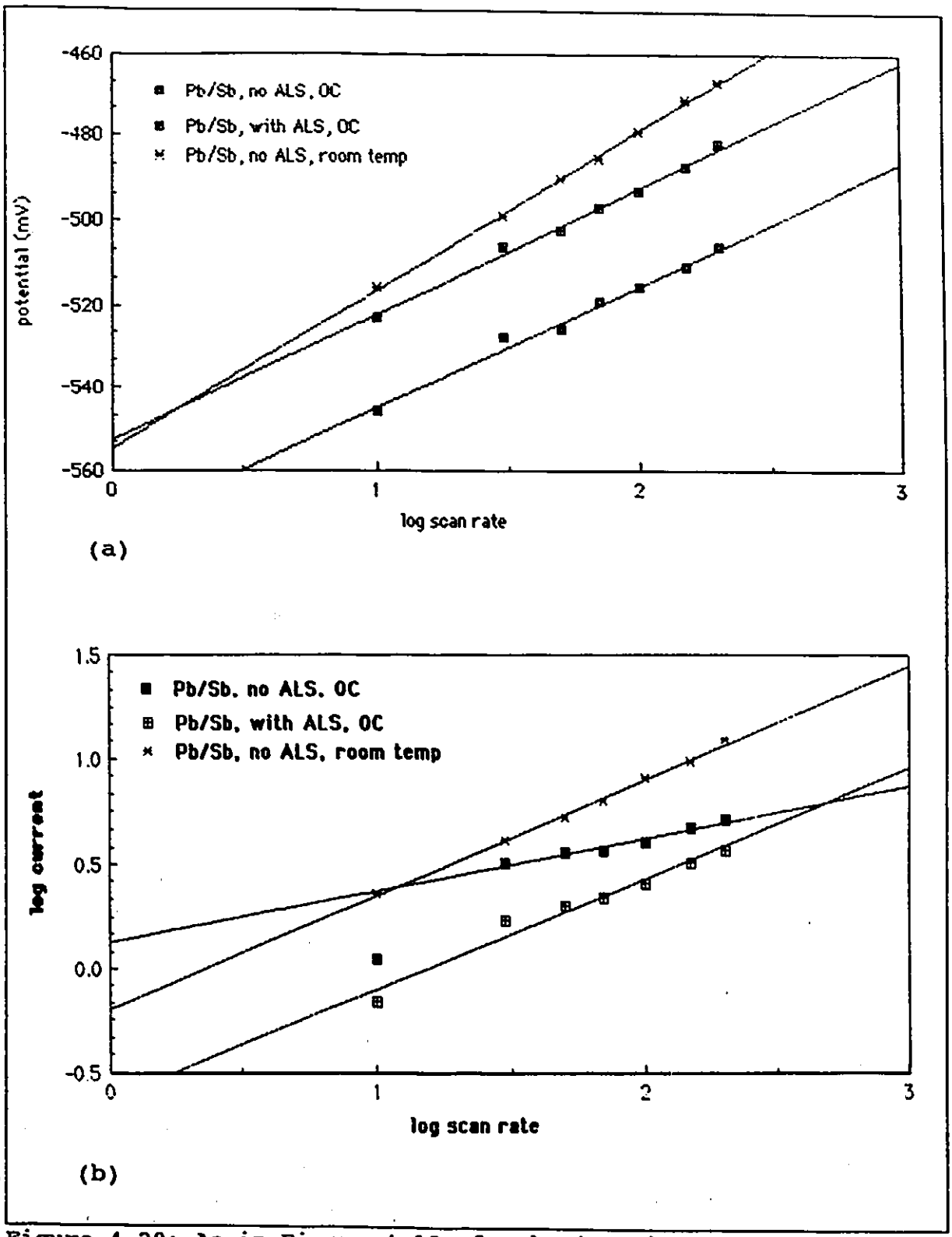

Figure 4.20: As in Figure 4.18, for lead-antimony.

TABLE 4.5

The electrochemical properties of lead and lead alloys at 0°C, with and without ALS added to the electrolyte. [Definitions: Tafel: Tafel slope (the slope of the curve of PAP vs. log (scan rate)), unit mV, No of e^-: number of electrons transferred, PAC slope: the slope of the curve of log (current) vs. log (scan rate), R^2: regression coefficient, (including the result at scan rate of 10 mV/s).]

Anodes	Pb		Pb/Ca		Pb/Sb	
Paramet.	no ALS	w. ALS	no ALS	w. ALS	no ALS	w. ALS
Tafel	31	29	30	28	30	30
No of e^-	2	2	2	2	2	2
PAC slope	0.49	0.54	0.49	0.55	0.48	0.53
R^2	88.8%	95.9%	91.1%	94.0%	87.3%	96.8%

proportional to the third root of the scan rate instead of the square root). The addition of ALS increased the regression coefficient (when the result at scan rate of 10 mV/s is also counted), and increased the slope to around 0.5 (see Table 4.5). Neither the temperature, nor the presence of the expander changed the Tafel slopes of lead and lead-calcium significantly (both around 30 mV). Hence, the number of electrons remains the same as in the room temperature case. However, as a result of lowering the temperature, the Tafel slope of the lead-antimony is decreased significantly (36 mV at the room temperature compare to 30 mV at 0°C). Therefore, the number of electrons are increased from 1.6 (at room temperature) to 2.0 (at 0°C) for lead-antimony. Since the voltammograms are uncompensated for the "iR" drops across the electrode-electrolyte interface, it is difficult to isolate the reasons for variations in these Tafel slopes.

The performances of the three anodes at low temperature with and without the addition of ALS to the electrolyte are compared in Figures 4.21 and 4.22. Before ALS is added to the electrolyte, the PAPs of lead and lead-antimony are lower than that of lead-calcium. The addition of ALS brings the curves closer together by increasing the PAPs of lead and lead-antimony.

From another point of view, the electrochemical reaction occurs at more negative potentials (depolarization due to low temperature, see Figures 4.18 to 4.20). The addition of ALS increases the PAP to a value closer to that obtained at room temperature. The latter effect is negligible for lead-calcium.

The current densities of lead and lead-antimony are very close to and lower than that of lead-calcium. The addition of ALS causes a decrease in the current density of all three alloys. After the addition of ALS, the current density of lead-antimony is highest when compared to those of the other two alloys, which means ALS performs best with lead-antimony alloys.

4.6- POTENTIOSTATIC TRANSIENT MEASUREMENTS

Potentiostatic anodic transient experiments were performed on lead, lead-calcium, and lead-antimony alloys to understand the kinetics and mechanism of lead sulphate film formation. The effect of ALS was also investigated. In a typical experiment, the working electrode was preconditioned at a potential beyond the hydrogen evolution potential (HEP), -1300 mV vs. SCE, for 15 seconds so that

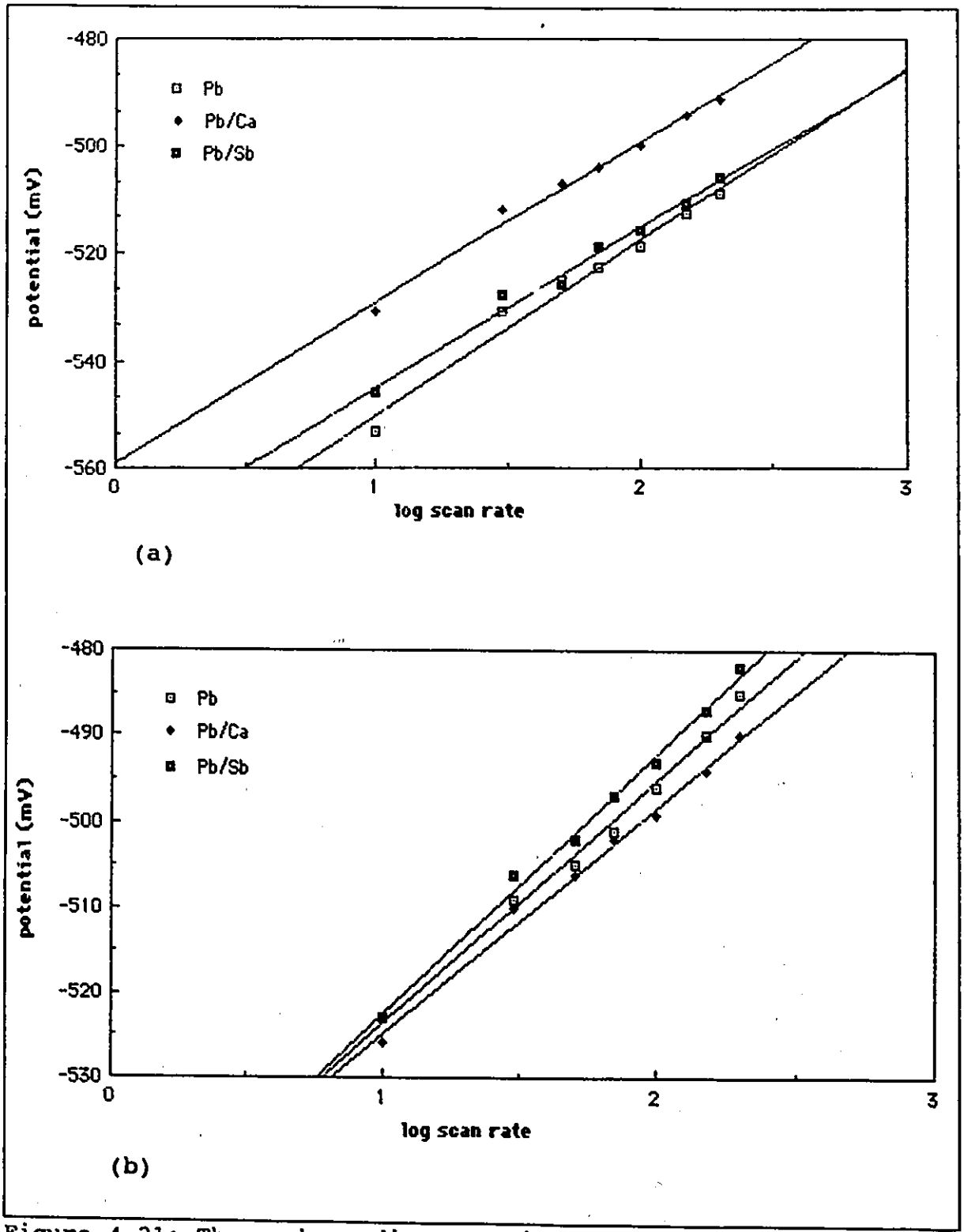

Figure 4.21: The peak anodic potential comparison of lead, lead-calcium, and lead-antimony at 0°C. (a): without ALS, (b): with ALS.

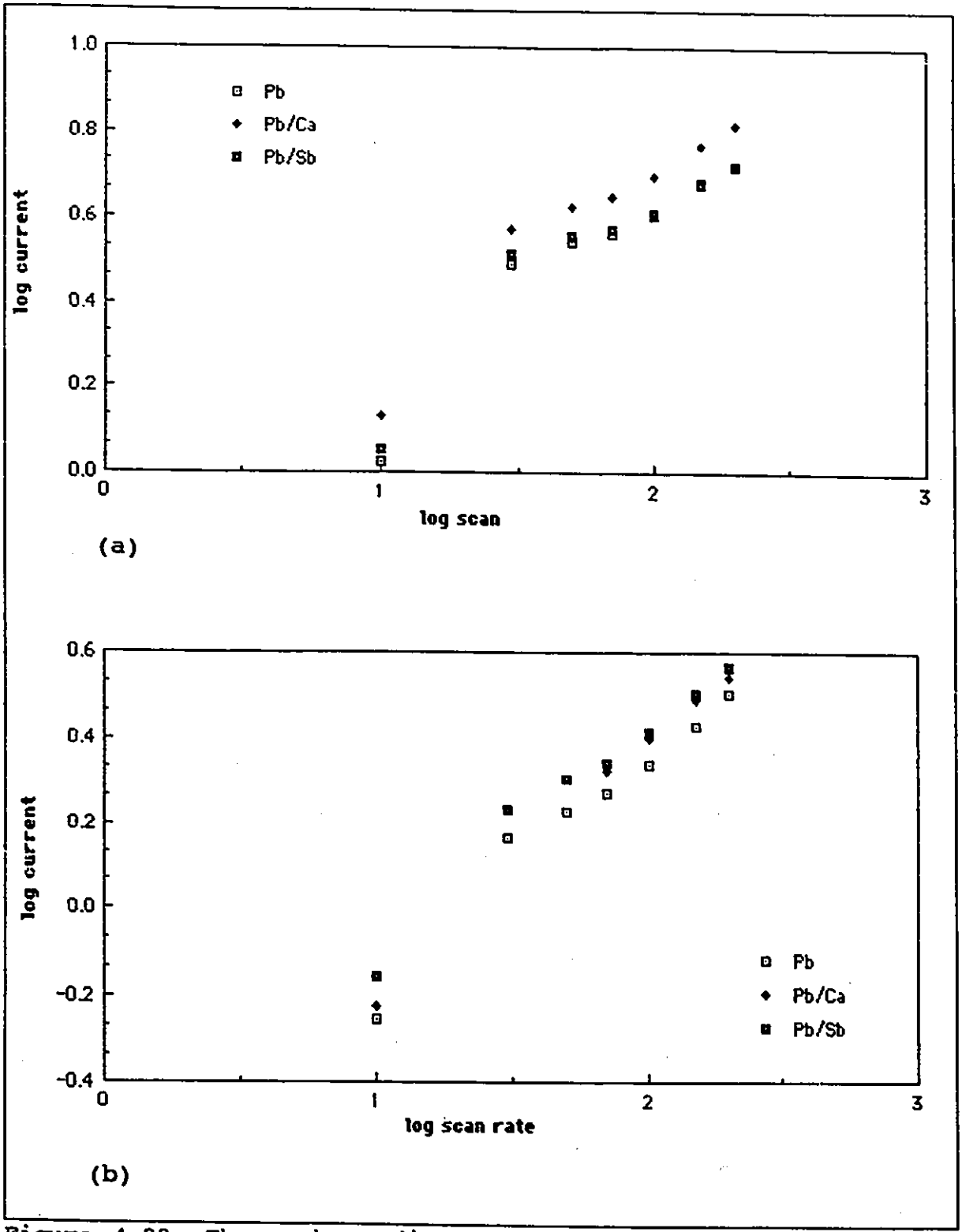

Figure 4.22: The peak anodic current comparison of lead, lead-calcium, and lead-antimony anodes at room temperature and 0°C. (a): without ALS, (b): with ALS.

the prior anodic film was reduced at steady-state cathodic current. Then the electrode potential was stepped to peak anodic potential. The resulting current-time curve was recorded. The time taken for the current to reach steady state t_{max}, the height of the current peak i_{max}, and the area underneath the curve (the charge transferred) were calculated. The crystal growth models were used to fit the transient curves and interpret the nature and nucleation of film growth.

Typical current vs. time curves for lead, lead-calcium, and lead-antimony in the presence and the absence of ALS are shown in Figure 4.23. The distinct shapes of the transient arises because the current initially increases as the lead sulphate nuclei form and grow. The size of the growing centres becomes limited in all directions as the centres overlap. Therefore the "rate of increase" diminishes and the current goes through a maximum. The current then asymptotically approaches zero at the final stages of this process when the centres overlap completely and hinder charge transfer across the electrode-electrolyte interface.

Table 4.6 compares the maximum current (i_{max}) and maximum time (t_{max}) with and without ALS addition to the electrolyte. The t_{max} is defined as the time required for the electrode to passivate (or the time taken for the current to reach a steady-state value).

The first important thing to be noticed is the reduced i_{max} and increased t_{max} in the presence of ALS. The reduction of i_{max} in the presence of ALS is a confirmation of the current reducing effect which was previously observed in the cyclic voltammetry data. The

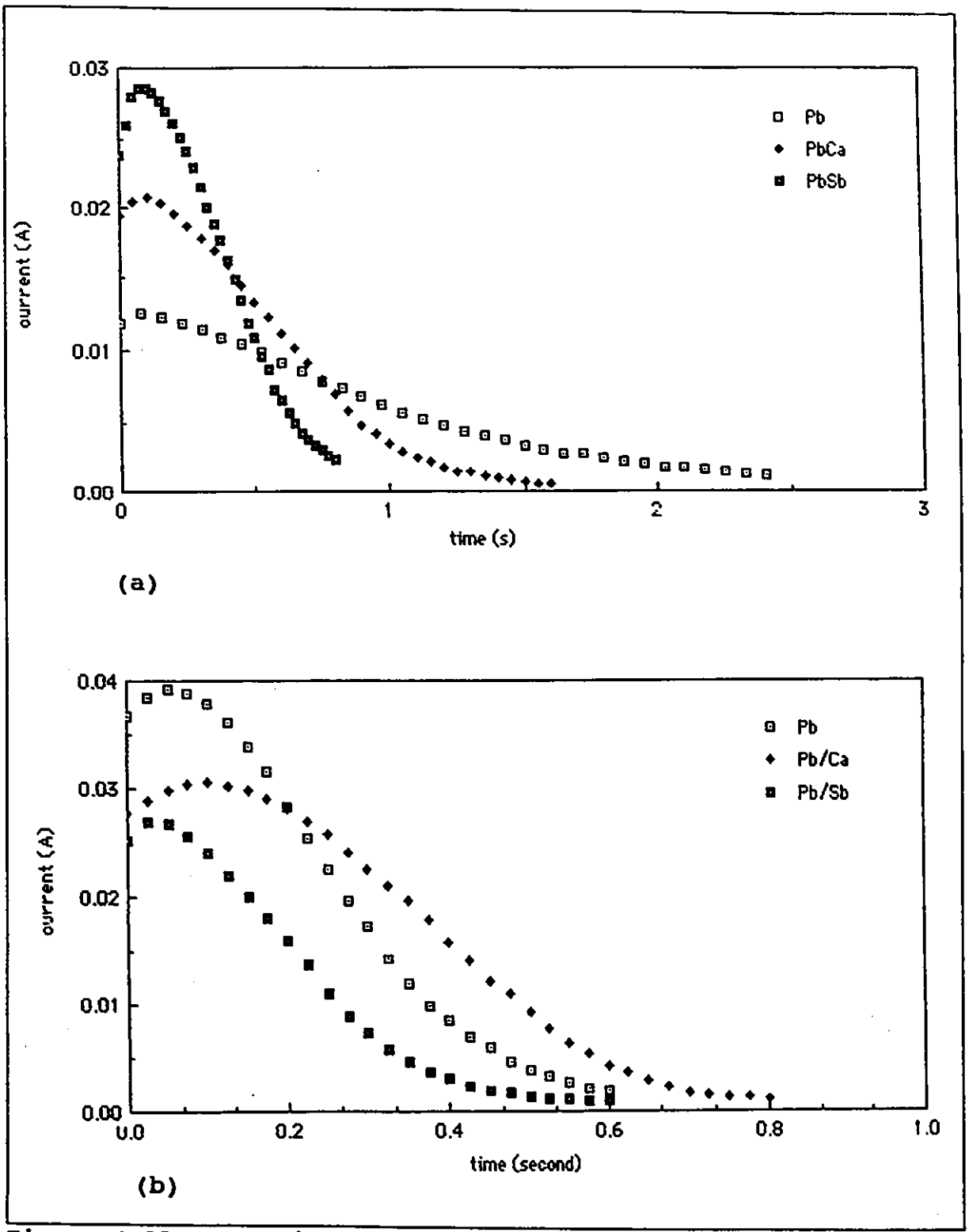

Figure 4.23: Comparison of transients of lead, lead-calcium, and lead-antimony alloys in the presence (a), and absence (b) of ALS, in stagnant 30% sulphuric acid at room temperature.

TABLE 4.6

Comparison of the maximum current density (i_{max}), $time_{max}$, and charge transferred in the transient experiment for lead and lead alloys in stagnant 30% sulphuric acid at room temperature.

	i_{max} (mA/Cm^2)		t_{max} (Sec)		Charge mAs/Cm^2	
	no ALS	w. ALS	no ALS	w. ALS	no ALS	w.ALS
Pb	34	17	0.7	2.0	19	20
Pb/Ca	26	21	0.8	1.3	20	20
Pb/Sb	30	29	0.5	0.8	15	18

increased t_{Max} represents the delay in nucleation and growth and consequent passivation of the anode. This favourable effect of ALS is in agreement with the trend that was reported earlier in the published literatures [Bode, 1977; Mahato, 1977, 1980; Simon, 1974; Brennan, 1973, 1974, 1976].

The charge consumed during the anodic reaction was estimated by integrating the area underneath the i-t transients. The values of charge transfer under different conditions are shown in the last two columns of Table 4.6. The addition of ALS has the best effect on the lead-antimony alloy with an average increase of 20% in the charge transfer. This implies that the film formation rates are reduced, and that transport processes in the film are favoured under these conditions. This improvement brings the ALS assisted performance level of the lead-antimony alloy anode to that comparable to lead and lead-calcium (18 mC/cm^2 for lead-antimony compared to 20 mC/cm^2 for lead and lead-calcium in the presence of ALS). The effect of the presence of ALS on charge transfer is negligible in lead and lead calcium with approximately 5% and 0%

TABLE 4.7

The regression factors of the ln(i/t) vs. t^2 curves of lead and lead alloy anodes.

	Pb		Pb/Ca		Pb/Sb	
	no ALS	w. ALS	no ALS	w. ALS	no ALS	w. ALS
R^2	97.6%	97.7%	99.4%	97.2%	93.3%	98.8%

increase respectively.

In order to study the electrocrystallization of lead sulphate particles, several 2 and 3 dimensional nucleation and growth models were examined (discussed in section 2.2). The shape of the i-t curves themselves illustrate clearly that they are not consistent with the 3-dimensional models (the curves approach zero, whilst in 3-dimensional growth models the curves approach a non-zero constant). Therefore, the data obtained from the transient experiment of each anode was tested to fit the 2-dimensional models (Equations 2.37, 2.41, 2.42, and 2.43). The best fitting model was found to be Equation 2.42 for all cases:

$$i=\left(\frac{2nF\pi MN_0k^2ht}{\rho}\right)\exp\left(-\pi M^2N_0k^2t^2/\rho^2\right) \qquad (2.42)$$

The plots of ln(i/t) vs. t^2 for lead, lead-calcium, and lead-antimony are shown in Figure 4.24. The regression factors for the linear portions of these curves are shown in Table 4.7. With an exception of lead-antimony in pure 30% sulphuric acid, all data points are linear with R^2 coefficients greater than 97%. Therefore, it can be concluded that the crystals form instantaneously in a

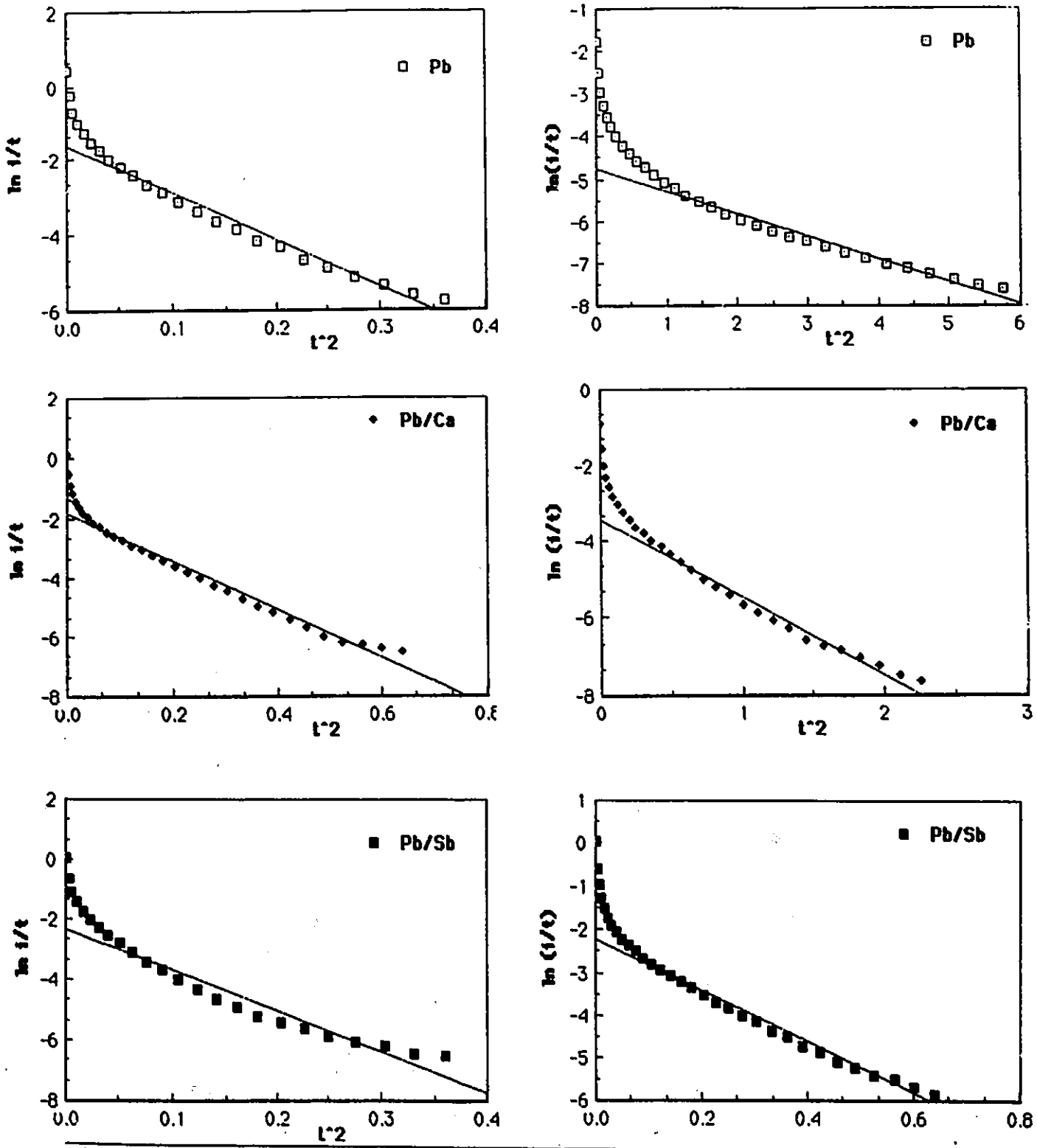

Figure 4.24: Plots of ln (i/t) vs. t^2 for lead, lead-calcium, and lead-antimony. Left column: without ALS, right column: with ALS.

disk shape and have a 2-dimensional growth (see Table 2.2). The transient for lead-antimony alloy in no ALS-added electrolyte does not satisfactorily fit any growth model. However, the ln(i/t) vs. t^2 still gives the best result.

4.7- SCANNING ELECTRON MICROSCOPY (SEM), AND X-RAY PHOTOELECTRON SPECTROSCOPY (XPS).

The morphology and the composition variations of the anodes resulting from the application of the cyclic voltammetry techniques were verified by the surface analysis techniques SEM and XPS. The morphology changes of the anode as a result of cycling were examined by micro-photographs using SEM techniques, while the quality of the materials present on the electrode surface were analyzed using XPS techniques. The experiments were performed on fresh (after 5 cycles) and old (after 500 cycles) anodes in the presence and absence of ammonium ligno-sulphonate (ALS).

In general, under the same conditions, similar morphologies were observed for all three anodes. Therefore, one typical anode microphotograph is shown in each case which represents similar morphologies of the other two. Figure 4.25 shows the surface morphology of a lead calcium electrode before undergoing any electrochemical process. The surface is highly porous and no deposition has occurred on the surface. The high porosity of the electrode creates a higher contact area between the active material

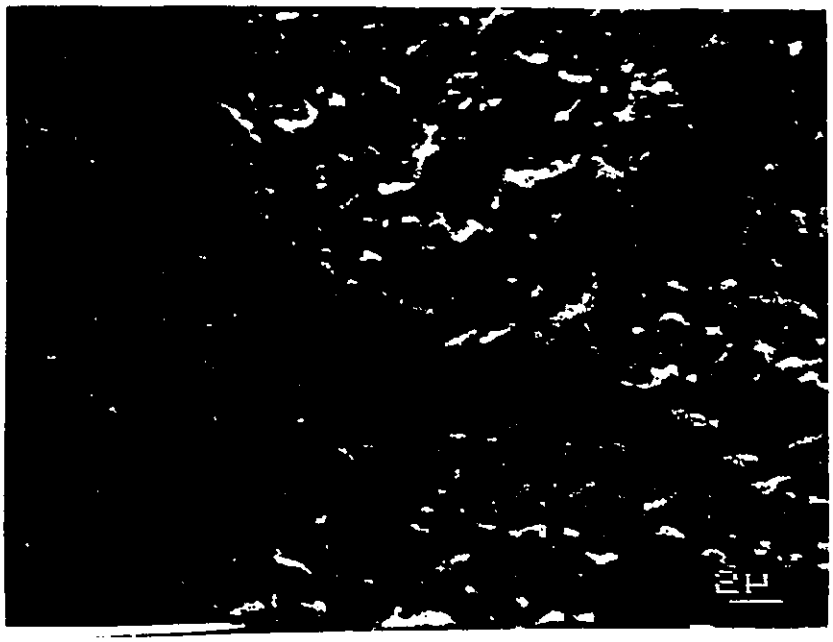

Figure 4.25: Morphology of a lead-calcium anode before being subject to any electrochemical changes.

and the electrolyte. This, in turn, results in more consumption of the active materials, thus, longer cycle life of the electrode.

The result of cycling of lead-antimony is shown in Figure 4.26 after 5 and 500 cycles. After 5 cycles, the surface is covered with fine needle-shaped lead sulphate crystals. The fine crystals cover the surface area without blocking the pore openings. The growth of dendrites is illustrated in the micro-photographs of the surface after 500 cycles. The dendrites are fully developed, overlapped, and cover the electrode surface. The formation of large individual lead sulphate crystals was also observed beside the dendritic sites (see figure 4.27). The formation of both types of lead sulphate are

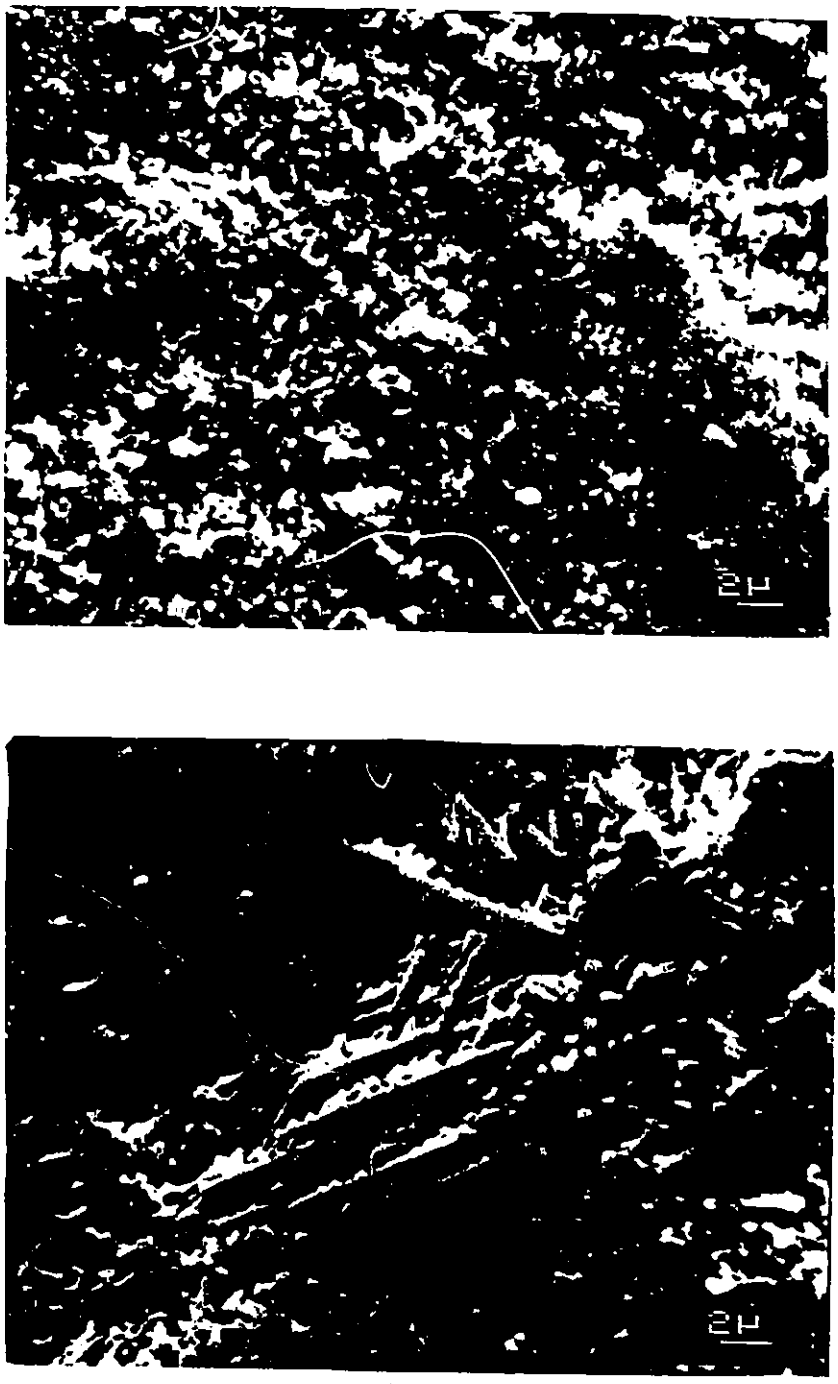

Figure 4.26: The deposition of lead sulphate crystals on the surface of a lead-antimony anode after 5 cycles (a) and 500 cycles (b). Note the formation of dendrites after 5oo cycles.

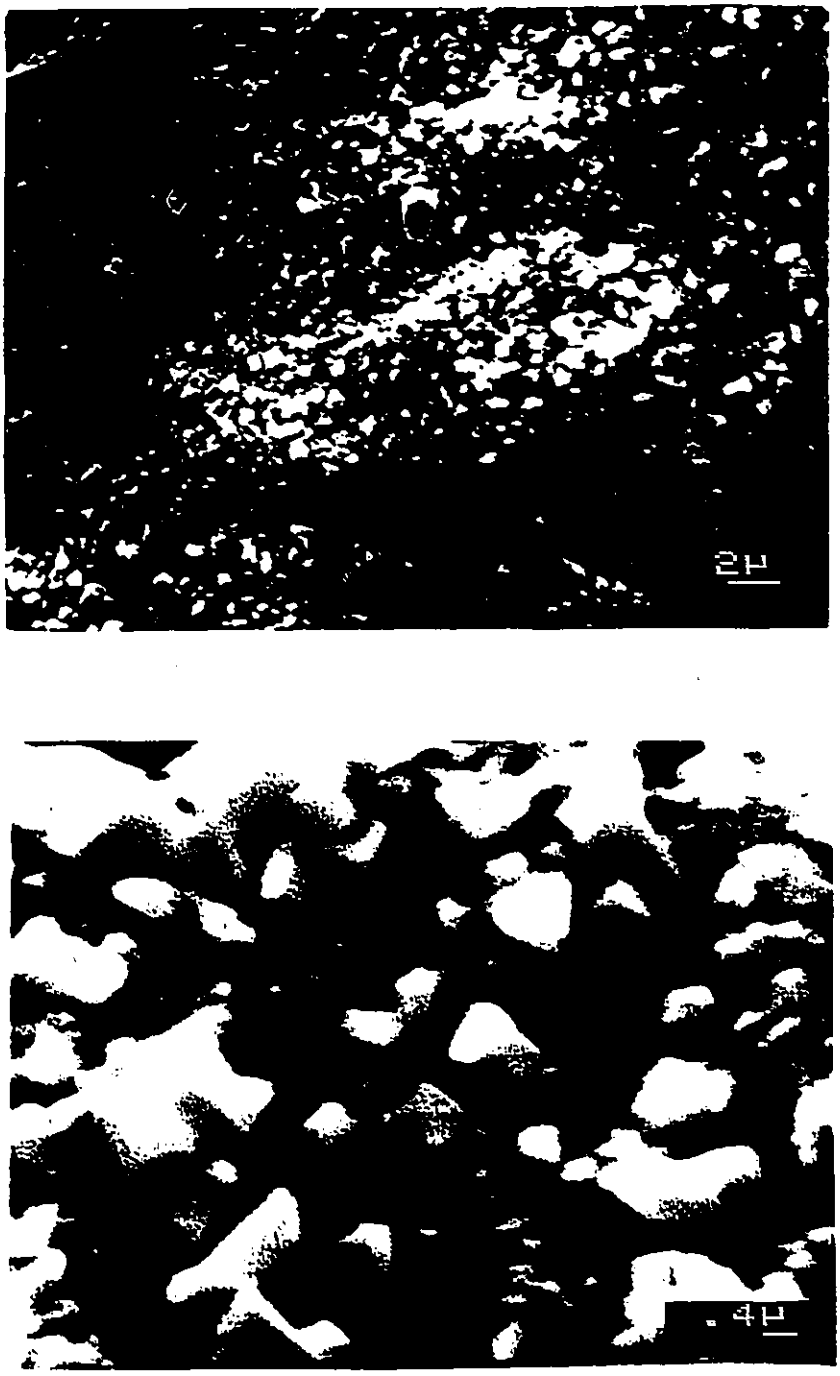

Figure 4.27: Lead sulphate crystals are formed both in the shape of dendrites and large individual crystals (a), and are sized in the range 0.3 to 1.3 μm (b).

reported in the literature. The size of the crystals was measured from micro-photographs of higher magnification shown in Figure 4.27, and found to be in the range of 0.3 to 1.3 μm. The large crystals and dendrites block the pore openings and decrease the electrolyte contact area considerably. The formation of these crystals which are known as the "hard" lead sulphates and are not reducible during the charge of the electrode, was previously reported by Pavlov [Pavlov, 1970]. These crystals accumulate on the surface and shorten the life of the electrode.

Figure 4.28 shows the microphotographs of lead sulphate crystals when ALS is added. As a result of the ALS addition, the crystals become smaller in size (range: 0.3 to 1.0 μm). The addition of ALS also eliminates dendrites, and hence, provides a more active area for the electrochemical reaction. An important observation is the increased amount of crystal covering the surface when ALS is added. This observation confirms the results obtained from the cyclic voltammetry and transient experiments in the previous sections reporting a decrease in the current density in the presence of ALS. The reduction was explained by formation of lead containing complexes of ALS with the same blocking function as lead sulphate (see Section 4.4). This XPS results reports the presence of an unknown lead containing compound at the surface when the electrodes were cycled in the presence of ALS. This compound might be a complex of lead and lignin which function the same way as lead sulphate. The spectrum of this compound is shown in Figure 4.29.

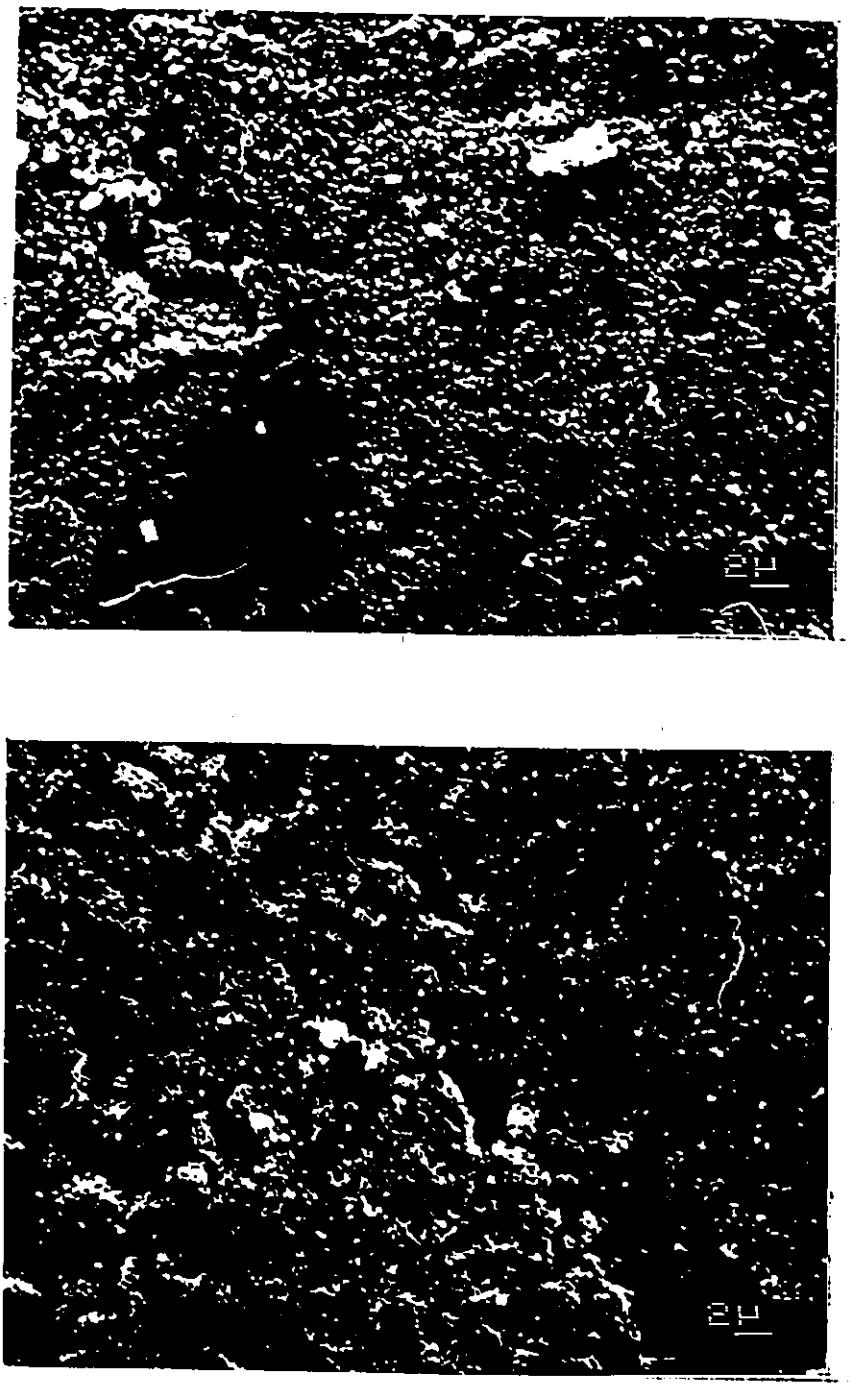

Figure 4.28: The formation of lead sulphate crystals in the presence of (ALS), (a): after 5 cycles, (b): after 500 cycles. Note the smaller size of crystals and elimination of dendrites.

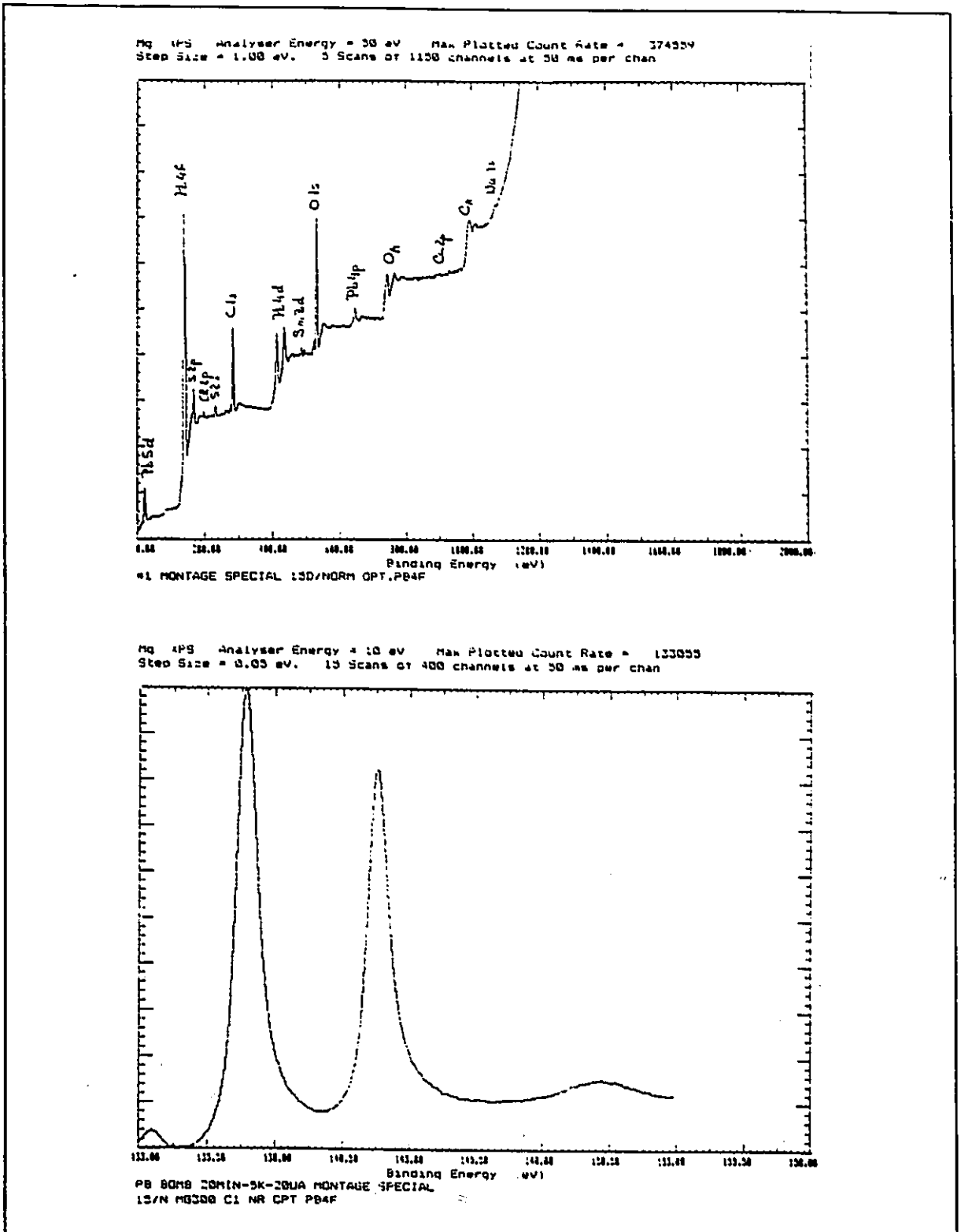

Figure 4.29: The X-ray spectroscopy of a lead anode in an ALS added sulphuric acid solution.

Based on the results obtained from SEM, and XPS it can be concluded that two different and competitive factors may be responsible for the rise and fall in the current density as well as the shift in PAP as a result of aging (discussed in Section 4.3, Figures 4.5 and 4.6): (i) morphological changes in the electrode structure, and (ii) the gradual growth of a lead sulphate film. The increase in the current density is due to the formation of a more porous active surface after each charge/discharge cycle. During charge, the reduced lead particles precipitate on the electrode surface and crystallize in a more porous arrangement with a higher active surface area. The new higher surface area exposes more active material from the electrode to the electrolyte. Hence, the current increases.

At the same time, a layer of hard lead sulphate accumulates on the surface of the electrode with each cycle. This film which is not reduced during charge, blocks the active area which decreases the current density.

In the early stages, the amount of the hard lead sulphate is small and decreases the current density by only a small amount. Since crystal rearrangement is the dominant factor, the current increases. However, with significant accumulation of hard non-conducting lead sulphate, the effect of the film can not be neglected. At a certain point, the effect of hard lead sulphate overcomes the effect of crystal rearrangement. At this point the overall current density passes through a maximum and starts to decrease. This phenomenon continues until the hard lead sulphate

centres overlap and collapse. Beyond this point, the lead sulphate does not grow any more and the current stabilizes.

The same mechanism accounts for retarding the PAP (causing the electrochemical reaction to occur at more cathodic potentials). Further formation of the resisting film creates a potential barrier which must be overcome before oxidation of active material become possible. In actual batteries, this phenomenon is manifest by the reduction in the open circuit voltage of the battery after several charge/discharge cycles.

CHAPTER FIVE: SUMMARY AND CONCLUSIONS

5.1- SUMMARY

The battery is one of the three critical components of remote photovoltaic/diesel/battery hybrid systems. The system life cycle costs can be significantly reduced by minimizing the maintenance requirements and maximizing the efficiency of the battery subsystem. Lead-acid batteries, either of sealed or flooded types, are currently being used in photovoltaic hybrid systems. The optimum use of lead-acid batteries in remote locations strongly depends on the performance of all components, e.g., cathode, anode, electrolyte, and separators. The anode performance, in turn, is usually influenced by various important factors such as the addition of alloying elements to lead as active material, the addition of chemical additives, i.e., expanders such as ammonium ligno-sulphonate, to the anode or to the electrolyte, the cycling strategies, the electrode aging, and the operational temperature.

As was mentioned in the literature review, the effects of these factors have been previously studied to some extent. Yet, systematic studies leading to an understanding of the effects of the alloying elements, the behaviour of the alloying elements, and the expanders under overcharge condition, and the behaviour of aged anodes, more particularly at low temperatures, are lacking in the published literature.

In this experimental study, the effect of the alloying elements in binary lead-calcium and lead-antimony, and ternary lead-calcium-tin and lead-antimony-selenium anodes was investigated using cyclic voltammetry, potentiostatic transient methods, and surface analysis techniques, i.e., SEM and XPS.

The significant effect of calcium in postponing the evolution of hydrogen during the charging process was observed. This favourable effect results in lower water loss and consequently less need for periodic battery electrolyte watering. However, the additions of both calcium and antimony lowered the discharge current output, re: anodic cycles of the cyclic voltammograms. The electrochemical studies suggest that this problem can be overcome by introduction of the third alloying elements of tin and selenium to lead-calcium and lead-antimony alloys respectively.

The addition of ammonium ligno-sulphonate was found to have the favourable effect of hindering the formation of large compact lead sulphate crystals and dendrites, and delaying the hydrogen evolution potential. ALS also postponed the onset of lead sulphate nucleation and crystal growth in favour of a dissolution-precipitation mechanism. The SEM microphotographs supported some of these observations. Ammonium ligno-sulphonate expander was expected to have an enhancing effect on the current density, while it showed an opposite effect under overcharge condition, both at 23 ± 1 °C and at 0 ± 0.2 °C.

The aged electrodes were different from the fresh ones by a small reduction in the current density and depolarization of the

peak anodic potential. However, the kinetics and the transport mechanism of old electrodes were observed to be independent of the aging.

The shape of the potentiostatic transients at potentials in the anodic region fit a model based on the growth kinetics being governed by instantaneous two-dimensional nucleation and growth followed by overlap.The SEM micro-photographs illustrate the formation of fine lead sulphate crystals at the early stages of cycling prior to the formation of larger crystals and dendrites at the later stages of cycling.

5.2- CONCLUSIONS

1- From electrochemical studies involving cyclic voltammetry, it can be concluded that:

i) addition of a third alloying element such as tin to lead-calcium or selenium to lead-antimony is important in overcoming the anode passivation effects;

ii) care should be exercised in avoiding overcharging the battery when ammonium ligno-sulphonate is used as a battery additive; and

iii) anode performance is significantly degraded at low temperatures.

2- From potentiostatic transient methods, it can be concluded that lead sulphate film formation in the anodic region is governed by

an instantaneous two-dimensional growth followed by a crystal overlap. This conclusion is important in understanding the rate of anodic film growth when applied to anodic passivation in practical batteries.

3- The scanning electron microscopic studies support the above conclusions.

CHAPTER SIX: REFERENCES

Archdale G. and Harrison J.A., "The Electrochemical Dissolution of Pb to Form $PbSO_4$ by a Solution-Precipitation Mechanism", J. Electroanal. Chem., 34, 21-6 (1972a).

Archdale G. and Harrison J.A., "The Anodic Dissolution of Pb in H_2SO_4", J. Electroanal. Chem., 39, 357-66 (1972b).

Archdale G. and Harrison J.A., "The Dissolution of Pb Amalgam in H_2SO_4", J. Electroanal. Chem., 43, 321-4 (1973a).

Archdale G. and Harrison J.A., "The Oxidation of Pb in H_2SO_4 in the Presence of A Battery Expander", J. Electroanal. Chem., 47, 93-101 (1973b).

Armstrong R.D., Fleischmann M., and Thirsk H.R., "The Anodic Behaviour of Mercury in Hydroxide ion Solution", J. Electroanal. Chem., 11, 208-23 (1966).

Asai K. Tsubota M., Yonezu K., and Ando K., "Discharge Behaviour of Electrodeposited PbO_2 and Pb Electrodes", J. Power Sources 7, 73-82 (1981/82).

Asai K., Tsubota M., Yonezo K., and Ando K.; "Capacity Limiting Mechanism of Lead-Acid Battery Plates", Power Sources 10, Proc. 14th International Power Source Symp., Brighton, UK, (1984).

Bagshaw N.E., "Lead-Strontium Alloys for Battery Grids", J. Power Sources, 2, 337-50 (1977).

Bass K., Ellis S.R., Johnson M., and Hampson N.A., "Electrochemical

Investigation of Lead-Calcium Alloys in Sulphuric Acid", J. Power Sources, 21, 151-6 (1987).

Bode H., in "Lead-Acid Batteries", John Wiley, New York, (1977).

Brennan M.P.J. and Hampson N.A., "Expander Action in Lead-Acid Battery. I", J. Electroanal. Chem., 48, 465-74 (1973).

Brennan M.P.J. and Hampson N.A., "Expander Action in Lead-Acid Battery. II", J. Electroanal. Chem., 52, 1-10 (1974a).

Brennan M.P.J. and Hampson N.A., "Expander action in Lead-Acid Battery. III", 54, 263-8 (1974b).

Burbank J., "Crystallization of $PbSO_4$ on Anodes of Lead-Antimony Alloy", J. Electrochem. Soc.; 118, 4, 525-9 (1971a).

Burbank J., "Anodic Crystallization on Pure and Antimonial Lead in Sulphuric Acid", NRL Report 7256; Washington D.C., (1971b).

Burbank J., "Cyclic Anodic Coatings on Pure and Antimonial Lead in H_2SO_4", Power Sources 3, Oriel Press, Newcastle upon Tyne, 13-34 (1971c).

Caldwell T.W. and Sokolov U.S., "Effect of Metallurgical Structure on Hydrogen Evolution on Lead Alloys", Power Sources 5, Academic Press, NY, 73-95 (1975).

Carr J.P., Hampson N.A., and Taylor R., "Fast Linear Sweep Voltammetry Studies on Polycrystalline Lead and Electrodeposited Lead Dioxide in Aqueous Sulphuric Acid", J. Electroanal. Chem., 33, 109-20 (1971).

Chiku T. and Nakajima K., "Formation of $PbSO_4$ Crystallites on Pb in the Lead-Acid Cell", J. Electrochem. Soc., 118, 9, 1395-8 (1971).

Costa P. and Mambelli A., "Production of Battery Grids Based on the Reclamation of Antimony-Containing Alloys From Used Battery Scraps", Proc. 37th International Foundry Congress, Brighton, (1970).

Ekdunge P., Rybalka K.V., and Simonsson D., "Rechargeable Kinetics and Structural Changes in the Porous Lead Electrode in H_2SO_4 Solution", Electrochem. Acta, 32, 4, 659-67 (1987).

Ekdunge P. and Simonsson D., "The Discharge Behaviour of the Porous Lead Electrode in the Lead-Acid Battery. I", J. App. Electrochem., 19, 127-35 (1989).

Energy, Mines and Resources Canada, "Photovoltaic system design manual", (1989).

Farrinton Lockwood Co. Ltd., "Lead-Acid Battery Expander Project", Kanata, Ontario, Canada, (1989).

Fleming A. N. and Harrison J.A., The Electrochemical Oxidation of Pb to form $PbSO_4$", Electrochem. Acta, 21, 905-12 (1976).

Fleming A.N. and Harrison J.A., in "Electrochemistry of Lead", (A.T. Kuhn, ed.); Academic Press, NY, (1979).

Hampson N.A., Jones P.C., and Phillips R.F., "Electrochemical Reactions at PbO_2 Electrodes. III", Can. J. Chem., 46, 1325 (1968).

Hoffmann G. and Vielstich W., "The Influence of the Organic Expanders on the Kinetics of the Lead Electrode", J. Electroanal. Chem., 180, 565-76 (1984).

Ijomah M.N.C., "Electrochemical Behaviour of Some Lead Alloys", J. Electrochem. Soc, 134, 12, 2960-6 (1987).

Iliev V and Pavelov D., "The Effect of the Expander upon the Two Types of Negative Active Mass Structure in Lead-Acid Batteries", J. Appl. Electrochem., 15, 39-52 (1985).

Independent Battery Manufacturers Assoc. Inc., " Grid Metal Manual", Largo, Florida, (1973).

Indian Lead Zinc Information Centre, "Lead-Acid Batteries, a Reference and Data Book", Elsevier, Lausanne, (1977).

Integrated Power Corp., "Photovoltaic and Hybrid Remote Power Systems", Rockville, Maryland, USA (1988).

Jensen H.E., Proc. 11th Power Sources Conf., Atlantic City, NJ, 73-7 (1957).

Laitinen H.A. and Watkins N.H., "Mechanism of Anodic Deposition and Cathodic Stripping Of PbO_2 on Conductive Tin Oxide", J. Electrochem. Soc., 123, 6, 804-9 (1976).

Linden D., in "Handbook of Batteries and Fuel Cells", McGraw-Hill, New York (1984).

Mahato B.K., "Aspects of the Role of Lignin Additives in Pasted Lead Electrodes", J. Electrochem. Soc., 124, 11, 1663-7 (1977).

Mahato B.K., "Lead-Acid Battery Expander I", J. Electrochem. Soc., 127, 8, 1679-87 (1980).

Mahato B.K., "Lead-Acid Battery Expander II", J. Electrochem Soc., 128, 7, 1416-22 (1981).

Mahato B.K. and W.H. Tiedemann, "Linear Potential Sweep of Lead-Acid Battery Electrodes Containing Traces Te, Sb, As, Co, and Ni", J. Electrochem. Soc., 130, 11, 2139-44 (1983).

Mahato B.K., Strebe J.L., Wilkinson D.F., and Bullock K.R., "Effect of Antimony on Lead-Acid Battery Negative", J. Electrochem. Soc., 132, 1, 19-23 (1985).

McDonald D.D., "Transient Techniques in Electrochemistry", Plenum Press, London (1977).

Pavlov D. and Popova R., "Mechanism of Passivation Processes of the Lead Sulphate Electrode", Electrochem. Acta, 15, 1483-91 (1970).

Pavlov D., in "Power Sources for Electric Vehicles", (McNicol and D.A.J. Rand, eds.), Elsevier (1984).

Pavlov D. and Ignatova S., "Breathing of the Lead-Acid Battery Negative Plate During Cycling", J. Appl. Electrochem., 17, 715-23 (1987).

Prengaman R.D., "Advanced Lead Alloys for Battery Making", Proc. 8th International Lead Conf., LDA, 69-77 (1983).

Rosen M.J., in "Surfactant and Interfacial Phenomena"; John Wiley, New York (1978).

Ruetschi P. and Angstadt R.T., "Anodic Oxidation of Lead at Constant Potential", J. Electrochem. Soc., 111, 12, 1323-30 (1964).

Ruetschi P., "ion Selectivity and Diffusion potentials in Corrosion Layers of $PbSO_4$ Films on Pb in H_2SO_4", J. Electrochem. Soc., 120, 3, 331-6 (1973).

Ruetschi P., "Review on the Lead-Acid Battery Science and Technology", J, Power Sources, 2, 3-24 (1977/78).

Sato H., "Development of Sealed Lead-Acid Batteries for Solar Power

Systems", J. Power Sources, 28, 173-80 (1989).

Sharpe T., "The Adsorption of Lignosulphonate onto Lead Surface. I", Electrochem. Acta, 14, 635-9 (1969).

Simon A.C., Caulder S.M., and Ritchie E.J., "Effect of Antimony Trioxide on the Microstructure of the Lead Dioxide Electrode", J. Electrochem. Soc., 117, 10, 1264-5 (1970).

Simon A.C., Caulder S.M., Gurlusky P.J., and Pierson J.R., "The Structure of the $Pb/PbSO_4$ Electrode in the Reduced State and the Changes produced by Lignin Derivatives and $BaSO_4$", Electrochem. Acta, 19, 739-43 (1974).

Simon A.C., Caulder S.M., Gurlusky P.J., and Pierson J.R., "The Effect of the Additives on the Reaction Mechanism of the $Pb/PbSO_4$ Electrode", J. Electrochem. Soc., 121,4, 463-67 (1974).

Simonsson D., Ekdunge P., Lindgren M., "Kinetics of the Porous Lead Electrode in the Lead-Acid Battery", J. Electrochem. Soc., 135, 7, 1613-18 (1988).

Sol Magazine, EMR Report, "PV Market Study Released", 72, 12, (1989).

Southampton Electrochemistry Group, "Instrumental Methods in Electrochemistry", Ellis Horwood Ltd., Chichester, England (1985).

Szava G.J., "Role of Organic Expander in Modern Lead-Acid Batteries", J. Power Sources, 23, 119-24 (1988).

Szava G.J., "Mechanisms by Which Organic Expanders Improve the Performance of Lead-Acid Batteries", J. Power Sources, 28,

149-53 (1989).

Tabe Mohammadi A., Donepudi V.S., Girgis M., and Adams W.A., "Photovoltaic/Diesel/Battery Hybrid Energy Storage: Lead-Acid Battery Characterization Research Activities." Canadian Chemical Engineering Graduate Student Conference" (Abstracts), Calgary, Alberta, Canada (1990a).

Tabe Mohammadi A., Donepudi V.S., Girgis M., and Adams W.A., "Electrochemical Studies on Some Lead Alloy Anodes in Photovoltaic Lead-Acid Battery Electrolyte", 177th Electrochemical Society Meeting (Abstracts), Montreal, Quebec, Canada (1990b).

Tabe Mohammadi A., Donepudi V.S., Girgis M., and Adams W.A., "Effects of Ammonium Ligno-Sulphonate on the Behaviour of Lead and Lead-Calcium Anodes in 30% Sulphuric Acid Solution", 41st Meeting of International Society of Electrochemistry (Abstracts), Prague, Czechoslovakia (1990c).

Thirsk H.R., and Harrison J.A., "A Guide to the Study of Electrode Kinetics", Academic Press, London (1972).

Valeriote E.M., "Composite Cell Testing of Corrosion Resistant Pasted Lead-Acid Battery Grids", J. Electrochem. Soc., 128, 1423-33 (1981).

Webster S., Mitchell P.J., and Hampson N.A., "Electroreduction Processes of Lead and Lead Alloys in 5M H_2SO_4", J. Electrochem. Soc., 133, 1, 137-9 (1986).

Webster S., Mitchell P.J., and Hampson N.A., "An Electrochemical Investigation into the Properties of Solid Lead-Bismuth Alloys

in 5M H_2SO_4", Proc. Electrochem. Eng. Symp. Series 98, Pergamon Press (1988).

Weininger J.L. and Morelock J.R., " Structural Transformation of the PbO_2 Active Material During Cycling", J. Electrochem. Soc., 122, 461-7 (1975).

Weissman E.A., in "Lead-Acid Storage Batteries"; Marcel Dekker Inc., New York (1977).

Williams J.D., J. Metallurgia, 74, 105 (1966).

Willinganz E., Proc. 13th Power Sources Conf., Atlantic City, NJ, 73-5 (1959).

Zachlin A.C., "Function and Behaviour of the Components of Expanders for the Negative Plates of Lead-Acid Storage Batteries", J. Electrochem. Soc., 98, 325-33 (1951).

APPENDIX I: DEFINITIONS

Active Material The material in the electrodes of a cell or battery which takes part in the electrochemical reactions of charge or discharge.

Ampere (A) Electron or current flow representing the flow of one coulomb per second past a given point in the circuit.

Ampere-Hour (Ah) A measurement of quantity of electricity computed as the product of current (in ampere) and time (in hours).

Anode The electrode in an electrochemical cell where oxidation takes place. During discharge, the negative electrode of the cell is anode. During charge, the situation reverses and the positive electrode of the cell is anode.

Battery Two or more electrochemical cells electrically interconnected in an appropriate series/parallel arrangement to provide the required operating voltage and current levels. Under common usage, the term "battery" is often also applied to a single cell.

Capacity The total number of ampere-hours or watt-hours that can be withdrawn from a fully charged cell or battery under specified conditions of discharge.

Cathode The electrode in an electrochemical cell where reduction takes place. During discharge, the positive electrode of the cell is the cathode. During charge, the situation reverses, and the negative electrode of the cell is cathode.

Cell The basic electrochemical unit used to store or generate electrical energy.

Charge The conversion of electrical energy, provided in the form of a current from an external source, into chemical energy within a cell or battery.

Charge Acceptance The ability of a battery to accept charge under specified conditions.

Charge/Discharge Cycle A sequence of a charge and subsequent discharge under specified conditions.

Charge, State of Condition of cell in terms of the rated capacity remaining in the cell at a given point in time.

Closed Circuit Voltage (CCV) The potential or voltage at the terminals of an electrical device when current is flowing.

Coulomb The quantity of electricity when one ampere flows for one second, representing 6.24×10^{18} electrons.

Current (i) The rate of transfer of electrical energy measured in ampere.

Current Density The current per unit active area of the surface of an electrode.

Cycle Life the number of cycles under specified conditions before a device fails to meet specified performance criteria.

Deep Discharge Withdrawal of at least 80% of the rated capacity of a cell or battery.

Depolarization The reduction in the polarization of an electrode.

Depth of Discharge The ratio of the quantity of electricity (usually in ampere-hours) removed from a cell or battery on discharge to its rated capacity.

Discharge The conversion of chemical energy of a cell or battery into electrical energy and withdrawal of the electrical energy into a load.

Double Layer The region in the vicinity of electrode-electrolyte interface where the concentration of mobile ionic species has been changed to values differing from the bulk equilibrium value by the potential difference across the interface.

E^0 Variously, symbol for **Electrode Potential, Standard Electrode Potential.**

e- Symbol for **Electron.**

Electrolyte The ionic-conducting medium within an electrochemical cell that provides the ion transport mechanism between the positive and negative electrodes.

Grid In batteries, a frame work for a plate or electrode which supports or retain the active materials and acts as a current collector.

Half Cell An electrode (either the anode or cathode) immersed in a suitable electrolyte.

Hybrid The combination of different component technologies on a single substrate.

Maintenance-Free Battery A secondary battery which does not require periodic "topping up" to maintain electrolyte volume.

Open Circuit Voltage (OCV) The difference in potential between the terminals of a cell or voltage when the circuit is open (no-load condition).

Overcharge The forcing of a current through a cell after all the active material have been converted to the charged state. In other words, charging in excess of that needed to return full capacity to the cell.

Passivation The phenomenon by which a metal, although in conditions of thermodynamic instability, remains indefinitely unattacked because of certain surface conditions.

Polarization The change in potential of a cell or electrode from its equilibrium value caused by a passage of an electric current.

Standard Electrode Potential (E^0) The equilibrium electrode potential when all the constituents taking part in the electrode reaction are in standard state.

Storage Battery A secondary battery designed for use in a fixed location.

APPENDIX II: ABSTRACTS

Abstract 1: Presented at the "Canadian Chemical Engineering Graduate Students Conference", Calgary, Alberta, Canada, 1-4 May 1990.

PHOTOVOLTAIC-DIESEL-BATTERY HYBRID ENERGY STORAGE: LEAD-ACID BATTERY CHARACTERIZATION RESEARCH ACTIVITIES

by

A. Tabe Mohammadi, G. Song, S. Donepudi, M. Girgis,

and W.A. Adams

(The Electrochemical Science and Technology Centre,

Dep. of Chemical Engineering, University of Ottawa)

Centralized electric grids based on thermal, hydroelectric, and nuclear power generation technologies provide power to most densely populated locations within Canada and other parts of the world. However, the same is not true for remote locations including Northern Canadian regions. Alternate energy options therefore have to be explored to meet the basic needs of remote communities, such as lighting, water pumping, and communications.

Various ways of storage and generating power are by means of: traditional diesel engine/generator, wind, solar thermal power generators and stand-alone or hybrid photovoltaic with diesel and battery sub-systems.

A conceptual PV-diesel-battery hybrid system is shown in Figure 1, and it consists of the following sub-systems:

- Photovoltaic array,
- Computer controller,
- Battery storage system,
- DC-AC convertor, and
- Diesel generator.

It is hoped that this strategy is capable of reducing diesel fuel consumption, thus minimizing frequent maintenance as well as environmental pollution. Since the battery is one of the critical components of the system, a careful evaluation and incorporation of batteries of known characteristics is required to reduce diesel demand.

Although lead-acid batteries have been known for nearly 150 years, their behaviour changes depending on the load profile for intended application as well as differences in battery performance characteristics that strongly depend on battery design and manufacturing. Therefore, we should determine the load demand in PV-diesel-battery systems and then establish the optimum charge-discharge strategy in order to meet the system load demand.

Since last year, several research activities have been in progress in this area which are in the two following principal areas:

(i) Characterization of PV lead-acid batteries by incorporating known charge-discharge strategies, development of the control algorithms, and

(ii) Electrochemical and surface analytical studies with the anodes of PV lead-acid batteries. In the present studies, flooded and sealed lead-acid batteries of nominal capacities (of 70 and 100 Ah respectively) were characterized using well-defined charging and discharging strategies in order to develop control algorithms. A system operating with this algorithm would eventually meet the number of cycles required by this battery system and has the advantage of being independent of the history and the age of the battery as well as the initial state of charge of the battery.

In parallel studies, some lead alloys have been subjected to electrochemical evaluations using conventional potential perturbation methods and surface analytical techniques. The thrust of this work was to investigate and understand the electrochemical factors that are influential in altering the performance characteristics of the PV lead-acid batteries. Cyclic voltamograms for pure Pb, Pb/Sb, and Pb/Ca alloys are compared in figure 2. Preliminary results show a noticeable reduction in the potential in the onset of hydrogen gas evolution in the case of the Pb/Sb electrodes. The Pb/Ca alloy had a little effect on the gassing phenomena. In addition to a significant shift in hydrogen overpotential, the presence of Sb (or Ca) results in lowering of charging efficiency.

In this presentation the current status of these activities will be summarized.

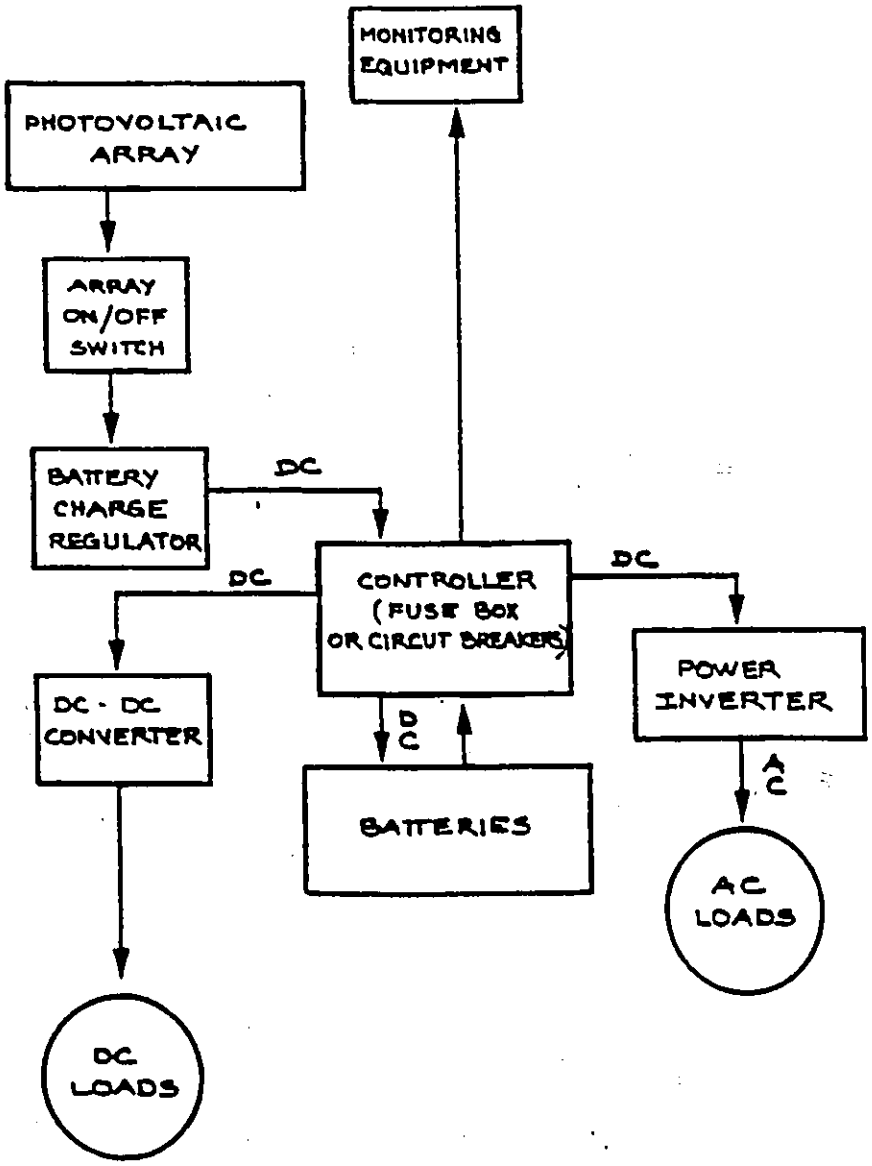

Figure 1: Basic Photovoltaic Configuration

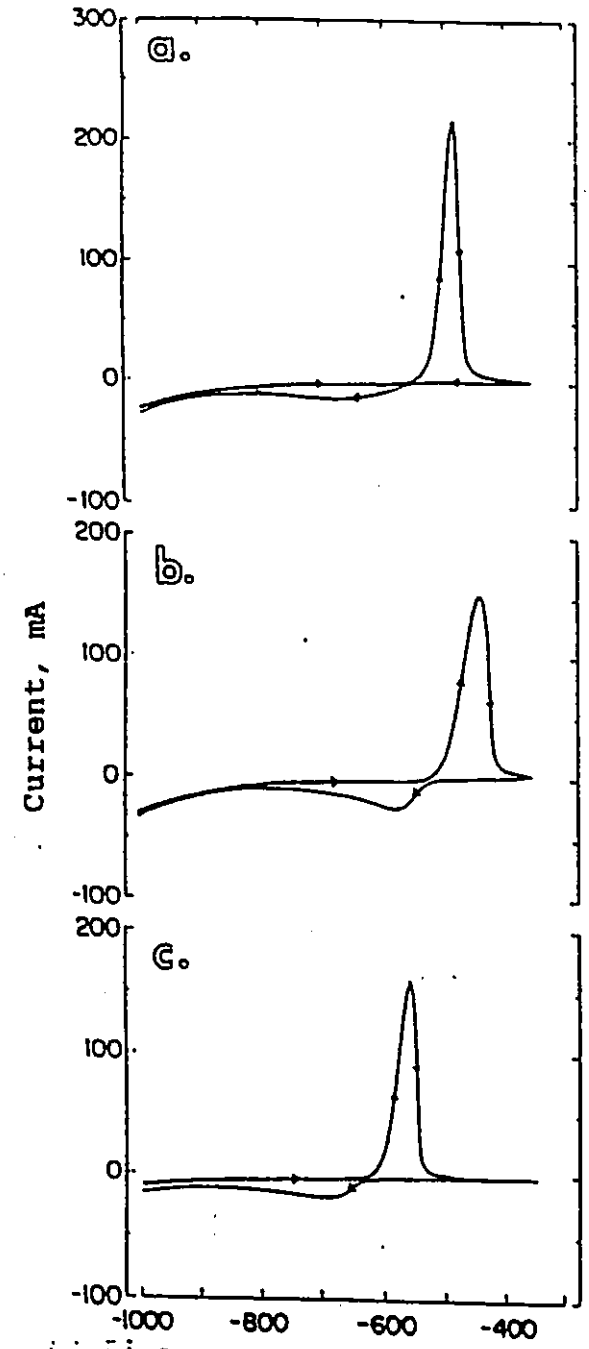

Figure 2: Cyclic voltamograms of : (a) pure lead, (b) lead/antimony (1.66 wt.%), and (c) lead/calcium (0.9 wt.%) alloys in unstirred sulphuric acid solution at room temperature. Sweep rate = 50 mV.S-1

Abstract 2: Presented at the "177th Electrochemical Society Meeting ", Montreal, Quebec, Canada, 6-10 May 1990.

Electrochemical Studies on Some Lead Alloy Anodes in Photovoltaic Lead-Acid Battery Electrolytes.

A. Tabe Mohammadi, M. Girgis, V.S. Donepudi, and W.A. Adams.
Electrochemical Science and Technology Centre,
University of Ottawa, Ottawa, Ontario, Canada.

A successful operation of remote photovoltaic/battery/diesel hybrid systems requires batteries with a well-defined behaviour under different conditions of utilization (storage, charge, and discharge) in conjunction with the other components, i.e., solar array, diesel generator and inverters. Therefore, it is important to conduct studies of various aspects such as: (i) characterization of commercially available batteries under various charge/discharge regimes simulating the functioning of a PV/ battery/diesel hybrid system. The testing and developing algorithms, and (ii) the investigation of fundamental electrochemical and surface analytical properties in order to understand the processes that take place in PV batteries. In the present studies flooded and sealed lead-acid batteries of nominal capacities of 70 and 100Ah respectively, were characterized using well-defined charging and discharging strategies in order to develop control algorithms. A system operation with these algorithms would meet the number of cycles required by this battery system and have the advantage of being independent of the past history and the age of the battery as well as the initial S.O.C. of the battery.

In parallel studies, some lead alloys have been subjected to electrochemical evaluation using conventional potential perturbation methods and surface analytical techniques. The thrust of this work was to investigate and understand the electrochemical factors that are influential in altering the performance characteristics of PV lead-acid batteries. The preliminary results show a noticeable reduction in the potential for the onset of hydrogen gas evolution in the case of the Pb/Sb electrode. The Pb/Ca alloy had a little effect on the gassing phenomenon. In addition to a significant shift in hydrogen overpotential, the presence of Sb (or Ca) results in a lowering of charging efficiency. Mahato et. al. (1,2) observed a similar behaviour. It is believed that such a reaction is competitive with $PbSO_4$ formation. This may be associated with a change in morphology of the $PbSO_4$ crystals themselves. In the second case, the supersaturation of Pb^{2+} ions in the vicinity of the electrode surface would increase and thus, excessive crystallization overvoltage would be required for the reaction to proceed. The same trend has been observed for the Pb/Ca alloy, but for different reasons, such as the formation of PbCa complexes.

References

1- B. K. Mahato, J.I. Strebe, D.F. Wilkinson, and K.R. Bullock, J. Electrochem. Soc., 132, 19 (1985).
2- B.K. Mahato and W. A. Tiedman, J. Electrochem. Soc., 130, 2139 (1983).
3- J. Burbank, J. Electrochem. Soc., 118, 525 (1971).

Abstract 3: Presented at the "41st Meeting of International Society of Electrochemistry", 20-25 August 1990, Prague, Czechoslovakia.

EFFECT OF AMMONIUM LIGNO-SULPHONATE ON THE BEHAVIOUR OF LEAD, LEAD-0.09% CALCIUM, AND LEAD-1.66% ANTIMONY ALLOY ANODES IN 30% SULPHURIC ACID SOLUTIONS.

A. Tabe Mohammadi, V.S. Donepudi, M. Girgis,
G. Song, and W.A. Adams
The Electrochemical Science and Technology Centre
University of Ottawa (ESTCO), Ottawa, Ontario, Canada

There is an ongoing photovoltaic hybrid energy storage program at "ESTCO" comprised of: i) characterization of lead-acid batteries for photovoltaic/diesel/battery hybrid applications, and ii) investigation of the electrochemical behaviour of lead, lead-0.09% calcium, and lead-1.66% antimony alloys in stagnant 30% sulphuric acid solutions, usual electrolytes of lead-acid batteries.

In these electrochemical investigations, conventional cyclic voltammetry techniques are used, supplemented by surface analyses using XPS techniques. The influence of alloy composition as well as that of ammonium ligno-sulphonate (ALS) were investigated. ALS, a large molecule having the structure shown in Figure 1, is added to open the pore structure of the sulphate film which enhances the battery operating characteristics at low temperature by modifying the porous film to allow easy access for reactants and products.

Based on open-circuit potential measurements and cyclic voltammetry (up to 10 cycles), it can be inferred that a critical concentration of ALS exists beyond which the trends in potential

and current variations with concentration are reversed, Figures 2a, 2b, and 2c show some results at room temperature.

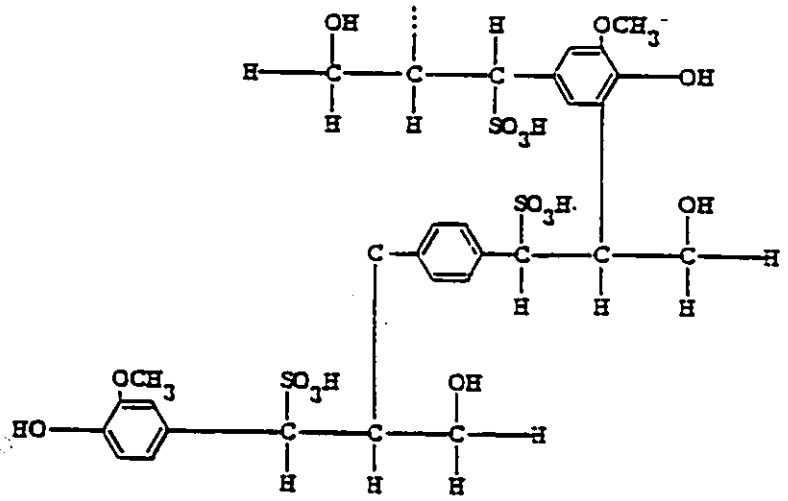

Figure 1: Ammonium Ligno-sulphonate structure

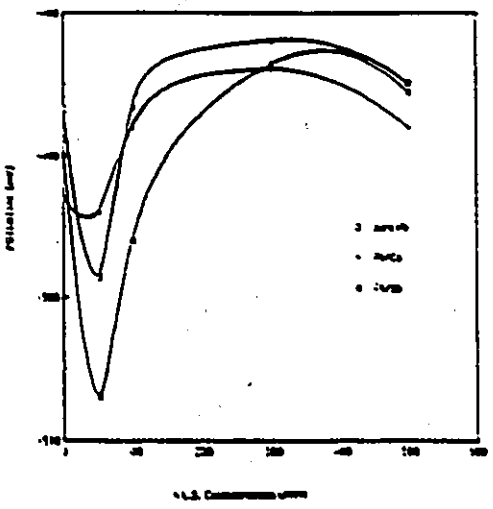

Figure 2a: Anodic peak potential variations with ALS concentration.

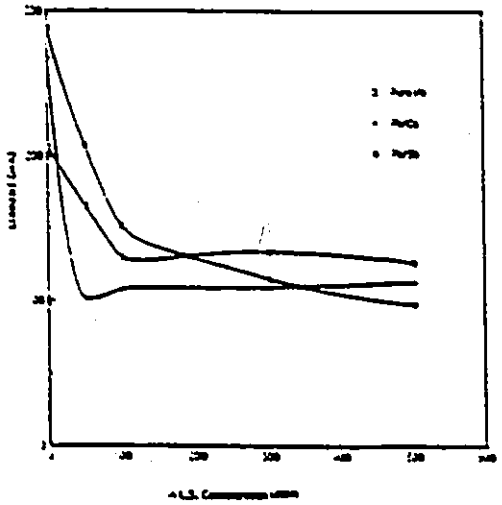

Figure 2b: Anodic peak current variations with ALS concentration..

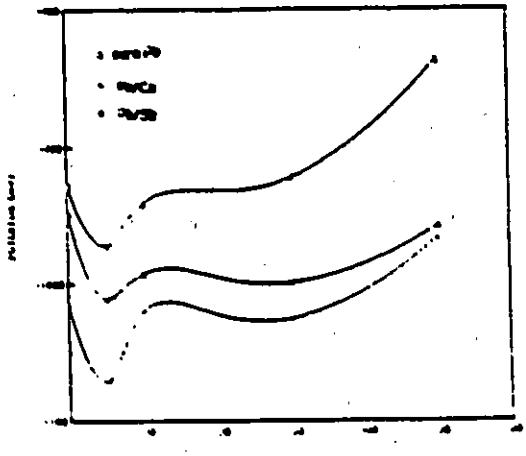

Figure 2c: Gassing potential variations with ALS concentrations.